Chapter 5

Failure Theories

5.1 Preliminary Discussions

The modes of failure discussed in Chapter 2 were presented as an overview of the possible mechanisms which trigger a failure. Assessing failure requires an accurate and thorough stress analysis in which the largest stresses (principal stresses) that occur at a critical point in the component under evaluation must be estimated. In addition to defining the principal stresses, one must also be aware of the type of material they are working with. Ductile and brittle materials will typically fail in different manners, and their failure is predicted by different theories. Similarly, when fatigue is being considered, the overall strength of the material is reduced as the number of load cycles increases.

5.2 Multiaxial States of Stress and Strain

Under the most complicated loading conditions, a machine part may be subjected to forces and moments produced by various combinations of direct axial loads, bending loads, direct or transverse shearing loads, torsional loads, and/or surface contact loads. As noted in 4.2, no matter how complicated the geometry of the part or how many different external forces and moments are being applied, the force system can always be resolved into just three resultant forces and three resultant moments, each defined with respect to an arbitrarily chosen x-y-z coordinate system. The origin of the selected x-y-z coordinate system may be placed at any desired critical point within the part. The most complicated state of stress that can be produced in a small elemental volume of material at the critical point is the *triaxial state of stress*[1]; *any* triaxial state of stress may be fully specified relative to the chosen x-y-z coordinate system by specifying the three normal stress components σ_x, σ_y, σ_z, and the three shearing stress components τ_{xy}, τ_{yz}, and τ_{zx}.

Principal Stresses

It can be shown[2] that if the selected x-y-z coordinate axes, together with the elemental volume of material, are rotated in three-dimensional space, about the fixed origin, a *unique* new orientation may be found for which the shearing stress components vanish on all faces of the newly oriented elemental volume. This unique orientation, for which the shearing stress components on all faces of the elemental cube are zero, is called the *principal orientation*. For the principal orientation, the three mutually perpendicular planes of zero

[1]See Figure 4.1. [2]For example, see ref. 1, Ch. 4.

shear are called *principal planes*, and the normal stresses on these principal planes (planes of zero shear) are called *principal normal stresses*, or just *principal stresses*.

The importance of principal stresses lies in the fact that among them will be the *largest normal stress* that can occur on *any* plane passing through the point, for the given loading. The principal stresses are usually designated σ_1, σ_2, and σ_3. There are always *three* principal stresses, but some of them may be zero.

There is a *second* special orientation of coordinate axes that may be found, for which the shearing stresses on the faces of the rotated volume element reach *extreme values*. Of the three extreme values, one is a maximum, one is a minimum, and the third is a minimax value. This orientation is called the *principal shearing orientation*, and the shearing stresses on these three mutually perpendicular *principal shearing planes* are called *principal shearing stresses*. The principal shearing planes may have nonzero normal stresses acting on them, depending upon the type of loading, but *normal* stresses on *planes of principal shear* are *not* principal stresses.

The importance of principal shearing stresses lies in the fact that among them will be the largest or *maximum shearing stress* that can occur on any plane passing through the point, for the given loading. The principal shearing stresses are usually designated τ_1, τ_2, and τ_3.

Stress Cubic Equation

Depending upon whether its material behaves in a *brittle* or a *ductile* manner, failure at the governing critical point of a machine part is dependent upon the principle normal stresses, the principal shearing stresses, or some combination of these. In any event, it is important for a designer to be able to calculate principal normal stresses and principal shearing stresses for any combination of applied loads. To do this, the *general stress cubic equation*[3] may be employed to find the principal stresses σ_1, σ_2, and σ_3 as a function of the readily calculable components of stress σ_x, σ_y, σ_z, τ_{xy}, τ_{yz}, and τ_{zx} relative to any selected x-y-z coordinate system. The general stress cubic equation, developed from equilibrium concepts, is

$$\sigma^3 - \sigma^2(\sigma_x + \sigma_y + \sigma_z) + \sigma(\sigma_x\sigma_y + \sigma_y\sigma_z + \sigma_z\sigma_x - \tau_{xy}^2 - \tau_{yz}^2 - \tau_{zx}^2) - (\sigma_x\sigma_y\sigma_z + 2\tau_{xy}\tau_{yz}\tau_{zx} - \sigma_x\tau_{yz}^2 - \sigma_y\tau_{zx}^2 - \sigma_z\tau_{xy}^2) = 0 \quad (5\text{-}1)$$

Since all normal and shearing stress components are real numbers, all three roots of (5-1) are real; these three roots are the principal normal stresses σ_1, σ_2, and σ_3.

It is also possible to find the *directions* of principal stress vectors (and principal shearing stress vectors) if necessary.[4]

Furthermore, it can be shown that the magnitudes of the principal shearing stresses may be calculated from

$$|\tau_1| = \left|\frac{\sigma_2 - \sigma_3}{2}\right| \quad (5\text{-}2)$$

$$|\tau_2| = \left|\frac{\sigma_3 - \sigma_1}{2}\right| \quad (5\text{-}3)$$

$$|\tau_3| = \left|\frac{\sigma_1 - \sigma_2}{2}\right| \quad (5\text{-}4)$$

[3]For example, see ref. 1, p. 97. [4]See, for example, ref. 1,

To summarize, if loads and geometry are known for a machine part, a designer may identify the critical point, arbitrarily select a convenient x-y-z coordinate system, and calculate the resultant six stress components σ_x, σ_y, σ_z, τ_{xy}, τ_{yz}, and τ_{zx}. Equations (5-1) through (5-4) may then be solved to find the principal normal stresses and the principal shearing stresses. This procedure works for all cases; if the case is biaxial, one of the principal stresses will be zero, and if it is uniaxial, two principal stresses will be zero.

Example 5.1 Multiaxial States of Stress; Principal Stresses

A hollow cylindrical 4340 steel member has a 1.0-inch outside diameter, wall thickness of 0.25 inch, and length of 30.0 inches. As shown in Figure E5.1A, the member is simply supported at the ends, and symmetrically loaded at the one-third points by 1000-lb loads. The tubular bar is simultaneously subjected to an axial force of 5000-lb tension and a torsional moment of 3000 in-lb. For the critical point at midspan, determine (a) the principal stresses and (b) the principal shearing stresses.

Solution

a. Since the vertical transverse loads and end supports are symmetric, the vertical components (z-components) produce pure bending, with the maximum bending moment extending over the entire middle span. Therefore bending stress (tensile) will be maximum at the lower extreme fiber all along the center span between the 1000-lb transverse loads. The axial tensile force produces uniform axial (x-component) tensile stress throughout the wall. The torsional shearing stress produced by torque T will be maximum at the outer fibers throughout the tube. Based on these observations, the midspan critical point A is depicted in Figure E5.1B. The resultant state of stress at critical point A due to bending, tension, and torsional shear is shown in Figure E5.1C.

The stress components σ_x and τ_{xy} may be evaluated as follows:

$$\sigma_x = \frac{Mc}{I} + \frac{F_a}{A}$$

and

$$\tau_{xy} = \frac{Ta}{J}$$

From the dimensions of the tube

$$I = \frac{\pi(d_o^4 - d_i^4)}{64} = \frac{\pi(1.0^4 - 0.5^4)}{64} = 0.046 \text{ in}^4$$

and

$$J = 2I = 0.092 \text{ in}^4$$

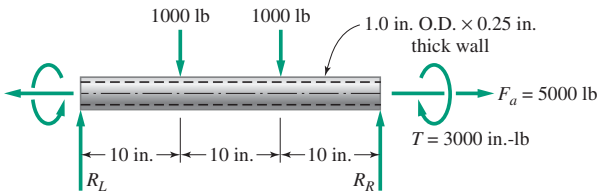

Figure E5.1A
Hollow bar loaded by forces and torques.

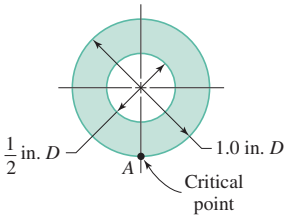

Figure E5.1B
Critical point location.

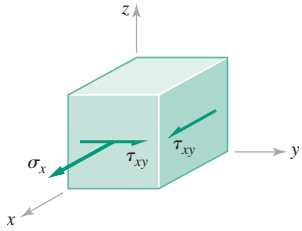

Figure E5.1C
State of stress at critical point A.

Example 5.1 Continues

Therefore

$$\sigma_x = \frac{[(1000)(10)]\left(\frac{1.0}{2}\right)}{0.046} + \frac{5000}{0.589} = 117{,}200 \text{ psi}$$

and

$$\tau_{xy} = \frac{(3000)\left(\frac{1.0}{2}\right)}{0.092} = 16{,}300 \text{ psi}$$

For the state of stress at critical point A depicted in Figure E5.1C, the stress cubic (5-1) reduces to

$$\sigma^3 - \sigma^2\sigma_x + \sigma(-\tau_{xy}^2) = 0$$

giving three roots

$$\sigma = \frac{\sigma_x}{2} \pm \sqrt{\left(\frac{\sigma_x}{2}\right)^2 + \tau_{xy}^2}$$

and

$$\sigma = 0$$

These may be rewritten as

$$\sigma_1 = \frac{\sigma_x}{2} + \sqrt{\left(\frac{\sigma_x}{2}\right)^2 + \tau_{xy}^2}$$

$$\sigma_2 = \frac{\sigma_x}{2} - \sqrt{\left(\frac{\sigma_x}{2}\right)^2 + \tau_{xy}^2}$$

$$\sigma_3 = 0$$

Substituting for σ_x and τ_{xy}, the principal stresses become

$$\sigma_1 = \frac{117{,}200}{2} + \sqrt{\left(\frac{117{,}200}{2}\right)^2 + (16{,}300)^2}$$

$$= 58{,}600 + 60{,}825 = 119{,}425 \text{ psi}$$

$$\sigma_2 = 58{,}600 - 60{,}825 = -2225 \text{ psi}$$

$$\sigma_3 = 0$$

b. From (5-2), (5-3), and (5-4) and using results from above the principal shearing stresses become

$$|\tau_1| = \left|\frac{-2225 - 0}{2}\right| = 1113 \text{ psi}$$

$$|\tau_2| = \left|\frac{0 - 119{,}425}{2}\right| = 59{,}713 \text{ psi}$$

$$|\tau_3| = \left|\frac{119{,}425 - (-2225)}{2}\right| = 60{,}825 \text{ psi}$$

Example 5.2 Principal Stress

It is desired to assemble a cast-iron hub to a steel shaft using an interference fit for retention. The system is subjected to a vertical load P and a torque T as shown in Figure E5.2 (a). At the critical location the stress field is given by the stresses shown in Figure E5.2 (b)

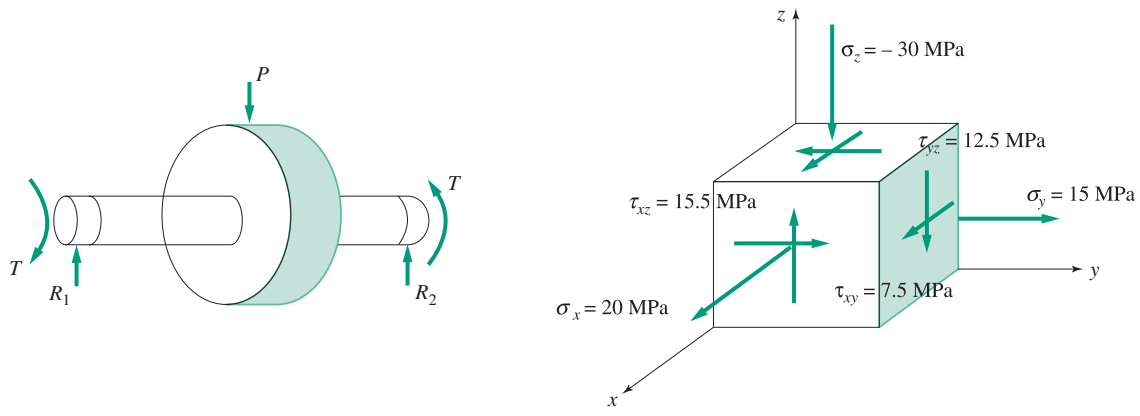

Figure E 5.2
Cast-iron hub fit to a steel shaft and associated state of stress at the critical location.

Solution

The stress cubic equation is given as

$$\sigma^3 - \sigma^2 I_1 + \sigma I_2 - I_3 = 0$$

where

$$I_1 = \sigma_x + \sigma_y + \sigma_z$$
$$I_2 = \sigma_x\sigma_y + \sigma_y\sigma_z + \sigma_x\sigma_z - \tau_{xy}^2 - \tau_{yz}^2 - \tau_{zx}^2$$
$$I_3 = \sigma_x\sigma_y\sigma_z + 2\tau_{xy}\tau_{yz}\tau_{zx} - \sigma_x\tau_{yz}^2 - \sigma_y\tau_{zx}^2 - \sigma_z\tau_{xy}^2$$

are the stress invariants. The above values can be written in matrix form as

$$\sigma = \begin{bmatrix} \sigma_x & \tau_{xy} & \tau_{xz} \\ \tau_{xy} & \sigma_y & \tau_{yz} \\ \tau_{xz} & \tau_{yz} & \sigma_z \end{bmatrix} = \begin{bmatrix} 20 & 7.5 & 15.5 \\ 7.5 & 15 & -12.5 \\ 15.5 & -12.5 & -30 \end{bmatrix} \text{MPa}$$

Using any number of programs, such as Maple, Matlab, etc., the above can be solved for the roots of the polynomial equation or the matrix equation can be solved for the eigenvalues, which are the principal stresses of the system. These are given as

$$\sigma_1 = 26.22 \text{ MPa}, \qquad \sigma_2 = 16.94 \text{ MPa}, \qquad \sigma_3 = -38.16 \text{ MPa},$$

Mohr's Circle Analogy for Stress

For biaxial states of stress the stress cubic equation (5-1) degenerates to the form

$$\sigma^3 - \sigma^2(\sigma_x + \sigma_y) + \sigma(\sigma_x \sigma_y - \tau_{xy}^2) = 0 \tag{5-5}$$

if stress components lie only in the xy plane. If stress components lie only in the yz plane or the zx plane, the stress cubic yields the same formal expression with solely yz subscripts or solely zx subscripts, respectively. The principal stress solutions for (5-5) are (see Example 5.1)

$$\sigma_1 = \frac{\sigma_x + \sigma_y}{2} + \sqrt{\left(\frac{\sigma_x - \sigma_y}{2}\right)^2 + \tau_{xy}^2} \tag{5-6}$$

$$\sigma_2 = \frac{\sigma_x + \sigma_y}{2} - \sqrt{\left(\frac{\sigma_x - \sigma_y}{2}\right)^2 + \tau_{xy}^2} \tag{5-7}$$

$$\sigma_3 = 0 \tag{5-8}$$

Examination of (5-6) and (5-7) suggests that these equations are formally the same as the equation of a circle plotted on the $\sigma-\tau$ plane, since the equation of such a circle on an xy plane has the form

$$(x - h)^2 + (y - k)^2 = R^2 \tag{5-9}$$

where h and k are the x-y coordinates of the center of the circle, and R is the radius. An *analogy* (refer to the discussion of the "membrane analogy" in 4.4) was developed by *Mohr*[5] in 1882 in which he successfully postulated that a circle plotted on the $\sigma-\tau$ plane could be used to represent *any* biaxial state of stress because the governing equations are formally the same for a circle as for a biaxial state of stress. Such plots have come to be known as *Mohr's circles* for stress. For example, a biaxial state of stress in the xy plane (see principal stress solutions in (5-6), (5-7), and (5-8)) may be represented by a circle[6] with center on the σ-axis of a $\sigma-\tau$ plot if in (5-9) x and y are replaced by σ and τ respectively, and

$$h = \frac{\sigma_x + \sigma_y}{2} \tag{5-10}$$

$$k = 0 \tag{5-11}$$

$$R = \sqrt{\left(\frac{\sigma_x - \sigma_y}{2}\right)^2 + \tau_{xy}^2} \tag{5-12}$$

Figure 5.1 shows such a plot. To successfuly utilize Mohr's circle as a stress analysis tool the following sign conventions should be adopted:

1. Normal stresses should be plotted as positive if tensile, and negative if compressive.
2. Shearing stresses should be plotted as positive if they produce a clockwise (CW) couple, and negative if they produce a counterclockwise (CCW) couple. (This convention is used *only* for Mohr's circle applications.)

The plotting procedure, illustrated in Figure 5.1, is to plot point A (tensile σ_y and CW τ_{xy} couple), then point B (tensile σ_x and CCW τ_{xy} couple), then pass a circle through A and B. The location of center C and magnitude of radius R may be established geometrically

[5]See ref. 1. [6]For example, see ref. 1, or ref. 8, Ch. 10.

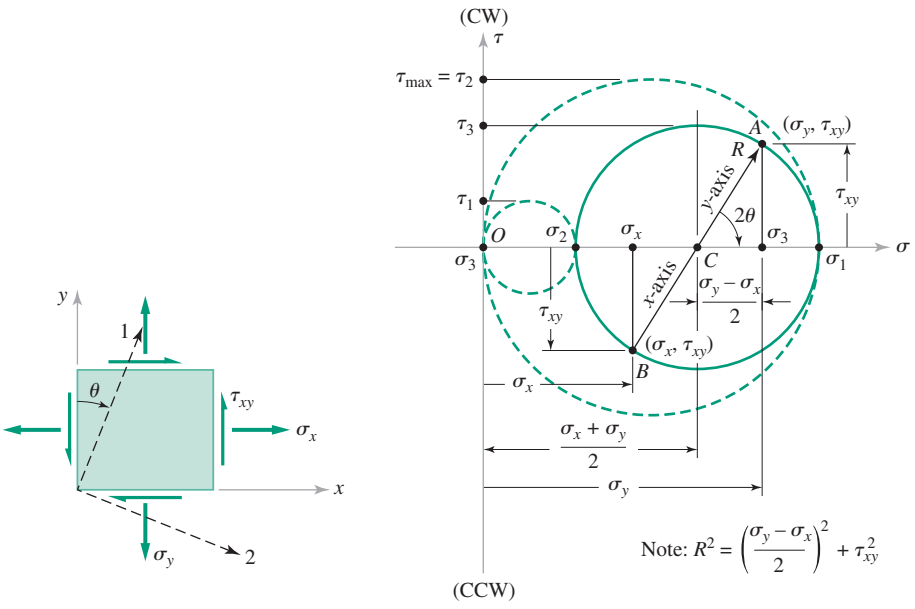

(*a*) Biaxial element at critical point.

(*b*) Mohr's circle for *xy* biaxial state of stress shown in (a); note that $\sigma_3 = 0$ for this biaxial case.

Figure 5.1
Mohr's circle for a biaxial state of stress in the *x-y* plane.

as shown, and principal stresses σ_1 and σ_2 pinpointed where the circle intersects the σ-axis (shear is 0 on the σ-axis). The principal shearing stress τ_3 may also be found as shown (see (5-4)). The third principal stress, $\sigma_3 = 0$, should not be ignored; plot σ_3 at the origin of the $\sigma-\tau$ plane and then construct two additional Mohr's circles, one through $\sigma_2 - \sigma_3$ and another through $\sigma_1 - \sigma_3$. From these circles τ_1 and τ_2 may be found as shown. If the maximum shearing stress for this state of stress is needed for failure prevention calculations, it will be the largest of τ_1, τ_2, and τ_3; for the case illustrated in Figure 5.1 this is $\tau_{max} = \tau_2$. Note specifically that τ_{max} is *not* τ_3, which is based on the initially plotted *solid* circle. If $\sigma_3 = 0$ had not been plotted, the *dashed* circles would have been missed, and, therefore, the true maximum shearing stress would have been missed.

It is also possible to find the orientation of the principal axes from the Mohr's circle construction, using the expression

$$2\theta = \tan^{-1} \frac{2\tau_{xy}}{\sigma_y - \sigma_x} \tag{5-13}$$

where the double angle 2θ is shown in Figure 5.1(b), measured *from* the ray *CA to* the principal stress ray σ_1. This corresponds to the rotation angle θ in Figure 5.1(a) measured in the same direction as 2θ, *from* the *y*-axis *to* the principal axis 1. A consequence of this procedure is that principal axis 2 will be perpendicular to axis 1 in the *x-y* plane, and principal axis 3 will be mutually perpendicular to axes 1 and 2.

Example 5.3 Mohr's Circle for Stress; Principal Stresses

Using the Mohr's circle analogy, solve the problem posed in Example 5.1 to find

a. The principal stresses

b. The principal shearing stresses

Example 5.3 Continues

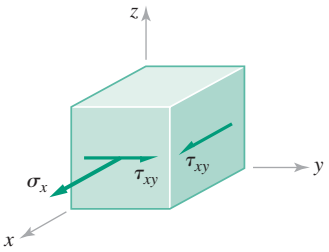

Figure E5.3A
State of stress at critical point *A*.

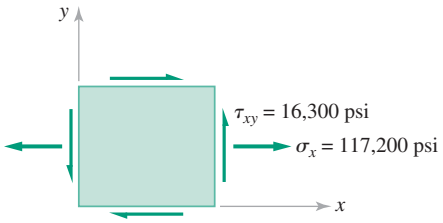

Figure E5.3B
Biaxial *xy* element from Figure E5.3A.

Figure E5.3C
Mohr's circle constructed for biaxial element shown in Figure E5.3B.

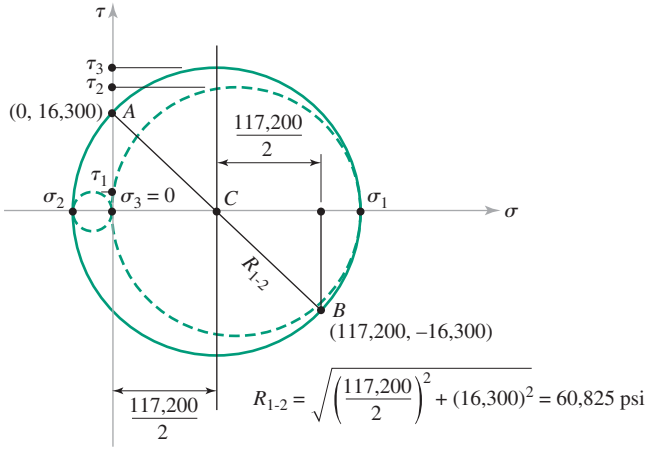

Solution

Reviewing the analysis of Example 5.1, the state of stress at the critical point *A* is shown in Figure E5.3A, repeated from Figure E5.3C.

Also, the magnitudes of σ_x, σ_y, and τ_{xy} were determined in Example 5.1 to be

$$\sigma_x = 117,200 \text{ psi}$$
$$\sigma_y = 0$$
$$\tau_{xy} = 16,300 \text{ psi}$$

a. Using the Mohr's circle analogy to find principal stresses, the *xy* plane of Figure E5.3A may be redrawn as shown in Figure E5.3B. Mohr's circle may next be constructed as shown in Figure E5.3C by plotting points *A* and *B* as shown, passing a circle through them and finding principal stresses σ_1 and σ_2 semigraphically. The third principal stress, $\sigma_3 = 0$, is plotted at the origin.

From Figure E5.3C, the following values may be found graphically

$$\sigma_1 = \overline{C} + \overline{R} = \frac{117,200}{2} + 60,825 = 119,425 \text{ psi}$$
$$\sigma_2 = \overline{C} - \overline{R} = \frac{117,200}{2} - 60,825 = -2225 \text{ psi}$$

and for this *biaxial* state of stress

$$\sigma_3 = 0$$

These values are the same as those found in Example 5.1 by solving the stress cubic equation.

b. To find the principal shearing stresses, the remaining two (dashed) Mohr's circles are constructed, and the principal shearing stresses are found to be, from the radii of the three circles,

$$|\tau_1| = R_{2-3} = \frac{2225}{2} = 1113 \text{ psi}$$
$$|\tau_2| = R_{1-3} = \frac{119{,}425}{2} = 59{,}713 \text{ psi}$$
$$|\tau_3| = R_{1-2} = 60{,}825 \text{ psi}$$

These values are the same as those shown in Example 5.1. From these values it may be noted that

$$\tau_{max} = \tau_3 = 60{,}825 \text{ psi}$$

Strain Cubic Equation and Principal Strains

Just as stress is an important measure of loading severity, strain may also be an important parameter in assessing failure potential in a machine part. *Strain* is the term used to define the intensity and direction of the deformation at a given critical point, with respect to a specified plane or set of planes passing through the critical point. Analogous to state of stress, the state of strain at a point may be fully defined by six components of strain relative to any selected x-y-z coordinate system: three normal strain components and three shearing strain components. The normal strain components are usually designated ε_x, ε_y, and ε_z, and the shearing strain components γ_{xy}, γ_{yz}, and γ_{zx}. Just as the state of stress may be completely defined in terms of three principal stresses and their directions, the state of strain may be completely defined in terms of three principal strains and their directions. The principal strains may be determined from a general strain cubic equation analogous to the general stress cubic equation (5-1). The strain cubic equation is

$$\varepsilon^3 - \varepsilon^2[\varepsilon_x + \varepsilon_y + \varepsilon_z] + \varepsilon\left[\varepsilon_x\varepsilon_y + \varepsilon_y\varepsilon_z + \varepsilon_z\varepsilon_x - \frac{1}{4}(\gamma_{xy}^2 + \gamma_{yz}^2 + \gamma_{zx}^2)\right] - \left[\varepsilon_x\varepsilon_y\varepsilon_z + \frac{1}{4}(\gamma_{xy}\gamma_{yz}\gamma_{zx} - \varepsilon_x\gamma_{yz}^2 - \varepsilon_y\gamma_{zx}^2 - \varepsilon_z\gamma_{xy}^2)\right] = 0 \tag{5-14}$$

This equation is formally the same as the stress cubic equation (5-1) except that the normal strains, and the shearing strains divided by two, replace the normal stresses and shearing stresses. The three solutions of (5-14) are the three principal normal strains ε_1, ε_2, and ε_3.

Mohr's Circle Analogy for Strain

In some circumstances, a designer may be interested in finding stresses or strains at particular points in an existing machine part. Such an interest may stem from the need to improve failure resistance, to verify a calculation procedure, or some other requirement. In

these cases it is common to *bond* a strain gage or a strain rosette to the surface at one or more critical points.[7] Using the strain gage data to evaluate biaxial solutions of the strain cubic equation (5-14), the principal strains and their directions may be found. Use of a Mohr's strain circle to determine the principal strains is common.

Mohr's strain circles may be constructed using the techniques just described for Mohr's stress circles, except that normal and shearing strains are plotted on the cartesian axes ε and $\gamma/2$ rather than σ and τ. To utilize the resulting Mohr's strain circle solutions for principal strains, with the objective of estimating stresses at the critical point, relationships between stress and strain must be known.

Elastic Stress-Strain Relationships (Hooke's Law)

For a broad class of engineering materials it has been experimentally well established that a linear relationship exists between stress and strain so long as the material is not loaded beyond its elastic range. These linear elastic relationships were first presented in the seventeenth century by Robert Hooke, and have come to be known as the *Hooke's Law relationships*. They are

$$\varepsilon_x = \frac{1}{E}[\sigma_x - \nu(\sigma_y + \sigma_z)] \tag{5-15}$$

$$\varepsilon_y = \frac{1}{E}[\sigma_y - \nu(\sigma_z + \sigma_x)] \tag{5-16}$$

$$\varepsilon_z = \frac{1}{E}[\sigma_z - \nu(\sigma_x + \sigma_y)] \tag{5-17}$$

and

$$\gamma_{xy} = \frac{\tau_{xy}}{G} \tag{5-18}$$

$$\gamma_{yz} = \frac{\tau_{yz}}{G} \tag{5-19}$$

$$\gamma_{zx} = \frac{\tau_{zx}}{G} \tag{5-20}$$

where the elastic constants are

E = Young's modulus of elasticity
ν = Poisson's ratio
G = shear modulus of elasticity

Numerical values of these elastic constants are given in Table 3.9 for several engineering materials.

[7]A strain gage is a device designed to measure the displacement between two points some known distance apart. They may be mechanical, optical, electroresistive, piezoresistive, capacitive, inductive, or acoustical in nature. The electrical-resistance strain gage is often employed on the free surface of a machine part or specimen to find stresses there. It is usual to use an arrangement of three gages to measure three strains at known angles to each other, from which principal surface strains and directions may be found. These three-gage arrays are called *rosettes*. To convert strains to stresses, Young's modulus of elasticity and Poisson's ratio must also be known.

It should be noted that the Hooke's Law relationships are valid for any arbitrarily selected *x-y-z* cartesian coordinate system orientation, including the principal *1-2-3* orientation. The Hooke's Law relationships may also be inverted to give

$$\sigma_x = \frac{E}{(1 - \nu - 2\nu^2)}[(1 - \nu)\varepsilon_x + \nu(\varepsilon_y + \varepsilon_z)] \tag{5-21}$$

$$\sigma_y = \frac{E}{(1 - \nu - 2\nu^2)}[(1 - \nu)\varepsilon_y + \nu(\varepsilon_z + \varepsilon_x)] \tag{5-22}$$

$$\sigma_z = \frac{E}{(1 - \nu - 2\nu^2)}[(1 - \nu)\varepsilon_z + \nu(\varepsilon_x + \varepsilon_y)] \tag{5-23}$$

5.3 Stress Concentration

Failures in machines and structures virtually always initiate at sites of *local stress concentration* caused by geometrical or microstructural discontinuities. These stress concentrations, or *stress raisers*, often lead to local stresses many times higher than the nominal net section stress that would be calculated without considering stress concentration effects. An intuitive appreciation of the stress concentration associated with a geometrical discontinuity may be developed by thinking in terms of *force flow* through a member as it is subjected to external loads (see 4.3). The sketches of Figure 5.2 illustrate the concept. In Figure 5.2(a) the rectangular flat plate of width w and thickness t is fixed at its lower edge and subjected to a total vertical force F uniformly distributed along the upper edge. The dashed lines each represent a fixed quantum of force, and the local spacing between lines is therefore an indication of the local force intensity, or stress. In Figure 5.2(a) the lines are uniformly spaced throughout the plate, and the stress σ is uniform and calculable as

$$\sigma = \frac{F}{wt} \tag{5-24}$$

In the sketch of Figure 5.2(b) a flat rectangular plate of the same thickness is subjected to the same total force F, but the plate has been made wider and notched back to provide the same *net* section width w at the site of the notch. The lines of force flow may be visualized in very much the same way that streamlines would be visualized in the steady flow of a fluid through an obstructed channel with the same cross-sectional shape as the plate cross section. It may be noted in Figure 5.2(b) that no force can be supported across the notch, and therefore the lines of force flow must pass around the root of the notch, just as a flowing fluid must pass around the obstruction. In so doing, force-flow lines crowd

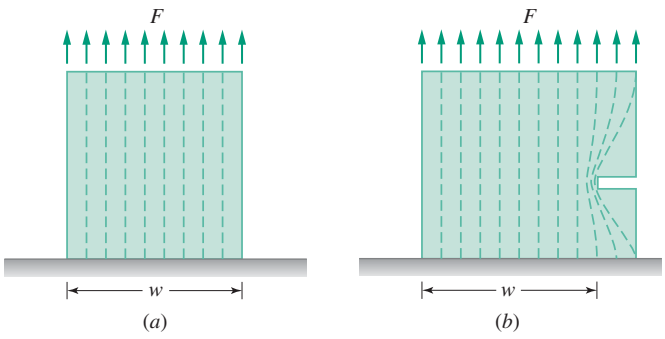

Figure 5.2
Intuitive concept of stress concentration. (a) Without stress concentration. (b) With stress concentration.

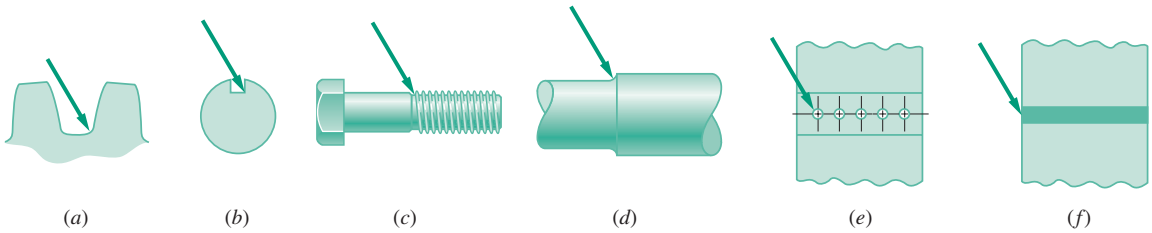

Figure 5.3
Some common examples of stress concentration. (a) Gear teeth. (b) Shaft keyway. (c) Bolt threads. (d) Shaft shoulder. (e) Riveted or bolted joint. (f) Welded joint.

together locally near the root of the notch, producing a higher force intensity, or stress, at the notch root. Even though the net section *nominal stress* is still properly calculated by (5-24), the *actual local stress* at the root of the notch may be many times higher than the calculated nominal stress.

Some common examples of stress concentration are illustrated in Figure 5.3. Discontinuities at the roots of gear teeth, at the corners of keyways in shafting, at the roots of screw threads, at the fillets of shaft shoulders, around rivet holes and bolt holes, and in the neighborhood of welded joints all constitute stress raisers that usually must be considered by a designer. The seriousness of the stress concentration depends on the type of loading, the type of material, and the size and shape of the discontinuity.

Stress Concentration Effects

For the purposes of studying stress concentration effects, stress raisers may be classified as being either *highly local* or *widely distributed*. Highly local stress raisers are those for which the volume of material containing the concentration of stress is a *negligibly small portion* of the overall volume of the stressed member. Widely distributed stress raisers are those for which the volume of material containing the concentration of stress is a *significant portion* of the overall volume of the stressed member. For the case of a highly local stress concentration, the overall size and shape of the stressed part would not be significantly changed by yielding in the region of the stress concentration. For a widely distributed stress concentration, the overall size and shape of the stressed part would be subject to significant changes by virtue of yielding in the region of stress concentration. Small holes and fillets would usually be regarded as highly local stress concentrations; curved beams, curved hooks, and eye-and-clevis joints would usually be categorized as cases of widely distributed stress concentration.

With the foregoing definitions made, stress concentration effects may be classified as shown in Table 5.1. From the table it may be noted that the effects of stress concentration

TABLE 5.1 Effects of Stress Concentration

Type of Stress Concentration	Type of Loading	Type of Material	Type of Failure	Stress Concentration Factor
Widely distributed	Static	Ductile	Widely distributed yielding	K_t (modified)
Widely distributed	Static	Brittle	Brittle fracture	K_t
Widely distributed	Cyclic	Any	Fatigue failure	K_f
Highly local	Static	Ductile	No failure (redistribution occurs)	$K_t \rightarrow 1$
Highly local	Static	Brittle	Brittle fracture	K_t
Highly local	Cyclic	Any	Fatigue failure	K_f

must be considered for all combinations of geometry, loading, and material with the possible exception of one, namely, the case of a *highly local* stress concentration in a *ductile* material subjected to *static* loading. In this case the local yielding is usually negligible and a stress concentration factor of unity may often be used. All other cases must be analyzed for potential failure because of the effects of stress concentration. The final column in Table 5.1 lists K_t or K_f as stress concentration factors. The factor K_t is the theoretical elastic stress concentration factor, which is defined to be the ratio of the actual maximum local stress in the region of the discontinuity to the nominal net section stress calculated by simple theory as if the discontinuity exerted no stress concentration effect; that is,

$$K_t = \frac{\text{actual maximum stress}}{\text{nominal stress}} = \frac{\sigma_{act}}{\sigma_{nom}} \tag{5.25}$$

It should be noted that the value of K_t is valid only for stress levels within the *elastic* range, and it must be suitably modified if stresses are in the plastic range.

The factor K_f is the fatigue stress concentration factor, which is defined to be the ratio of the effective fatigue stress that actually exists at the root of the discontinuity to the nominal fatigue stress calculated as if the notch has no stress concentration effect. K_f may also be defined as the ratio of the fatigue strength of an *unnotched* member to the fatigue strength of the same member *with a notch*. Thus, the fatigue stress concentration factor may be defined as

$$K_f = \frac{\text{effective fatigue stress}}{\text{nominal fatigue stress}} = \frac{S_N\,(\text{unnotched})}{S_N\,(\text{notched})} \tag{5-26}$$

Stress concentration factors are determined in a variety of different ways, including direct measurement of strain, utilization of photoelastic techniques, application of the principles of the theory of elasticity, and finite element analysis. Numerical values for a wide variety of geometries and types of loading are presented in reference 9. A few of the more common cases drawn from the literature are reproduced in Figures 5.4 through 5.12. Data for the important case of screw threads are sparse, but reference 9 reports a range of values for K_t from about 2.7 to 6.7 at the thread root of standard threads. Most (but not all) threaded fastener failures tend to occur in the thread at the nut face.

Multiple Notches

Sometimes it will be found that one stress raiser is superimposed upon another, such as a notch within a notch or a notch in a fillet. Although accurate calculation of the overall stress concentration factor is difficult for such combinations, reasonable estimates can be made.[8] Figure 5.13(a) illustrates a large notch with a smaller notch at its root. To estimate the combined influence of these notches, the stress concentration factor K_{t1} for the large notch is determined as if the small notch does not exist. This permits an estimate of the stress σ'_n at the root of the large notch by multiplying the nominal stress σ_n by K_{t1} to give

$$\sigma'_n = K_{t1}\sigma_n \tag{5-27}$$

Now, assuming that the stress σ'_n occurs throughout the zone within the dashed line near the notch root of Figure 5.13(a), σ'_n becomes the *nominal* stress as far as the *small* notch is concerned (because the entire small notch lies within the σ'_n field). Next, determining

[8]See ref. 6.

Figure 5.4
Stress concentration factors for a shaft with a fillet subjected to (a) bending, (b) axial load, or (c) torsion. (From ref. 2; adapted with permission of John Wiley & Sons, Inc.)

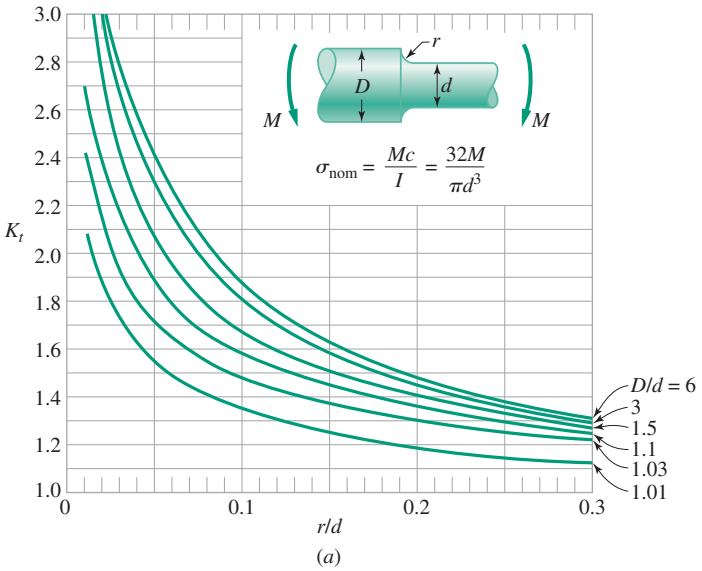

(a)

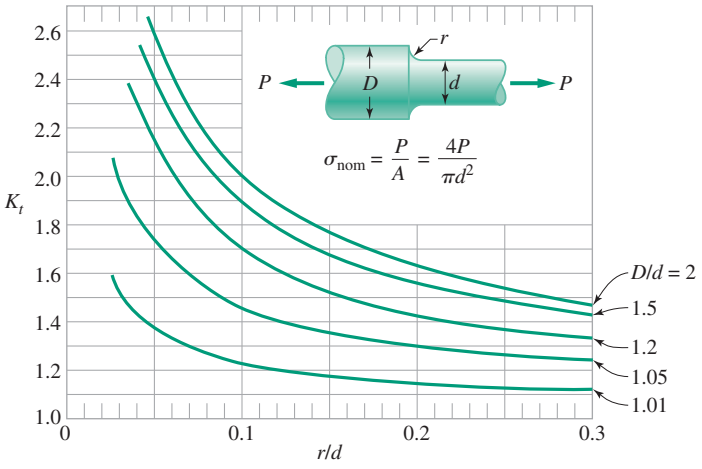

(b)

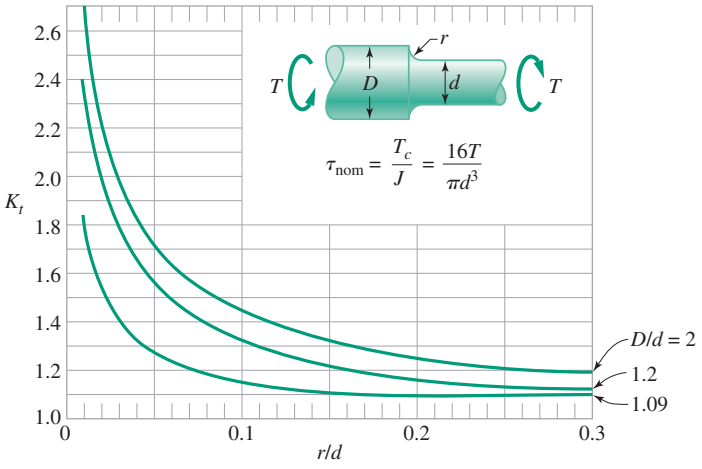

(c)

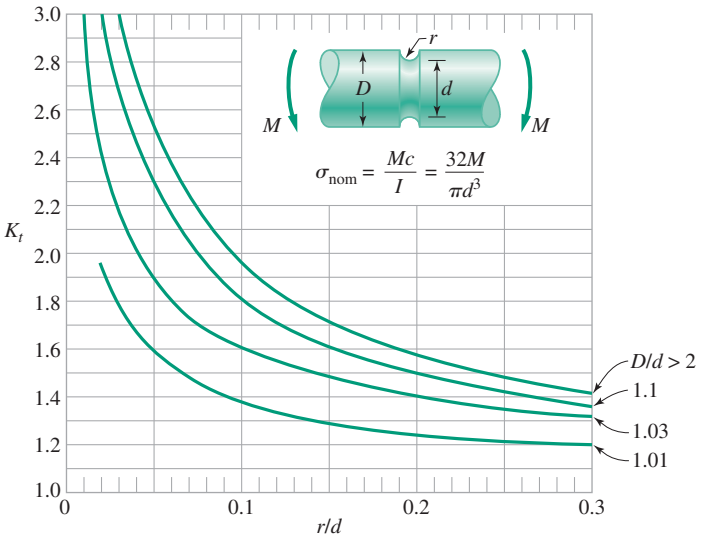

(a)

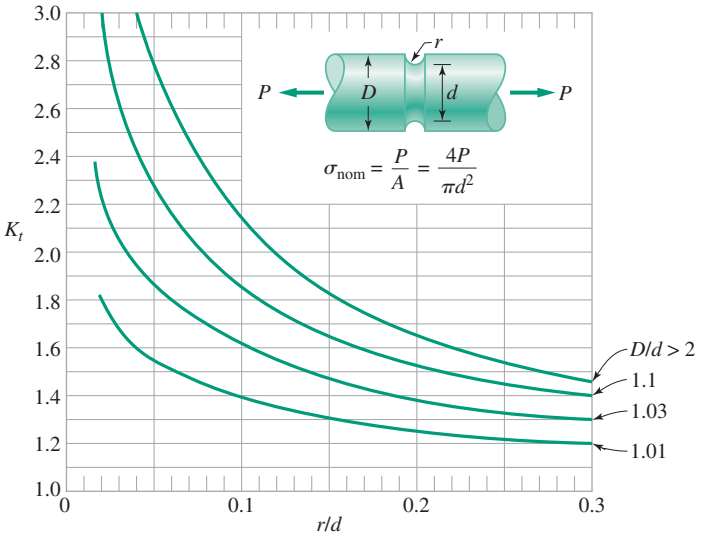

(b)

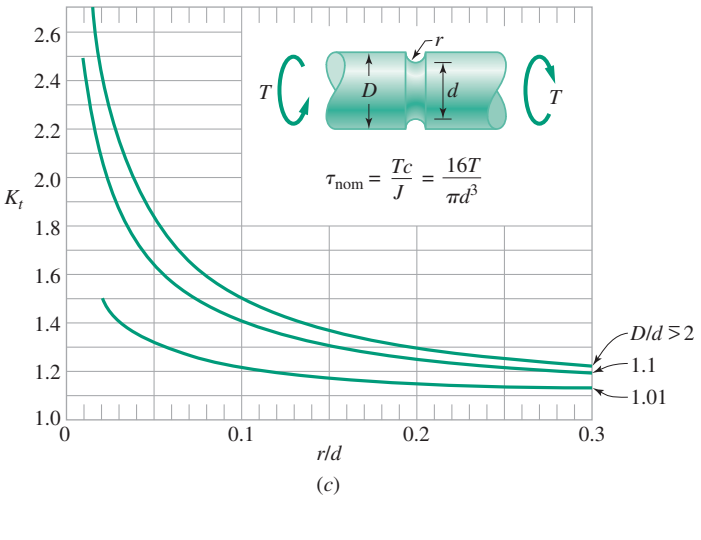

(c)

Figure 5.5
Stress concentration factors for a shaft with a groove subjected to (a) bending, (b) axial load, or (c) torsion. (From ref. 2; adapted with permission from John Wiley & Sons, Inc.)

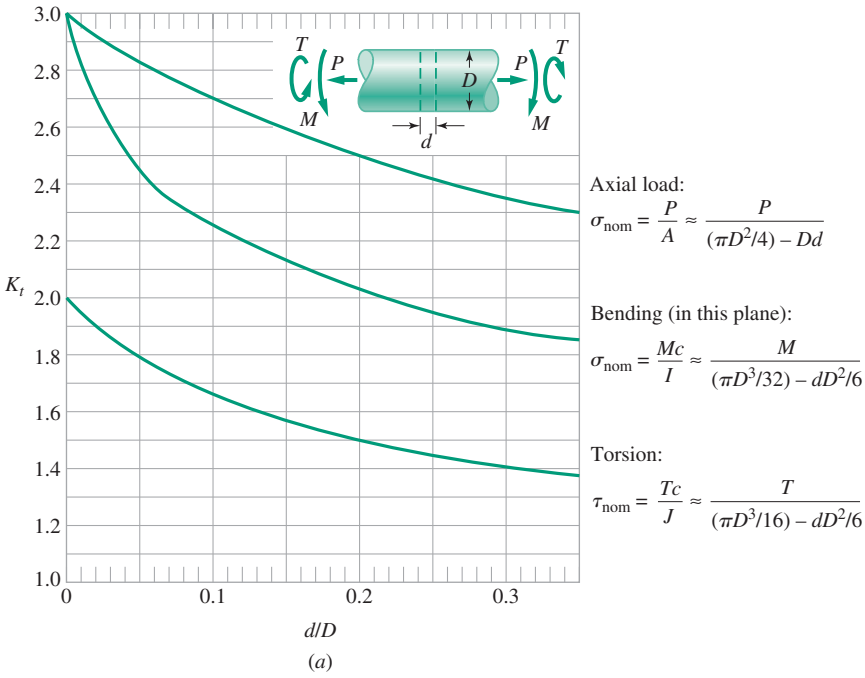

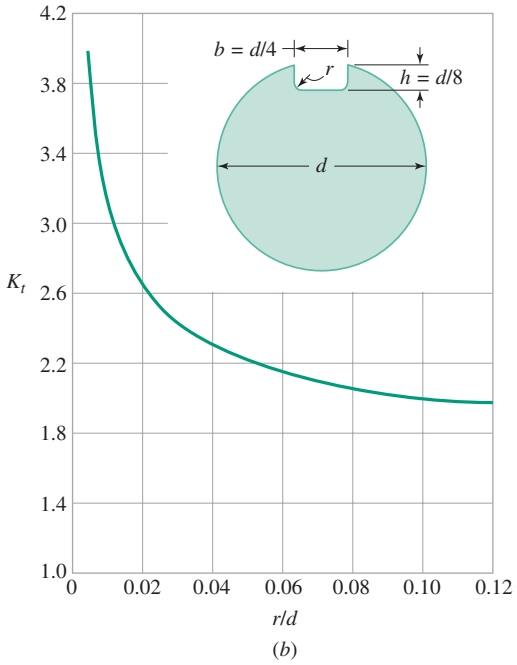

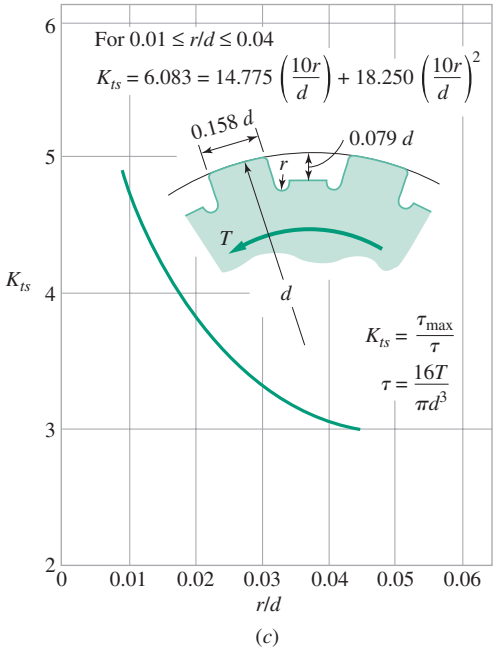

Figure 5.6

Stress concentration factors for (a) a shaft with a radial hole subjected to axial load, bending, or torsion (from ref. 3 with permission of the McGraw-Hill Companies), (b) a shaft with a straight parallel keyway subjected to torsion (from ref. 4, with permission of the McGraw-Hill Companies), and (c) a shaft with an eight-tooth spline subjected to torsion (from ref. 2, with permission from John Wiley & Sons, Inc.).

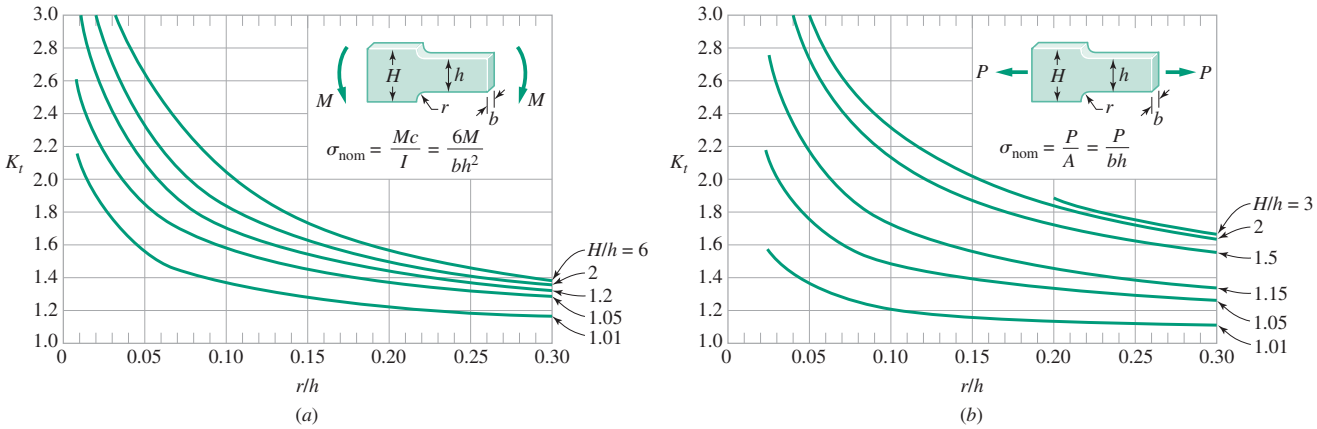

Figure 5.7
Stress concentration factors for a flat bar with a shoulder fillet subjected to (a) bending or (b) axial load. (From ref. 2; adapted with permission from John Wiley & Sons, Inc.)

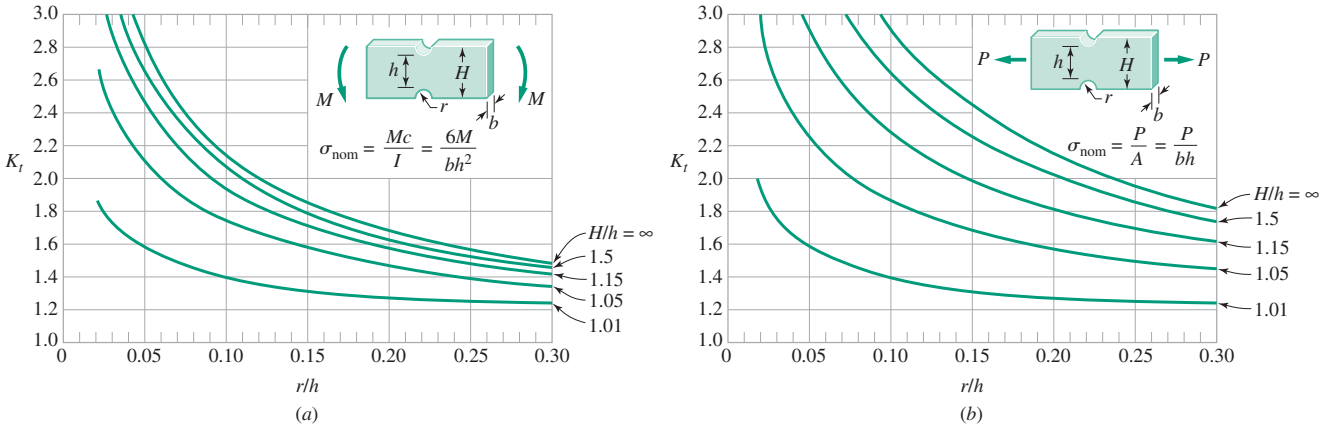

Figure 5.8
Stress concentration factors for a flat bar with a notch subjected to (a) bending or (b) axial load. (From ref. 2; adapted with permission from John Wiley & Sons, Inc.)

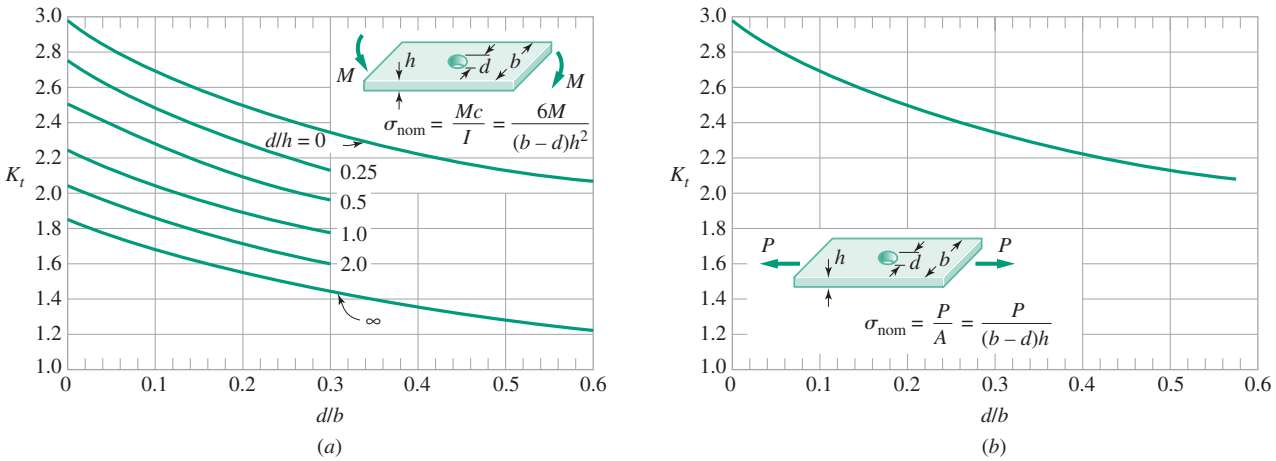

Figure 5.9
Stress concentration factors for a flat plate with a central hole subjected to (a) bending or (b) axial load. (From ref. 2; adapted with permission from John Wiley & Sons, Inc.)

Figure 5.10
Theoretical stress concentration factor K_t for a tension-side gear tooth fillet. Pressure angle is $\varphi = 20^o$. (From ref. 2; adapted with permission from John Wiley & Sons, Inc.)

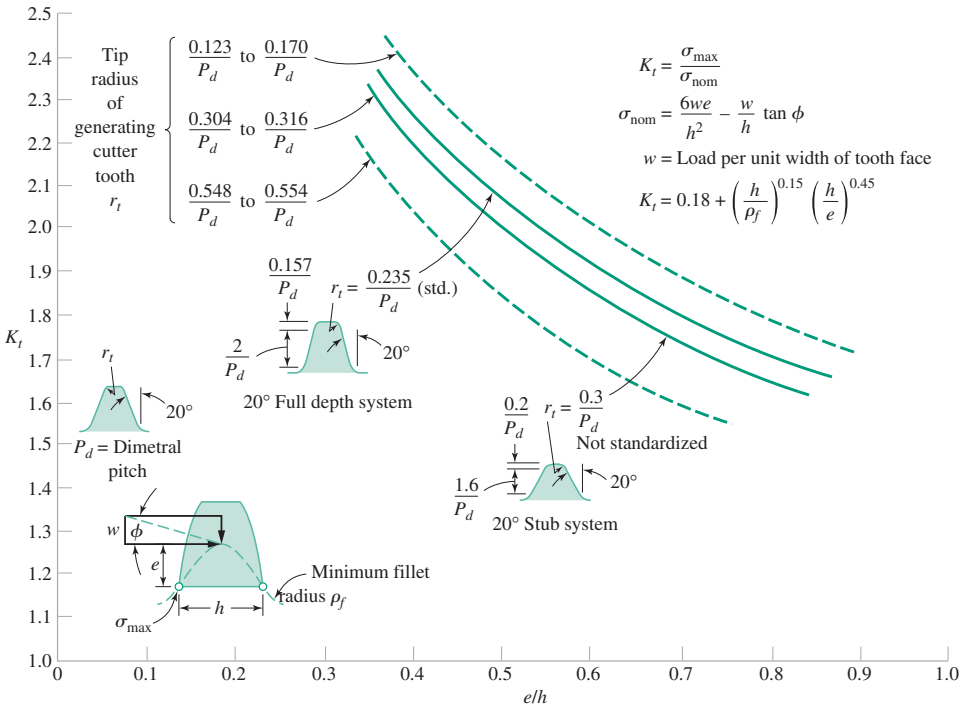

Figure 5.11
Stress concentration factors K_t for a crankshaft in bending. *Note:* When the inside of the crankpin and the outside of the journal are in line, $s = 0$ When the crankpin is closer, s is positive (as shown). When the crankpin's inner surface is farther away than $d/2$, S is negative. (From ref. 2; adapted with permission from John Wiley & Sons, Inc.)

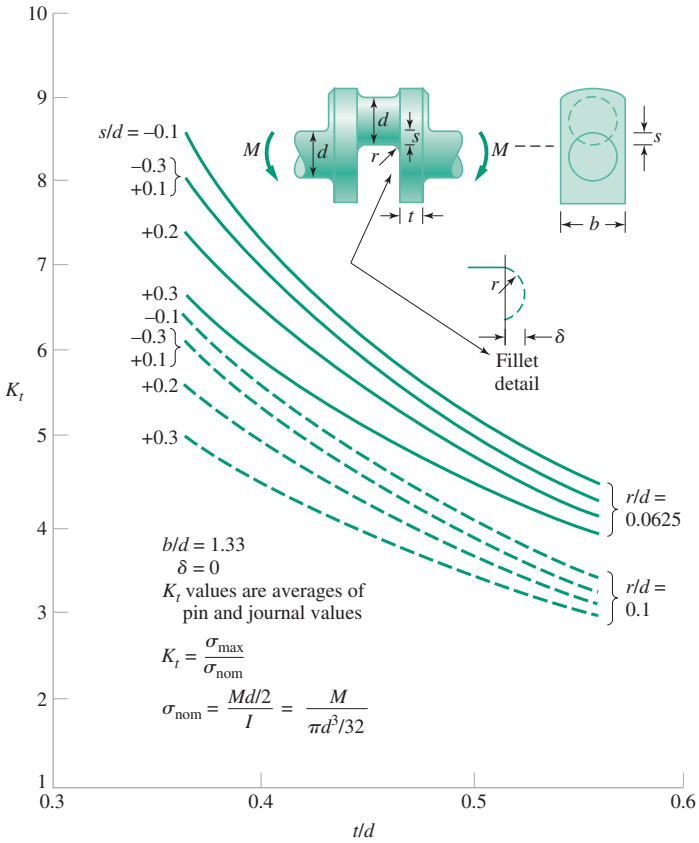

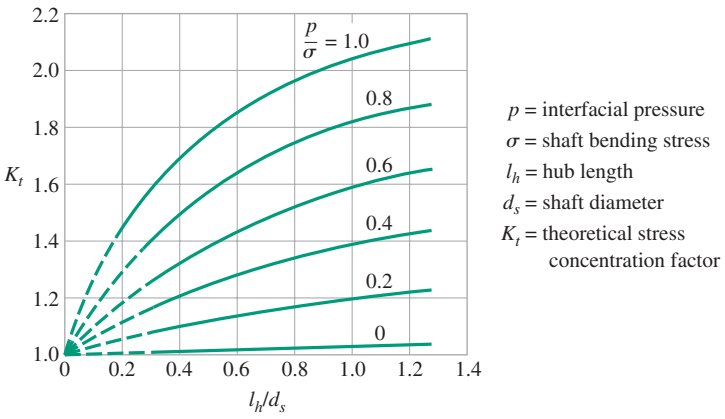

Figure 5.12
End-of-hub stress concentration factors for press fit assemblies subjected to bending moments. (From ref. 5; reprinted by permission of Pearson Education, Inc., Upper Saddle River, NJ.)

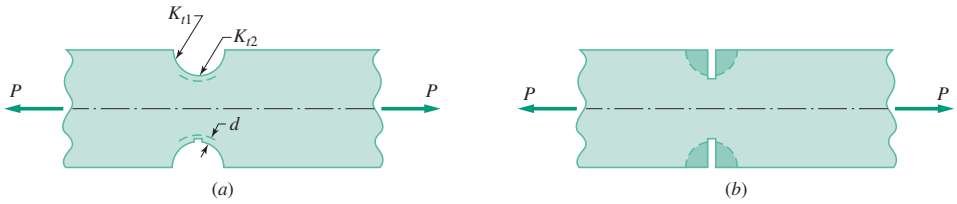

Figure 5.13
Stress concentration effects due to superimposed multiple notches. (After ref. 6; adapted with permission of The McGraw-Hill Companies.)

the stress concentration factor K_{t2} for the small notch acting alone, it may be multiplied times σ'_n to obtain the actual stress at the small notch root, or

$$\sigma_{actual} = K_{t2}\sigma'_n \tag{5-28}$$

Next, utilizing (5-27),

$$\sigma_{actual} = K_{t1}K_{t2}\sigma_n \tag{5-29}$$

Thus, the combined theoretical stress concentration factor K_{tc} for the multiple notch is the *product* of the stress concentration factors for the two notches considered individually, giving

$$K_{tc} = K_{t1}K_{t2} \tag{5-30}$$

This has been verified photoelastically.[9] The combined fatigue stress concentration factor K_{tc}, as for any other stress concentration factor, depends[10] on q and can be calculated from (5-92) by substituting K_{tc} for K_t in that equation. One technique for estimating a conservative value for K_{tc} is sketched in Figure 5.13(b). The technique assumes the notch of 5.13(a) to be filled in as shown by the crosshatched area. This leaves a single, deep, narrow notch, for which the theoretical stress concentration factor will always be *greater* than the stress concentration factor for the multiple notch.

Example 5.4 Stress Concentration of Flat Bar

Two flat bars with different configurations are shown in Figure E5.4 (a) and (b). Each carries a steady load of 4 kN. The material is gray cast iron ASTM A-48 (class 40). Determine the maximum stress induced for each of the conditions shown.

[9]Ibid. [10]See (5-91).

Example 5.4 Continues

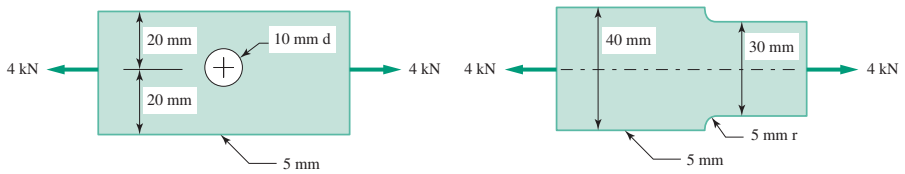

Figure E5.4
Flat bars supporting an axial load of 4 kN.

Solution

(a) The actual stress at the critical location adjacent to the hole is

$$\sigma_{act} = K_t \sigma_{nom}$$

The nominal stress is calculated as

$$\sigma_{nom} = \frac{P}{A_{net}} = \frac{4000}{0.005(0.040 - 0.010)} = 26.7 \text{ MPa}$$

From Figure 4.22(b) with $d/b = 10/40 = ¼$

$$K_t = 2.37$$

Hence, the actual stress becomes

$$\sigma_{act} = 2.37(26.7) = 63.3 \text{ MPa}$$

(b) The nominal stress is

$$\sigma_{nom} = \frac{P}{A_{net}} = \frac{4000}{0.005(0.03)} = 26.7 \text{ MPa}$$

From Figure 4.20(b) with r/h = 5/30 = 0.1667, and H/h = 40/30 = 1.333

$$K_t = 1.7$$

Hence, the actual stress becomes

$$\sigma_{act} = 1.7(26.7) = 45.4 \text{ MPa}$$

5.4 Combined Stress Theories of Failure

Predicting failure, or establishing a combination of material and geometry that will avert failure, is a relatively simple matter if the machine part is subjected to a *static uniaxial* state of stress. It is necessary only to have available the simple uniaxial stress-strain curve for the material of interest, which can be readily obtained from one or a few simple tension and compression experiments. For example, if yielding has been established as the governing failure mode for a *uniaxially* stressed machine part, failure of the part would be predicted when its maximum normal stress equals or exceeds the *uniaxial* yield strength of the material.

If a machine part is subjected to a *multiaxial* state of stress, the accurate prediction of failure becomes far more difficult. No longer can one accurately predict yielding, for example, when the maximum normal stress exceeds the *uniaxial* yield strength because the other two principal normal stress components at the critical point may also influence yielding behavior. Further, *multiaxial* yield strengths are generally unavailable because of the time and expense required to determine them experimentally. Therefore, when one desires to predict failure, or to pick a combination of material and geometry to avert failure, when the machine part is subjected to a multiaxial state of stress, it is usual to utilize an experimentaly validated theory that relates failure in the multiaxial state of stress to failure by the same mode in a simple uniaxial stress test. All such failure prediction theories are based on well-chosen *loading severity parameters* such as stress, strain, or strain energy density. Loading severity parameters must be *readily calculable* in the multiaxial state of stress and *readily measurable* in a simple uniaxial stress test. These theories, called *combined stress theories of failure*, all share a common postulate, namely, that *failure is predicted to occur when the maximum value of the selected loading severity parameter in the multiaxial state of stress becomes equal to or exceeds the value of the same loading severity parameter that produces failure in a simple uniaxial stress test using a specimen of the same material.*

Many combined stress failure theories have been proposed, but three have found wide acceptance because of their relatively good agreement with experimental results and reasonable simplicity in application. They are

1. Maximum normal stress theory
2. Maximum shearing stress theory
3. Distortion energy theory

Maximum Normal Stress Theory (Rankine's Theory)

In words, the maximum normal stress theory may be expressed as:

> Failure is predicted to occur in the multiaxial state of stress when the maximum principal normal stress becomes equal to or exceeds the maximum normal stress at the time of failure in a simple uniaxial stress test using a specimen of the same material. (5-31)

For a multiaxial state of stress, the maximum principal normal stress is the largest of the three roots to the stress cubic equation (5-1), that is, the largest of σ_1, σ_2, and σ_3. The maximum normal stress at the time of failure is equal to the uniaxial strength of the material corresponding to the governing failure mode. It should be noted that for some materials the failure strength under tensile loading may be different from the failure strength under compressive loading.

With these factors in mind, the word statement (5-31) may be expressed mathematically as *failure is predicted by the maximum normal stress theory to occur if (FIPTOI)*

$$\begin{aligned} \sigma_1 &\geq \sigma_{fail\text{-}t} \\ \sigma_2 &\geq \sigma_{fail\text{-}t} \\ \sigma_3 &\geq \sigma_{fail\text{-}t} \end{aligned} \tag{5-32}$$

or if

$$\begin{aligned} \sigma_1 &\leq \sigma_{fail\text{-}c} \\ \sigma_2 &\leq \sigma_{fail\text{-}c} \\ \sigma_3 &\leq \sigma_{fail\text{-}c} \end{aligned} \tag{5-33}$$

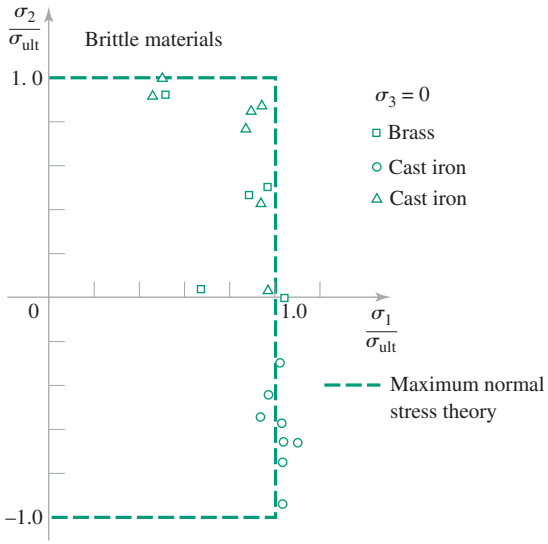

Figure 5.14
Comparison of biaxial ultimate strength data for brittle materials with the *maximum normal stress theory*.

where $\sigma_{fail\text{-}t}$ is the uniaxial *tensile* (+) failure strength of the material and $\sigma_{fail\text{-}c}$ is the uniaxial *compressive* (−) failure strength of the material, corresponding to the governing failure mode (usually yielding or ultimate rupture if loading is static).

The maximum normal stress theory provides good results for brittle materials, as illustrated in Figure 5.14, but should not be used for ductile materials.

Maximum Shearing Stress Theory (Tresca–Guest Theory)

In words, the maximum shearing stress theory may be expressed as

> Failure is predicted to occur in the multiaxial state of stress when the maximum shearing stress magnitude becomes equal to or exceeds the maximum shearing stress magnitude at the time of failure in a simple uniaxial stress test using a specimen of the same material. (5-34)

For a multiaxial state of stress the maximum shearing stress magnitude is the largest of the three principal shearing stresses τ_1, τ_2, and τ_3, given by (5-2), (5-3), and (5-4). For a *uniaxial* stress test, the only nonzero normal stress component is a principal stress component in the direction of the applied force. From (5-2), (5-3), and (5-4), in a uniaxial stress test at failure, two of the principal normal stresses are zero and the third is set equal to σ_{fail}, giving

$$\tau_{fail} = \frac{\sigma_{fail}}{2} \tag{5-35}$$

With these factors in mind, word statement (5-34) may be expressed mathematically as *failure is predicted by the maximum shearing stress theory to occur if (FIPTOI)*

$$\begin{aligned} |\tau_1| &\geq |\tau_{fail}| \\ |\tau_2| &\geq |\tau_{fail}| \\ |\tau_3| &\geq |\tau_{fail}| \end{aligned} \tag{5-36}$$

where τ_{fail} is the largest principal shearing stress at the time of failure in a *uniaxial* stress test, as given by (5-35).

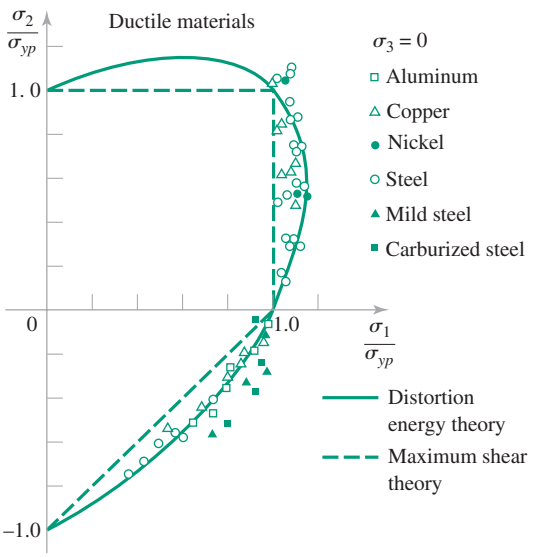

Figure 5.15
Comparison of biaxial yield strength data with the *maximum shearing stress theory* and the *distortion energy theory*.

The maximum shearing stress theory provides good results for ductile materials, as illustrated in Figure 5.15, but should not be used for brittle materials.

Distortion Energy Theory (Huber–von Mises–Hencky Theory)

In words, the distortion energy theory, sometimes called the von Mises theory, may be expressed as

> Failure is predicted to occur in the multiaxial state of stress when the distortion energy per unit volume becomes equal to or exceeds the distortion energy per unit volume at the time of failure in a simple uniaxial stress test using a specimen of the same material. (5-37)

The distortion energy theory, developed as an improvement over an earlier "total strain energy theory," is based on the postulate that the total strain energy U_T stored in a volume of stressed material may be divided into two parts: the energy associated solely with change in volume, U_v, termed *dilatation* energy, and the energy associated solely with change in shape, U_d, termed *distortion* energy. It was further postulated that failure, particularly under conditions of ductile behavior, is related *only* to the *distortion* energy. Thus

$$U_T = U_v + U_d \tag{5-38}$$

Dividing by the volume in each term, the distortion energy *per unit volume* may be expressed as

$$u_d = u_T - u_v \tag{5-39}$$

An expression for total strain energy per unit volume, u_T may be found[11] by calculating the work done in a triaxial state of stress by forces associated with σ_1, σ_2, and σ_3, acting over their respective areas, to induce the strains ε_1, ε_2, and ε_3, and their corresponding displacements.

[11]See equations (4-59), (5-1), (5-15), (5-16), and (5-17).

Employing Hooke's Law, the resulting expression for total strain energy per unit volume becomes

$$u_T = \frac{1}{2E}[\sigma_1^2 + \sigma_2^2 + \sigma_3^2 - 2\nu(\sigma_1\sigma_2 + \sigma_2\sigma_3 + \sigma_3\sigma_1)] \tag{5-40}$$

Likewise, the dilatation (volume changing) energy per unit volume may be found[12] as

$$u_v = \frac{3(1 - 2\nu)}{2E}\left[\frac{\sigma_1 + \sigma_2 + \sigma_3}{3}\right]^2 \tag{5-41}$$

Then substituting (5-40) and (5-41) into (5-39), the distortion energy per unit volume is found to be

$$u_d = \frac{1}{2}\left[\frac{1 + \nu}{3E}\right][(\sigma_1 - \sigma_2)^2 + (\sigma_2 - \sigma_3)^2 + (\sigma_3 - \sigma_1)^2] \tag{5-42}$$

To find the distortion energy per unit volume at the time of failure, $u_{d\text{-}fail}$, (5-42) is evaluated under *uniaxial failure* conditions, when two of the principal stresses are equal to zero and the third one is equal to the uniaxial failure strength σ_{fail}. Thus

$$u_{d\text{-}fail} = \left[\frac{1 + \nu}{3E}\right]\sigma_{fail}^2 \tag{5-43}$$

With (5-42) and (5-43) at hand, word statement (5-37) may be expressed mathematically as *failure is predicted by the distortion energy theory to occur if (FIPTOI)*

$$\frac{1}{2}[(\sigma_1 - \sigma_2)^2 + (\sigma_2 - \sigma_3)^2 + (\sigma_3 - \sigma_1)^2] \geq \sigma_{fail}^2 \tag{5-44}$$

The distortion energy theory provides very good results for ductile materials, as illustrated in Figure 5.15, but generally should not be used for brittle materials.

The left side of (5-44) is sometimes defined as the square of the *von Mises stress*, the *effective stress*, or the *equivalent uniaxial stress*, σ_{eq}, giving the expression

$$\sigma_{eq} = \sqrt{\frac{1}{2}[(\sigma_1 - \sigma_2)^2 + (\sigma_2 - \sigma_3)^2 + (\sigma_3 - \sigma_1)^2]} \tag{5-45}$$

For a biaxial state of stress, assuming $\sigma_3 = 0$, (5-45) becomes

$$\sigma_{eq} = \sqrt{\sigma_1^2 - \sigma_1\sigma_2 - \sigma_2^2} \tag{5-46}$$

In terms of rectangular components of stress, the von Mises criterion can be written as

$$\sigma_{eq} = \sqrt{\frac{1}{2}\left[(\sigma_x - \sigma_y)^2 + (\sigma_y - \sigma_z)^2 + (\sigma_z - \sigma_x)^2\right] + 3(\tau_{xy}^2 + \tau_{yz}^2 + \tau_{xz}^2)} \tag{5-47}$$

and for a biaxial state of stress, assuming that $\sigma_z = 0$, and $\tau_{xz} = \tau_{yz} = 0$, we have

$$\sigma_{eq} = \sqrt{\sigma_x^2 - \sigma_x\sigma_y + \sigma_y^2 + 3\tau_{xy}^2} \tag{5-48}$$

[12]For example, see ref. 1, p. 154.

Failure Theory Selection

Evaluation of the three failure theories just discussed in light of experimental evidence leads to the following observations:

1. For isotopic materials that fail by brittle fracture, the maximum normal stress theory is the best theory to use.
2. For isotropic materials that fail by yielding or ductile rupture, the distortion energy theory is the best theory to use.
3. For isotropic materials that fail by yielding or ductile rupture, the maximum shearing stress theory is almost as good as the distortion energy theory.
4. As a rule of thumb,[13] the maximum normal stress theory would be used for isotropic brittle materials (materials that exhibit a ductility of less than 5 percent elongation in 2 inches) and either the distortion energy theory or maximum shearing stress theory would be used for isotropic ductile materials (materials that exhibit a ductility of 5 percent or more in a 2-inch gage length). Where possible, a fracture mechanics analysis should be performed.

Example 5.5 Yielding Failure Prediction Under Static Multiaxial State of Stress

An aircraft wing flap actuator housing is made of cast magnesium alloy AZ63A-T4 (S_u = 276 MPa, S_{yp} = 97 MPa, e = 12% in 50 mm). The state of stress has been calculated for the suspected critical point and is shown in Figure E5.5. Would you predict failure due to yielding?

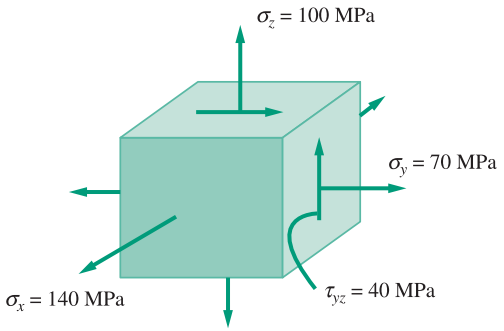

Figure E5.5
State of stress at suspected critical point.

Solution

For the state of stress shown, the stress cubic equation (5-1) becomes

$$\sigma^3 - \sigma^2(\sigma_x + \sigma_y + \sigma_z) + \sigma(\sigma_x\sigma_y + \sigma_y\sigma_z + \sigma_z\sigma_x - \tau_{yz}^2) - (\sigma_x\sigma_y\sigma_z - \sigma_x\tau_{yz}^2) = 0$$

Substituting numerical values (in MPa)

$$\sigma^3 - \sigma^2(140 + 70 + 100) + \sigma[(140)(70) + (70)(100) + (100)(140) - (40)^2]$$
$$- [(140)(70)(100) - 140(40)^2] = 0$$
$$\sigma^3 - 310\sigma^2 + 29\,200\sigma - 756000 = 0$$

[13]The 5 percent boundary between "brittle" and "ductile" behavior is an arbitrary but widely used rule of thumb.

Example 5.5 Continues

Since shearing stresses are zero on the x-plane, it is, by definition, a principal plane. Thus,

$$\sigma_x = \sigma_1 = 140 \text{ MPa}$$

is one of the three solutions of (1). Next, dividing (1) by $(\sigma - 140)$ gives

$$\sigma^2 - 170\sigma + 5400 = 0$$

whence

$$\sigma = \frac{170 \pm \sqrt{(170)^2 - 4(5400)}}{2} = 85 \pm 42.7$$

giving the solution

$$\sigma_2 = 127.7 \text{ MPa} \qquad \text{and} \qquad \sigma_3 = 42.3 \text{ MPa}$$

Since the elongation in 50 mm is given as 12 %, the material may be regarded as ductile; and the distortional energy theory of failure, given in (5-??) is the best theory to use. Thus, FIPTOI

$$\frac{1}{2}\left[(140 - 127.7)^2 + (127.7 - 42.3)^2 + (42.3 - 140)^2\right] \geq (97)^2$$

or FIPTOI

$$8495 \geq 9409$$

Since this condition *is not* met, *failure is not predicted* at the specified critical point.

Example 5.6 Thickness of Thin Cylindrical Pressure Vessel

A thin-walled cylindrical pressure vessel with closed ends is subjected to an internal pressure of 100 MPa. The internal diameter is 50 mm. If the yield stress for the pressure vessel is 400 MPa, what should be the wall thickness based upon (a) the maximum shear stress theory and (b) distortion energy theory?

Solution

The stresses in the cylindrical pressure vessel are (see Chapter 9) given as

$$\sigma_t = \frac{p_i d}{2t}, \qquad \sigma_t = \frac{p_i d}{4t}$$

where σ_1 is the tangential stress and σ_1 is the longitudinal stress. The tangential and longitudinal stresses are also the principal stresses in the pressure vessel. Thus, we have

$$\sigma_1 = \sigma_t = \frac{100(50)}{2t} = \frac{2500}{t}, \quad \sigma_2 = \sigma_1 = \frac{100(50)}{4t} = \frac{1250}{t}, \quad \sigma_3 = 0$$

(a) Maximum shear stress theory is given as

$$\tau_{max} = \frac{\sigma_1 - \sigma_3}{2} = \frac{2500 - 0}{2t} = \frac{1250}{t}$$

Thus, we have

$$\tau_{max} = \frac{1250}{t} = \frac{S_{yp}}{2} = \frac{400}{2} = 200$$

$$t = \frac{1250}{200} = 6.25 \text{ mm}$$

(b) Distortion energy theory is given by the following:

$$\sigma_{eq} = \sqrt{\sigma_1^2 - \sigma_1\sigma_2 + \sigma_2^2}$$

Hence,

$$\sigma_{eq} = S_{yp} = 400 = \frac{1}{t}\sqrt{2500^2 - 2500 \times 1250 + 1250^2} = \frac{2165.06}{t}$$

$$t = \frac{2165.06}{400} = 5.41 \text{ mm}$$

Example 5.7 Maximum Torque in Shaft Subjected to Bending

A 2.5-in diameter shaft is made of AISI 1020 cold-drawn steel. The shaft is subjected to a bending moment of 50,000 in-lb. Determine the maximum torque that can be applied to the shaft according to (a) the maximum shear stress theory and (b) the distortion energy theory.

Solution

The maximum bending stress occurs on the outer surface of the shaft and is given by

$$\sigma_x = \frac{Mc}{I} = \frac{32M}{\pi d^3}$$

The maximum shear stress due to torque T occurs on the outer surface of the shaft and is given by

$$\tau_{xy} = \frac{Tr}{J} = \frac{16T}{\pi d^3}$$

The principal stresses are obtained from

$$\sigma_{1,2} = \frac{\sigma_x}{2} \pm \sqrt{\left(\frac{\sigma_x}{2}\right)^2 + \tau_{xy}^2} = \frac{16M}{\pi d^3} \pm \sqrt{\left(\frac{16M}{\pi d^3}\right)^2 + \left(\frac{16T}{\pi d^3}\right)^2}$$

$$= \frac{16}{\pi d^3}\left[M \pm \sqrt{M^2 + T^2}\right]$$

(a) The maximum shear stress theory states that the maximum shear stress is

$$\tau_{max} = \frac{\sigma_1 - \sigma_2}{2} = \frac{16}{\pi d^3}\sqrt{M^2 + T^2} = \frac{S_{yp}}{2}$$

Example 5.7 Continues

Solving for torque T gives

$$T = \left(\left[S_{yp}(\pi^2)\left(\frac{d^3}{32}\right) \right]^2 - M^2 \right)^{1/2}$$

Thus, for AISI 1020 CD $S_{yp} = 51{,}000$ psi, we find

$$T = \left(\left[51{,}000(\pi)\left(\frac{2.5^3}{32}\right) \right]^2 - 50{,}000^2 \right]^{1/2} = 60170 \text{ in-lb}$$

(b) The distortion energy theory is given by

$$\sigma_{eq} = \sqrt{\sigma_1^2 - \sigma_1\sigma_2 + \sigma_2^2} = \frac{16}{\pi d^3}\sqrt{4M^2 + 3T^2}$$

Solving for torque T gives

$$T = \left\{ \frac{1}{3}\left(\left[S_{yp}\left(\frac{\pi d^3}{16}\right) \right]^2 - 4M^2 \right) \right\}^{1/2}$$

For AISI 1020 CD, we find

$$T = \left\{ \frac{1}{3}\left(\left[51{,}000\left(\frac{\pi(2.5)^3}{16}\right) \right]^2 - 4(50{,}000)^2 \right) \right\}^{1/2} = 69{,}478 \text{ in-lb}$$

Example 5.8 Factor of Safety for Shaft Subjected to Bending and Torsion

A simply supported stationary shaft, 50 mm in diameter and made of AISI 1060 hot-rolled steel, is subjected to a maximum bending moment of 3000 N-m and a maximum torque of 2000 N-m. Find the factor of safety corresponding to failure based on the distortion energy theory.

Solution

The bending stress is given as

$$\sigma_x = \frac{Mc}{I} = \frac{32M}{\pi d^3} = \frac{32(3000000)}{\pi(50)^3} = 244.46 \text{ MPa}$$

and the maximum torsional stress is

$$\tau_{xy} = \frac{Tr}{J} = \frac{16T}{\pi d^3} = \frac{16(2000000)}{\pi(50)^3} = 81.49 \text{ MPa}$$

The distortion energy theory is given as

$$\sigma_{eq} = \sqrt{\sigma_x^2 + 3\tau_{xy}^2} = \sqrt{(244.46)^2 + 3(81.49)^2} = 282.28 \text{ MPa}$$

For AISI 1060 hot-rolled steel, the yield strength is 372 MPa; thus the factor of safety is

$$n_d = \frac{S_{yp}}{\sigma_{eq}} = \frac{372}{282.28} = 1.32$$

5.5 Brittle Fracture and Crack Propagation; Linear Elastic Fracture Mechanics

When the material behavior of a machine part is brittle rather than ductile, the mechanics of the failure process are much different. As described in 2.3, in brittle fracture the part separates into two or more pieces due to the breaking of primary interatomic bonds, with little or no plastic flow. High-velocity crack propagation from preexisting flaws results in sudden and catastrophic failure. If material behavior is clearly brittle, and geometry and loading are simple, as for the axially loaded bar of Figure 2.1, failure by brittle fracture may be predicted when the stress σ, from (2-1), exceeds the material's ultimate strength S_u. Hence failure is predicted to occur if (FIPTOI)

$$\sigma \geq S_u \tag{5-49}$$

Thus for a uniaxial state of stress the failure prediction expression (5-49) for brittle fracture is formally the same as (2-18) for ductile rupture. If the loading is more complicated, and a multiaxial state of stress is produced by the loads, fracture may be predicted with reasonable accuracy through the use of the maximum normal stress theory of failure, as discussed in 5.4.

On the other hand, it has now been well established that *nominally ductile* materials may also fail by a brittle fracture response in the presence of cracks or flaws if the combination of crack size, geometry of the part, temperature, and/or loading rate lies within certain critical ranges. The prediction of brittle fracture in these circumstances has been based on the assumptions that the stress at a crack tip, where failure is initiated, may be calculated as if the material behavior is linear elastic and the state of stress is two-dimensional; thus the procedure is often referred to as *linear elastic fracture mechanics (LEFM).*

Three basic types of stress fields have been defined for crack-tip stress analysis, each one associated with a distinct mode of crack deformation, as illustrated in Figure 5.16. The crack opening mode, Mode I, is associated with local displacement in which the crack surfaces move directly apart. Modes II and III are forward sliding and tearing displacements respectively. Mathematical expressions have been developed for the *intensity* and *distribution* of stress near the crack tips for each of the three modes shown in Figure 5.16.[14] For failure prediction purposes, the crack-tip *stress-intensity factors*, developed from these mathematical expressions, provide a good measure of the seriousness of loading and geometry in any particular case. In general, the expressions for stress intensity factor, K, are of the form

$$K = C\sigma\sqrt{\pi a} \tag{5-50}$$

where σ is gross-section nominal stress, a is a crack-length parameter, and C is dependent upon the type of loading and the geometry away from the crack. Many values of C have

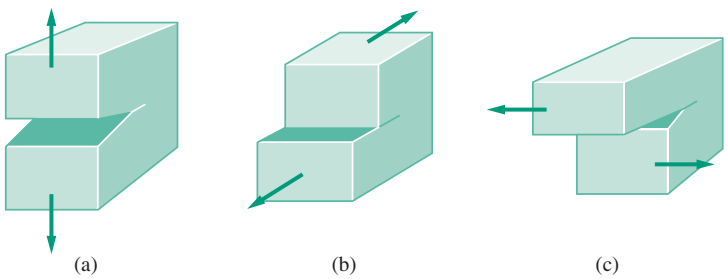

Figure 5.16
Basic modes of crack displacement. (a) Mode I, (b) Mode II, (c) Mode III. (To be read "Mode-one," "Mode-two," and "Mode-three.")

[14]See, for example, the Westergaard equations, ref. 1, pp. 54–55.

been published,[15] and several typical charts for selecting proper C values for through-the-thickness cracks are given in Figures 5.17 through 5.21. Figure 5.22 gives a chart for *surface flaw shape parameter* Q to be used in finding stress-intensity factors for part-through thumbnail-shaped surface cracks. The stress-intensity factor, K, calculated from (5-50), is a single-parameter measure of the seriousness of the stress field around the crack tip. The magnitude of K associated with the onset of rapid crack extension (initiation of brittle fracture) has been designated as *critical stress intensity*, K_c. Thus failure by brittle fracture may be predicted to occur for through-the-thickness cracks if (FIPTOI)

$$K = C\sigma\sqrt{\pi a} \geq K_c \tag{5-51}$$

or, for thumbnail-shaped surface cracks if

$$K = \frac{1.12}{\sqrt{Q}}\ \sigma\sqrt{\pi a} \geq K_c \tag{5-52}$$

For a given cracked plate, for example the case shown in Figure 5.19, the stress-intensity factor K increases proportionally with gross nominal stress σ, and also is a function of

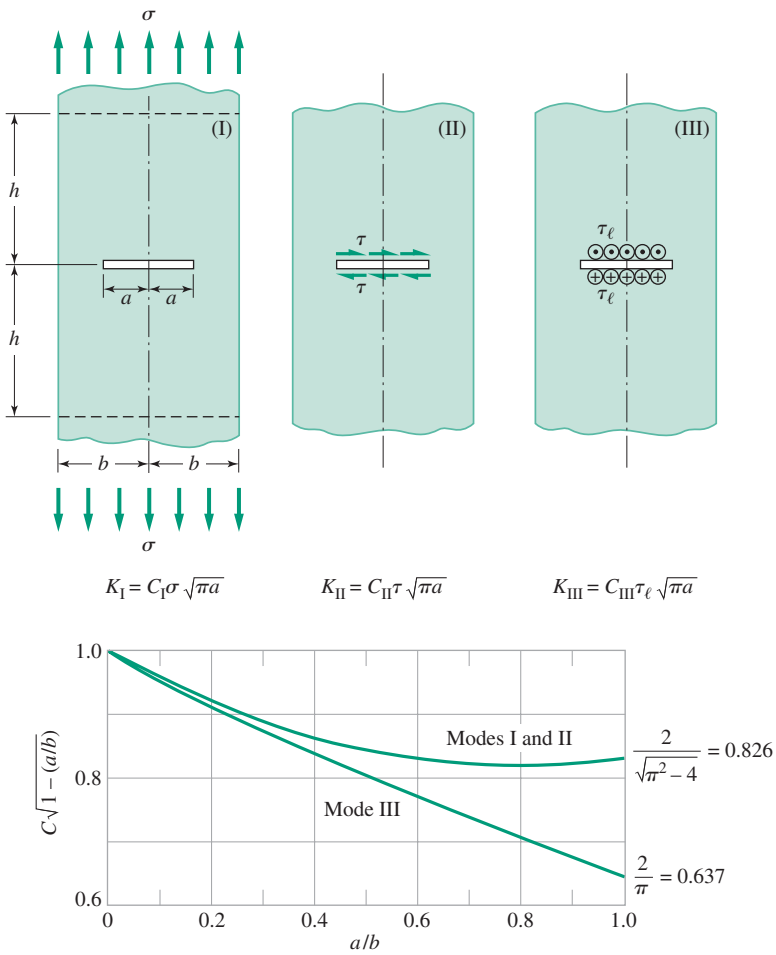

Figure 5.17
Stress-intensity factors K_I, K_{II} and K_{III}, for center-cracked test specimen. (Source: ref. 11, Del Research Corp.)

[15]See, for example, ref. 7.

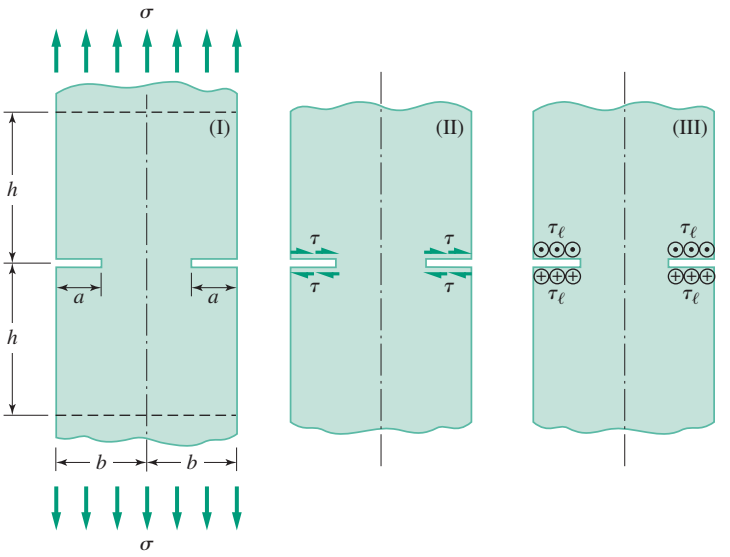

$K_I = C_I \sigma \sqrt{\pi a}$ $K_{II} = C_{II} \tau \sqrt{\pi a}$ $K_{III} = C_{III} \tau_\ell \sqrt{\pi a}$

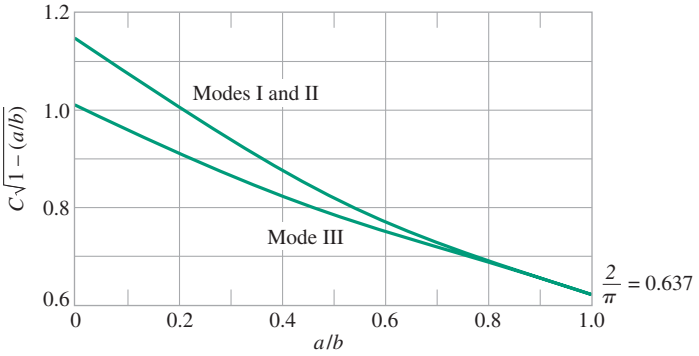

Figure 5.18
Stress-intensity factors K_I, K_{II} and K_{III}, for double-edge notch test specimen. (Source: ref. 7, Del Research Corp.)

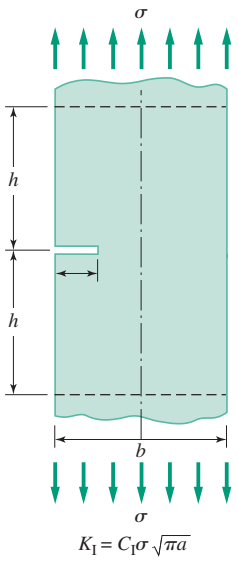

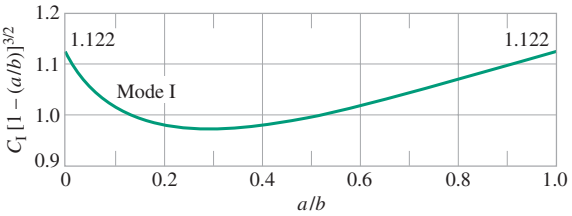

$K_I = C_I \sigma \sqrt{\pi a}$

Figure 5.19
Stress-intensity factors K_I, for single-edge notch test specimen. (Source: ref. 7, Del Research Corp.)

Figure 5.20
Stress-intensity factors K_I, for single through-the-thickness edge crack under pure bending moment. (Source: ref. 7, Del Research Corp.)

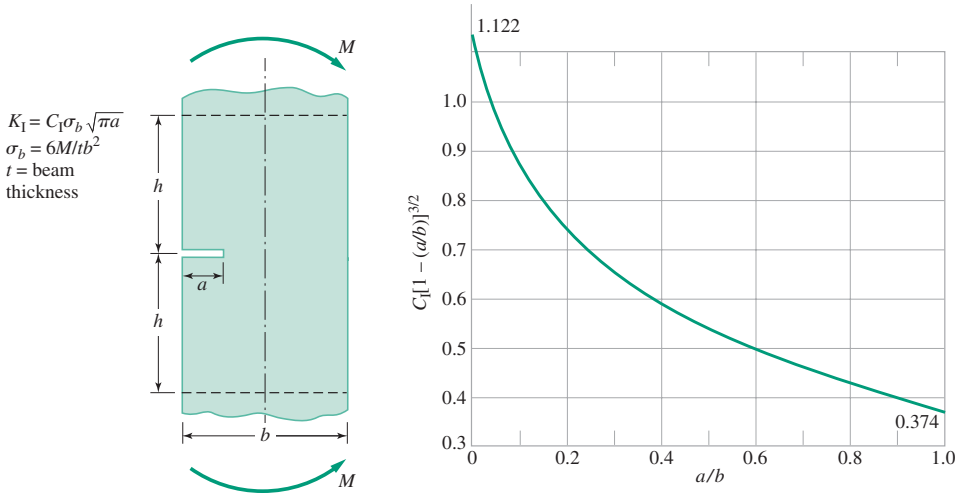

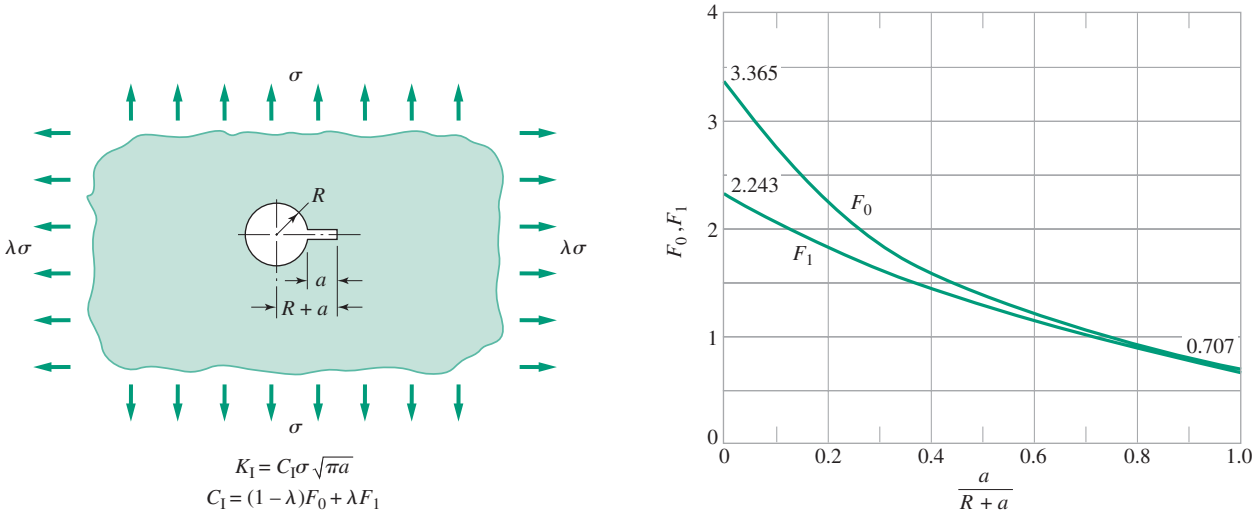

Figure 5.21
Stress-intensity factors K_I, for a through-the-thickness crack emanating from a circular hole in an infinite plate under biaxial tension. (Source: ref. 7, Del Research Corp.)

Figure 5.22
Surface flaw shape parameter. (From ref. 9; adapted by permission of Pearson Education, Inc., Upper Saddle River, N.J.)

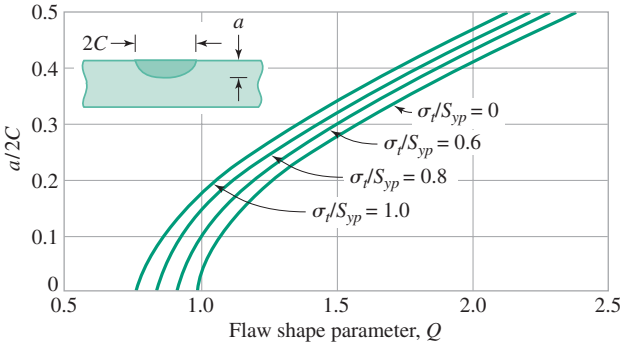

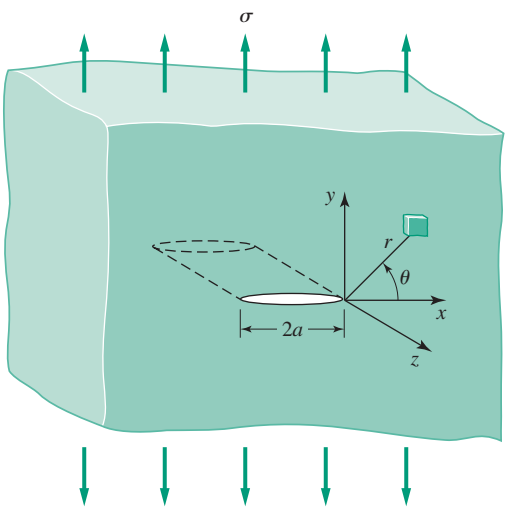

Figure 5.23
Coordinate system for infinite plate containing a through-the-thickness crack of length $2a$.

instantaneous crack length a. For the infinite plate shown in Figure 5.23, the crack is oriented so that its plane is perpendicular to the direction of applied uniaxial stress, σ, hence pure Mode 1 loading exists. The crack front extends uniformly all the way through the plate, so the crack is a through-the-thickness crack. The usual coordinate system for defining state of stress at the crack tip is shown. In studying material behavior it has been found that for a given material, depending upon the state of stress at the crack tip, the critical stress intensity K_c decreases to a lower limiting value as the state of strain at the crack tip approaches the conditions of plane strain.[16] This lower limiting value defines a basic material property, the *plane strain fracture toughness*, designated[17] K_{Ic}. Standard test methods have been established for the determination of K_{Ic} values.[18] A few data are given in Table 5.2. For the plane strain fracture toughness K_{Ic} to be a valid failure prediction criterion for a machine part, *plane strain* conditions[19] must exist at the crack tip; that is, the material must be *thick* enough to ensure plane strain conditions. It has been estimated empirically that for plane strain conditions the minimum material thickness B must be

$$B \geq 2.5\left(\frac{K_{Ic}}{S_{yp}}\right)^2 \tag{5-53}$$

If the material is *not* thick enough to meet the criterion of (5-53), *plane stress* better characterizes the state of stress at the crack tip, and K_c, the critical stress-intensity factor for failure prediction under plane stress conditions, may be estimated using a semiempirical relationship for K_c as a function of plane strain fracture toughness K_{Ic} and thickness B.[20] This relationship is

$$K_c = K_{Ic}\left[1 + \frac{1.4}{B^2}\left(\frac{K_{Ic}}{S_{yp}}\right)^4\right]^{1/2} \tag{5-54}$$

[16]For thick plates the surrounding material constrains the crack-tip zone to near-zero strain in the thickness direction, resulting in plane (biaxial) strain. See also 5.2.

[17]To be read "K-one-c."

[18]See ref. 8.

[19]*Plane strain (biaxial state of strain)* occurs when nonzero strain components exist in only two coordinate directions. See also 5.2.

[20]See refs. 13 and 14.

TABLE 5.2 Yield Strength and Plane Strain Fracture Toughness Data for Selected Engineering Alloys[1]

		Test Temperature		S_{yp}		K_{Ic}	
Alloy	Form	°F	°C	ksi	MPa	ksi$\sqrt{\text{in}}$	MPa$\sqrt{\text{m}}$
AISI 1045 steel	Plate	25	−4	39	269	46	50
AISI 1045 steel	Plate	0	−18	40	276	46	50
4340 steel (500°F temper)	Plate	70	21	217–238	1495–1640	45–57	50–63
4340 steel (800°F temper)	Forged	70	21	197–211	1360–1455	72–83	79–91
D6AC steel (1000°F temper)	Plate	70	21	217	1495	93	102
D6AC steel (1000°F temper)	Plate	−65	−54	228	1570	56	62
18 Ni maraging steel (300)	Plate	600	316	236	1627	80	87
18 Ni maraging steel (300)	Plate	70	21	280	1931	68	74
18 Ni maraging steel (300)	Plate	−100	−73	305	2103	42	46
A 538 steel	—	—	—	250	1722	100	111
2014-T6 aluminum	Forged	75	24	64	440	28	31
2024-T351 aluminum	Plate	80	27	54–56	370–385	28–40	31–44
6061-T651 aluminum	Plate	70	21	43	296	26	28
6061-T651 aluminum	Plate	−112	−80	45	310	30	33
7075-T6 aluminum	—	—	—	75	517	26	28
7075-T651 aluminum	Plate	70	21	75–81	515–560	25–28	27–31
7075-T7351 aluminum	Plate	70	21	58–66	400–455	28–32	31–35
Ti-6Al-4V titanium	Plate	74	23	119	820	96	106

[1]From refs. 10–12.

As long as the crack-tip plastic zone is in the regime of *small-scale yielding,*[21] this estimation procedure provides a good design approach. If the plastic zone size ahead of the crack tip becomes so large that the small-scale yielding condition is no longer satisfied, an appropriate *elastic-plastic fracture mechanics (EPFM)* procedure would give better results. For example, a *failure assessment diagram*[22] might be utilized; however such EPFM procedures are beyond the scope of this text.

To utilize (5-52) as a design or failure prediction tool, the stress-intensity factor K must be determined for the particular loading and geometry of the part or structure under consideration. The critical stress intensity is set equal to K_{Ic} if the minimum thickness criterion (5-53) is met, otherwise K_c is estimated from (5-54). If failure is predicted to occur using (5-52), redesign becomes necessary.

Example 5.9 Brittle Fracture

Two "identical" support straps of forged 2014-T6 aluminum, shown in Figure E5.8, have been inspected and found to contain through-the-thickness cracks. While the total crack length of 5 mm is the same for both straps, one strap (case A) involves two edge cracks, each with 2.5-mm length, opposite each other; while the other strap (case B) involves a single crack of 5-mm length at the center. The straps are of rectangular cross section 50 mm

[21]*Small-scale yielding* means that the crack-tip plastic zone size is small compared to the dimensions of the crack.

[22]See ref. 1, pp. 70–76.

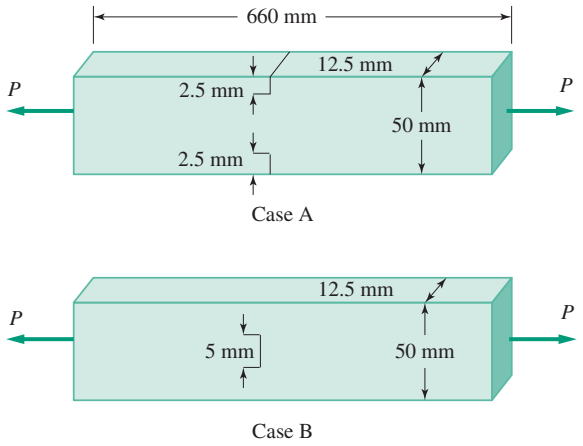

Figure E5.9
Cracked support bracket.

wide and 12.5 mm thick, and the straps are 660 mm in length. The straps are loaded by a direct tensile force $P = 220$ kN in the 660 mm direction, as shown.

a. For each case, what is the governing failure mode?

b. For each case, is failure predicted to occur?

c. Is center cracking or edge cracking the more serious configuration?

d. How would the analysis change if the strap thickness for each case had been 11 mm instead of 12.5 mm?

Solution

a. Both yielding and brittle fracture should be checked for each case. Property values from Table 5.2 are

$$S_{yp} = 440 \text{ MPa} \quad \text{and} \quad K_{Ic} = 31 \text{ MPa}\sqrt{\text{m}}$$

b. For each case, failure by both yielding and brittle fracture must be checked. For case A (edge cracks), to check for yielding, from (2-17) FIPTOI

$$\sigma \geq S_{yp}$$

Where

$$\sigma = \frac{P}{A_{net}} = \frac{220{,}000}{(0.05 - 0.005)(0.0125)} = 391 \text{ MPa}$$

Hence, FIPTOI $391 \geq 440$. Therefore, failure by yielding is not predicted for case A. To check brittle fracture, from (5-52) FIPTOI

$$C_A \sigma \sqrt{\pi a} \geq K_c$$

Using the Mode I curve from Figure 5.18, with $a = 2.5$, $b = 25$, and $a/b = 0.1$,

$$C_A \sqrt{1 - 0.1} = 1.07 \quad \rightarrow \quad C_A = 1.13$$

The cross-sectional stress is

$$\sigma = \frac{P}{A_g} = \frac{220{,}000}{(0.05)(0.0125)} = 352 \text{ MPa}$$

Example 5.9 Continues

Checking for plane strain, from (5-50) plane strain exists if

$$B \geq 2.5\left(\frac{K_{Ic}}{S_{yp}}\right)^2 = 2.5\left(\frac{31}{440}\right)^2 = 0.0124 \text{ m}$$

Since $B = 12.5$ mm, the plain strain condition is met and plain strain conditions prevail. Therefore,

$$K_c = K_{Ic} = 31 \text{ MPa}\sqrt{\text{m}}$$

and the failure criteria may be evaluated as FIPTOI

$$C_A\sigma\sqrt{\pi a} \geq K_c: \quad (1.13)(352)\sqrt{\pi(0.0025)} \geq 31$$

or if

$$35.2 \geq 31$$

Hence, failure by brittle fracture *is* predicted for case A.

For case B (center crack), the calculation for yielding failure is identical to the case A calculation, since the net cross-sectional area is the same in both cases. Therefore, failure by yielding is *not* predicted for case B. To check brittle fracture, from (5-52) FIPTOI

$$C_B\sigma\sqrt{\pi a} \geq K_c$$

Using the Mode I curve from Figure 5.17, with $a = 2.5$, $b = 25$, and $a/b = 0.1$,

$$C_B\sqrt{1 - 0.1} = 0.96 \quad \rightarrow \quad C_B = 1.01$$

The cross-sectional stress is the same as for case A. Thus, $\sigma = 352$ MPa. Since the material properties are the same as for case A, plain strain conditions prevail if and

$$K_c = K_{Ic} = 31 \text{ MPa}\sqrt{\text{m}}$$

Now the failure criteria may be evaluated as FIPTOI

$$(1.01)(352)\sqrt{\pi(0.0025)} \geq 31$$

or if

$$31.5 \geq 31$$

Hence, failure by brittle fracture is also predicted for case B, but only by a slight margin.

c. Since the stress-intensity factor K for case A ($35.2 \text{ MPa}\sqrt{\text{m}}$) is larger than for case B ($31.5 \text{ MPa}\sqrt{\text{m}}$), the edge-crack case (case A) is more serious.

d. If the strap thickness is reduced from 12.5 mm to 11 mm, the plain strain condition is no longer met and the nominal stress levels increase. To check for yielding for both cases A and B we compute the stress

$$\sigma = \frac{P}{A_{net}} = \frac{220\ 000}{(0.05 - 0.005)(0.011)} = 444 \text{ MPa}$$

FIPTOI $444 \geq 440$. Therefore, failure by yielding *is* predicted for both cases.

To check for brittle fracture, since only the thickness has changed, the values $C_A = 1.13$ and $C_B = 1.01$ remain unchanged. The gross-section stress for both cases becomes

$$\sigma = \frac{220{,}000}{(0.05)(0.011)} = 400 \text{ MPa}$$

Since plain strain conditions are not satisfied, from (5-51)

$$K_c = K_{Ic}\left[1 + \frac{1.4}{B^2}\left(\frac{K_{Ic}}{S_{yp}}\right)^4\right]^{1/2} = 31\left[1 + \frac{1.4}{(0.011)^2}\left(\frac{31}{440}\right)^4\right]^{1/2} = 35.1 \text{ MPa}$$

Then for case A, FIPTOI

$$(1.13)(400)\sqrt{\pi(0.0025)} \geq 35.1$$

or if

$$40.1 \geq 35.1$$

And failure by brittle fracture *is* again predicted for case A.
Similarly, for case B, FIPTOI

$$(1.01)(400)\sqrt{\pi(0.0025)} \geq 35.1$$

or if

$$35.8 \geq 35.1$$

So brittle fracture *is* again predicted for case B.

If loading conditions are more complicated, fracture mechanics procedures are available but much more involved. For example, in cases where the plane of a through-the-thickness crack is oriented at some other angle than perpendicular to the direction of σ, the applied stress field induces a combination of Mode I and Mode II loading on the crack. Mixed-mode fracture behavior presents an analytical challenge, and a designer would usually consult with a fracture mechanics specialist to evaluate such a problem. Likewise, a specialist would often be involved in addressing problems associated with high-rate loading, cyclic loading, or cases where LEFM conditions are not valid.

5.6 Fluctuating Loads, Cumulative Damage, and Fatigue Life

In modern engineering practice, repeated loads, fluctuating loads, and rapidly applied loads are far more common than static or quasistatic loads. By far, the majority of engineering design environments involve machine parts subjected to fluctuating or cyclic loads. Such loads induce fluctuating or cyclic stresses that often result in failure by *fatigue*. Fatigue is a progressive failure process that involves the *initiation* and *propagation* of cracks until one reaches an unstable size, triggering a sudden catastrophic separation of the affected part into two or more pieces. It is difficult to detect the progressive changes in material properties that occur during fatigue stressing, and fatigue failure may therefore

occur with little or no warning. Periods of rest, with the fatigue stress removed, do not lead to any significant healing or recovery from the effects of the prior cyclic stressing. Hence, the damage done during the fatigue process is *cumulative*. Fatigue failures have been recognized for over 150 years, but only with the advent of high-speed high-performance machinery, and the development of the aerospace industry, has widespread attention been directed toward trying to understand the fatigue process.

In recent years it has been recognized that the fatigue failure process involves three phases. A *crack initiation* phase occurs first, followed by a *crack propagation* phase; finally, when the crack reaches a critical size, the terminal phase of *unstable rapid crack growth to fracture* completes the failure process. Traditionally, the models for analysis and prediction of fatigue failure have lumped all three phases together in the *stress-life (S-N) approach*. Numerous analytical/empirical procedures and a large database have been developed to support the *S-N* approach. More recently, the separate modeling of each phase has been under intense development, and prediction models have now been set forth for each phase separately. This methodology may be referred to as the *fracture-mechanics (F-M) approach*.

Additionally, two domains of cyclic loading have been identified on the basis of whether the induced *cyclic strains* are predominantly *elastic* or predominantly *plastic*. When cyclic loads are relatively low, strain cycles are confined largely to the elastic range, and long lives or high numbers of cycles to failure are exhibited, the domain is called *high-cycle fatigue*. When cyclic loads are relatively high, significant levels of plastic strain are induced during each cycle, and short lives or low numbers of cycles to failure are exhibited, the domain is called *low-cycle fatigue*, or *cyclic strain-controlled fatigue*. Occasionally, a machine part may be subjected to intermixed loadings from both domains. High-cycle fatigue predominates in most design environments; therefore high-cycle fatigue analysis will be emphasized in this text. Low-cycle fatigue analysis is widely discussed in the literature.[23]

Fluctuating Loads and Stresses

Fluctuating loads and *loading spectra*, producing associated *stress spectra* in a machine part, reflect the design configuration and operational use of the machine. Perhaps the simplest fatigue stress spectrum to which a machine element may be subjected is a zero-mean sinusoidal stress-time pattern of constant amplitude and fixed frequency, applied for a specified number of cycles. Such a stress-time pattern, often referred to as a *completely reversed* or *zero-mean* cyclic stress, is illustrated in Figure 5.24(a). Using the sketches of Figure 5.24, we may define several useful terms and symbols; these include

$$\sigma_{max} = \text{maximum stress in the cycle}$$

$$\sigma_{min} = \text{minimum stress in the cycle}$$

$$\sigma_m = \text{mean cyclic stress} = \frac{\sigma_{max} + \sigma_{min}}{2}$$

$$\sigma_a = \text{alternating stress amplitude} = \frac{\sigma_{max} - \sigma_{min}}{2}$$

$$\Delta\sigma = \text{range of stress} = \sigma_{max} - \sigma_{min}$$

$$R = \text{stress ratio} = \frac{\sigma_{min}}{\sigma_{max}}$$

$$A = \text{amplitude ratio} = \frac{\sigma_a}{\sigma_m}$$

[23]For example, see refs. 1 or 15.

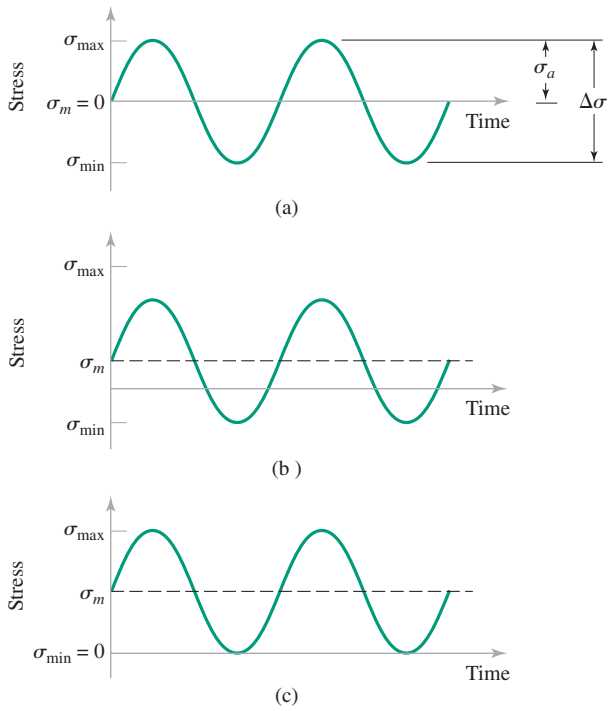

Figure 5.24
Several constant-amplitude stress-time patterns of interest. (a) Completely reversed; $R = -1$. (b) Nonzero-mean stress. (c) Released tension; $R = 0$.

Any two of the quantities just defined, except the combination σ_a and $\Delta\sigma$ or the combination A and R, are sufficient to completely describe the stress-time pattern.

A second type of stress-time pattern often encountered is the *nonzero-mean* spectrum shown in Figure 5.24(b). This pattern is very similar to the completely reversed case except that the mean stress is either tensile or compressive, in any event different from zero. The nonzero-mean case may be thought of as a static stress equal in magnitude to the mean σ_m with a superposed completely reversed cyclic stress of amplitude σ_a.

A special case of nonzero-mean stress, illustrated in Figure 5.24(c), is often encountered in practice. In this special case the minimum stress ranges from zero up to some tensile maximum and then back to zero. This type of stressing is often called *released tension*. For released tension it may be noted that $\sigma_m = \sigma_{max}/2$. A similar but less frequently encountered stress-time pattern is called released compression, where $\sigma_{max} = 0$ and $\sigma_m = \sigma_{min}/2$.

More complicated stress-time patterns are illustrated in Figure 5.25. In Figure 5.25(a) the mean stress is zero but there are two (or more) different stress amplitudes mixed together. In Figure 5.25(b), not only does the stress amplitude vary, but also the magnitude of

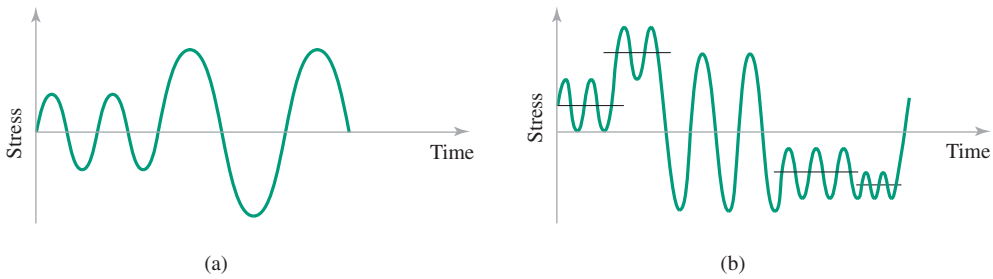

Figure 5.25
Stress-time patterns in which the amplitude changes or both mean and amplitude change to produce a more complicated stress spectrum. (a) Zero mean, changing amplitude. (b) Changing mean and amplitude.

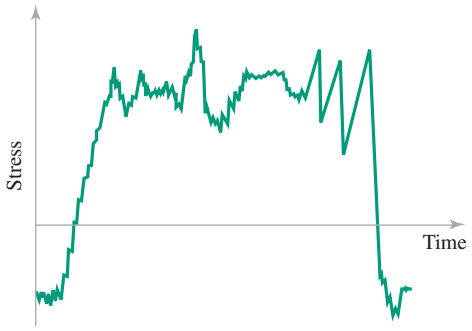

Figure 5.26
A quasi-random stress-time pattern that might be typical of an operational aircraft during any given mission.

the mean stress periodically changes, approaching a more realistic condition. Figure 5.26 illustrates a realistic stress-time pattern, as might be observed, for example, in an airframe structural member during a typical mission including refueling, taxi, takeoff, gusts, maneuvers, and landing. To effectively predict and prevent fatigue failures, procedures for assessing damage due to all of these various stress-time spectra are required.

Fatigue Strength and Fatigue Limit

Designing machine parts or structures that are subjected to fatigue loading is usually based on the results of laboratory fatigue tests using small polished specimens of the material of interest. To be successful in using small-specimen data, a designer must be aware of the merits and limitations of such data, including influences of size, surface finish, geometry, environment, speed, and many other factors. Basic fatigue data in the high-cycle life range are usually displayed on a plot of cyclic stress versus life. These plots, called *S-N curves*, constitute design information of fundamental importance for machine parts subjected to cyclic or repeated loadng.

Figure 5.27 illustrates the characteristic appearance of an *S-N* curve for a ferrous material. The curve is constructed by fitting it to data collected from laboratory tests of a large number of specimens at various cyclic stress amplitudes and zero-mean stress. Because of

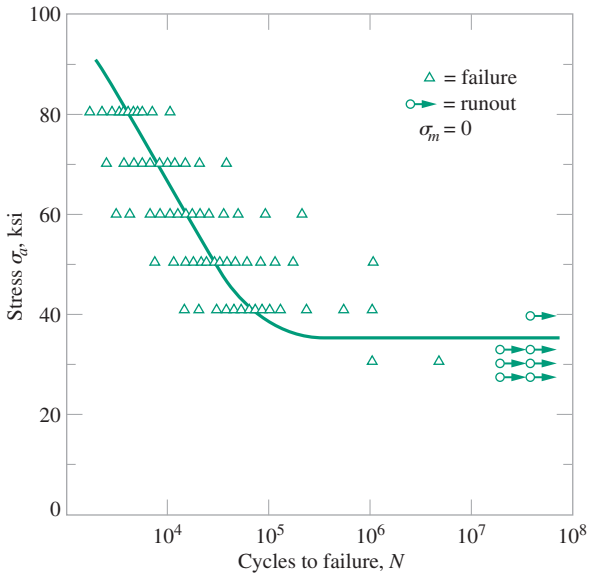

Figure 2.27
Plot of stress-life (*S-N*) data as they might be collected by laboratory fatigue testing of a new alloy.

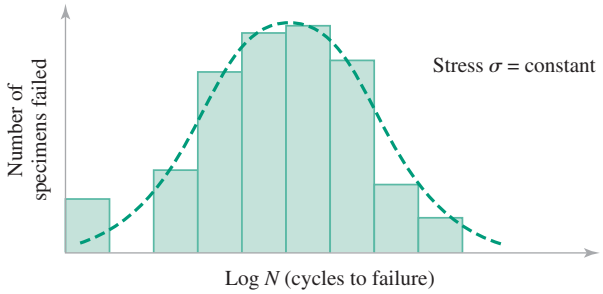

Figure 5.28
Distribution of fatigue specimen failures at a constant stress level as a function of logarithm of life.

the *scatter* of fatigue life data at any given stress level, the construction of the most appropriate curve through the data becomes a design issue of importance. A statistical description of fatigue failure data is usually used to facilitate construction of the most appropriate *S-N* curve. Using this approach, one would construct for each test stress level a *histogram*, such as the one shown in Figure 5.28, which shows the *distribution* of failures as a function of the logarithms of lives for the sample tested. Computation of the sample *mean* and *standard deviation*[24] permits estimation of the *probability of failure (P)* at each stress level. Points of equal probability of failure may then be connected to obtain curves of constant probability of failure on the *S-N* plot. A family of such *S-N-P* curves is shown in Figure 5.29 for 7075-T6 aluminum alloy. It is also of interest that the *reliability (R)* is defined to be 1 minus the probability of failure; hence $R = (1-P)$. Thus in Figure 5.29, the 10 percent probability of failure curve ($P = 0.10$) may alternatively be designated as the 90 percent reliability curve ($R = 0.90$), and some references may be found in the literature to these so-called *R-S-N* curves.

Usually, references in the literature to "the" *S-N* curve refer to the *mean* or 50 percent probability of failure curve unless otherwise specified. The mean *S-N* curves of Figure 5.30 distinguish two commonly observed types of response to cyclic loading. The

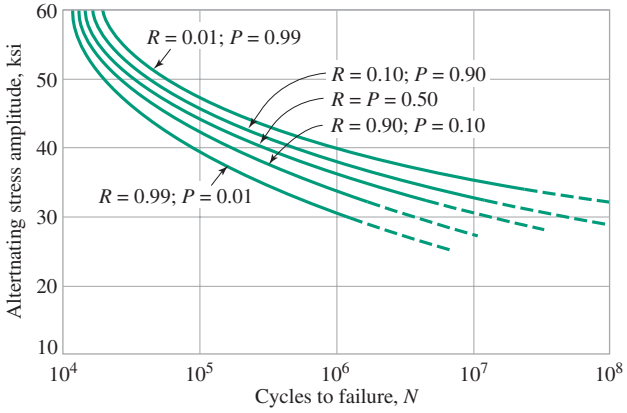

Figure 5.29
Family of *S-N-P* curves, or *R-S-N* curves for 7075-T6 aluminum alloy. Note: P = probability of failure; R = reliability = 1 − P. (Adapted from ref. 16, p. 117, Copyright © 1969, by permission from John Wiley & Sons, Inc.)

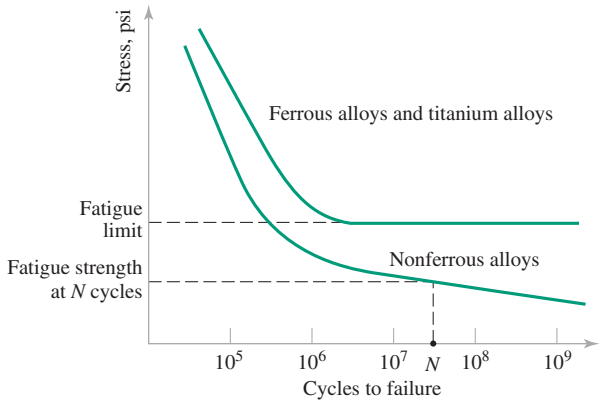

Figure 5.30
Two types of material response to cyclic loading.

[24]See, for example, ref. 1, Ch. 9.

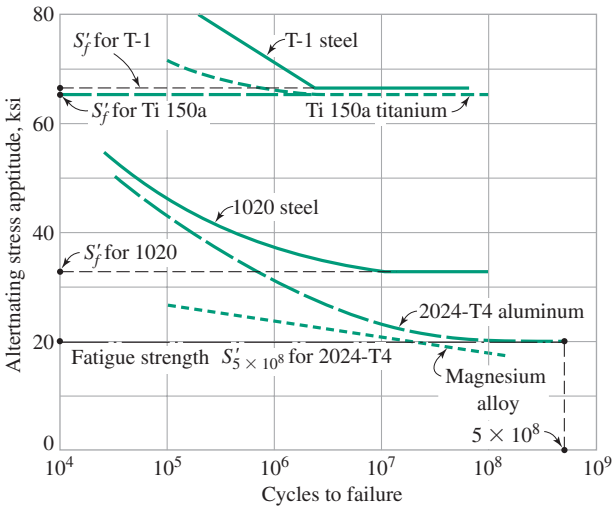

Figure 5.31
Effect of material composition on the *S-N* curve. Note that ferrous and titanium alloys exhibit well-defined fatigue limits whereas other alloy compositions do not. (Data from refs. 17 and 18.)

ferrous alloys and titanium exhibit a steep branch in the shorter life range, leveling off to approach a stress asymptote at longer lives. This stress asymptote is called the *fatigue limit*, S_f or S'_f (formerly called endurance limit) and is the stress level below which an infinite number of cycles could theoretically be sustained without failure. The symbol S_f is commonly used to denote fatigue limit of an *actual machine part*, while S'_f is fatigue limit of the material based on *small polished specimens*. The nonferrous alloys do not exhibit an asymptote, and the curve of stress versus life continues to drop off indefinitely. For such alloys there is *no fatigue limit*, and failure as a result of cyclic stress is only a matter of applying enough cycles. To characterize the failure response of most nonferrous materials, and of ferrous or titanium alloys in the finite life range, the term *fatigue strength at a specified life*, S_N or S'_N, is used; S_N denotes finite-life fatigue strength of a *component*, while S'_N is finite-life fatigue strength of the material based on *small polished specimens*. The specification of *fatigue strength* without specifying the corresponding life is meaningless. The specification of a *fatigue limit* always implies infinite life. Use of these terms is illustrated in Figure 5.31, which depicts *S-N* curves for several alloys.

Estimating *S-N* Curves

When designing a machine part to be subjected to fluctuating loads it is essential to obtain an *S-N* curve for the candidate material for which heat treatment, operating temperature, and other operating conditions match the application. If such an *S-N* curve can be found in the literature or in an available database, the curve may be used directly to design the part. If not, it may be possible to find an *S-N* curve for small polished specimens of the candidate material and modify it by using a series of appropriate factors as discussed later in connection with Table 5.3. If *S-N* data cannot be found for the candidate material it becomes necessary either to perform laboratory fatigue tests on small polished specimens (a lengthy and expensive process) or to attempt to estimate the basic *S-N* curve for the material. Although there is no direct connection between static strength and fatigue strength, purely empirical relationships *have* been documented by examining large bodies of existing data. These empirical observations allow a designer to estimate *S-N* curves from static ultimate tensile strength (S_{ut}) values. These estimated *S-N* curves are often accurate enough for the design task at hand, especially at the preliminary design stage. For

TABLE 5.3 Strength-Influencing Factors That May Affect *S-N* Curves

Influencing Factor	Symbol	Approximate Range	"Typical" Value[1]
Material composition	—	—	Specific *S-N* data required
Heat treatment	—	—	Specific *S-N* data required
Operating temperature	—	—	Specific *S-N* data required
Grain size and direction	k_{gr}	0.4–1.0	1.0
Welding	k_{we}	0.3–0.9	0.8
Geometrical discontinuity	k_f	0.2–1.0	Reciprocal of K_f; see 4.8
Surface condition	k_{sr}	0.2–0.9	0.7
Size effect	k_{sz}	0.5–1.0	0.9
Residual surface stress	k_{rs}	0.5–2.5	Specific data required; see 4.11
Fretting	k_{fr}	0.1–0.9	0.35 if fretting exists, 1.0 if no fretting; also see 2.11
Corrosion	k_{cr}	0.1–1.0	Specific data required
Operating speed	k_{sp}	0.9–1.2	1.0
Strength reliability required	k_r	0.7–1.0	0.9; also see Table 2.3
Configuration of stress-time pattern	—	—	See later section titled *Cumulative Damage Concepts and Cycle Counting*
Nonzero-mean stress	—	—	See later section titled *Nonzero-Mean Stress*
Damage accumulation	—	—	See later section titled *Cumulative Damage Concepts and Cycle Counting*

[1]These "typical" values may be used for solving problems in this text or for making preliminary design estimates when actual conditions are poorly known. However, any *critical* design situation would require a literature/database search or supporting laboratory experiments to establish more accurate values.

wrought-ferrous alloys, the *mean S-N* curve may be estimated for polished specimens by plotting on a semilog plot of strength versus log life the following:

1. Plot $S'_N = S_{ut}$ at $N = 1$ cycle.
2. Plot $S'_f = 0.5S_{ut}$ at $N = 10^6$ cycles if $S_{ut} \leq 200$ ksi

   or,

   Plot $S'_f = 100$ ksi at $N = 10^6$ cycles if $S_{ut} > 200$ ksi
3. Connect (1) with (2) by a straight line.
4. Construct a horizontal straight line from (2) toward very long lives.

This estimated mean (50 percent reliability) *S-N* curve may be supplemented if desired by using the standard normal variable X of Table 5.4 to calculate and construct estimated *S-N* curves with higher reliabilities.

TABLE 5.4 Strength Reliability Factors as a Function of Reliability Level

Reliability R (percent)	Corresponding Standard Normal Variable X (see Table 2.9)	Strength Reliability Factor k_r
90	1.282	0.90
95	1.645	0.87
99	2.326	0.81
99.9	3.090	0.75
99.995	3.891	0.69

For cast irons and cast steels a similar procedure may be used except that

$$S'_f = 0.4S_{ut} \quad \text{at} \quad N = 10^6 \text{ cycles} \quad \text{if} \quad S_{ut} \leq 88 \text{ ksi}$$

or

$$S'_f = 40 \text{ ksi} \quad \text{if} \quad S_{ut} > 88 \text{ ksi}$$

Guidelines for other alloys have been published as follows:[25]

Titanium alloys:	$S'_f = 0.45S_{ut}$	to	$0.65S_{ut}$	at	$N = 10^6$ cycles
Aluminum alloys:	$S'_N = 0.4S_{ut}$			at	$N = 5 \times 10^8$ cycles
Magnesium alloys:	$S'_N = 0.35S_{ut}$			at	$N = 10^8$ cycles
Copper alloys:	$S'_N = 0.2S_{ut}$	to	$0.5S_{ut}$	at	$N = 10^8$ cycles
Nickel alloys:	$S'_N = 0.3S_{ut}$	to	$0.5S_{ut}$	at	$N = 10^8$ cycles

It is very important to emphasize that these guidelines provide only *estimates*, to be used when pertinent *S-N* data are unavailable, and must be used with caution.

Stress-Life (*S-N*) Approach to Fatigue

For uniaxial states of cyclic stress the traditional *S-N* approach to fatigue design is straightforward in concept. Data are required for the material of interest, including effects of size, surface finish, geometry, and environment, and information is required on the cyclic loading to be applied to the part. From these, the size and shape of the part to provide the desired cyclic life may be determined. To implement the *S-N* approach, material data are best presented as *S-N* curves, such as those shown in Figure 5.30 or 5.31, or Figure E5.10 of Example 5.10. For example, if a part to be made of 2024-T4 aluminum has a design life requirement of 5×10^8 completely reversed stress cycles, its fatigue strength S'_N at a life $N = 5 \times 10^8$ cycles may be read from Figure 5.31 as 20,000 psi. This assumes that the part operates under conditions matching the conditions used to obtain the data for Figure 5.31. Also, since $S_{N=5\times10^8} = 20{,}000$ psi is a fatigue *failure* strength, an appropriate safety factor would typically be imposed for safe operation, as discussed in Chapter 2.

Factors That May Affect *S-N* Curves

As already mentioned, published *S-N* curves, unless otherwise labeled, are typically *mean value* curves for *small polished specimens*. Actual machine parts subjected to cyclic or fluctuating stress levels exhibit *S-N* responses different from small, polished-specimen curves, depending upon differences in composition, processing, environment, and operational factors. Thus the fatigue strength or fatigue limit of an actual machine part (S_N or S_f) is nearly always different (usually lower) from the fatigue strength or fatigue limit S'_N or S'_f read from a published *S-N* curve for small polished specimens of the same material. Furthermore, published *S-N* curves for small polished specimens are somewhat dependent upon the test method used to obtain the underlying data. The test method of choice in modern practice is to use computer-controlled closed-loop axial push-pull fatigue testing machines that apply uniformly distributed cyclic direct stresses to small polished specimens. Most *S-N* data presented in this textbook may be assumed to have been produced by uniform uniaxial cyclic stresses on small polished specimens, unless otherwise noted. Older small specimen *S-N* data found in the literature may have been obtained from cyclic *bending* tests, using either rotating or reciprocating bending machines. If such bending data are used as the basis for

[25] See ref. 6

obtaining fatigue strength or fatigue limit estimates for an actual machine part, as in (5-55) or (5-56), the fatigue limit values from the cycle bending data should be reduced by about 10 percent (because of the bending-stress gradients; see Figure 4.3) to be compatible with the uniformly stressed push-pull small specimen data used in this textbook.

The factors that may cause differences between the fatigue response of actual machine parts and small polished specimens are shown in Table 5.3 and briefly discussed in the following paragraphs. More detailed discussions may be found in the fatigue literature.[26]

To obtain an estimate for fatigue strength or fatigue limit of an actual machine part from small-polished-specimen *S-N* data and a knowledge of operational and environmental requirements for the part, the usual procedure is to utilize an expression of the form

$$S_f = k_\infty S'_f \tag{5-55}$$

or

$$S_N = k_N S'_N \tag{5-56}$$

depending upon whether fatigue limit, or fatigue strength corresponding to a design life of N cycles, is required. From Table 5.3 the expressions for k_∞ and k_N may be written as the products of pertinent influencing factors. Thus

$$k_\infty = (k_{gr} k_{we} k_f k_{sr} k_{sz} k_{rs} k_{fr} k_{cr} k_{sp} k_r)_\infty \tag{5-57}$$

and

$$k_N = (k_{gr} k_{we} k_f k_{sr} k_{sz} k_{rs} k_{fr} k_{cr} k_{sp} k_r)_N \tag{5-58}$$

It should be recognized that the various factors may have different values for finite-life design requirements as compared to infinite-life design specifications. Also, it should be noted that these procedures assume that no interactions occur between or among the various strength-influencing factors, an assumption not always justified. For example, the surface condition effect and corrosion effect may interact, or other effects may interact to produce unknown influences on the fatigue strength or fatigue limit. For this reason it is always advisable in practice to subject the final design to full-scale prototype testing under simulated service conditions.

Approximate ranges and "typical" values for many of the strength-influencing factors are shown in Table 5.3. While these may be helpful guidelines in approximating the fatigue strength or fatigue limit of a machine part, more specific values are usually required for any critical design situation, and a search of fatigue databases or fatigue literature is common practice. The following brief remarks relative to the entries of Table 5.3 are offered as additional guidance.

Material composition is the most basic factor in determining fatigue strength. As noted in the discussion of Figure 5.30, materials divide themselves into two broad groups with respect to *S-N* failure response. The ferrous alloys and titanium exhibit a rather well-defined fatigue limit, which is well established by the time 10^7 cycles of stress have been applied. The other nonferrous alloys do not exhibit a fatigue limit at all, and their *S-N* curves continue to fall off at lives of 10^8, 10^9, and larger numbers of cycles.

Heat treatment is also a strong influencing factor on the fatigue strength, just as it is in the case of static strength. Small-polished-specimen *S-N* data for which the specimen heat treatment corresponds to that proposed for the actual part under consideration is very useful in determining fatigue response of the part.

[26]See for example, ref. 1, 6, 17, 19–23.

Operating temperature may have a significant influence on fatigue strength. Generally, the fatigue strength is somewhat enhanced at temperatures below room temperature and diminished at temperatures above room temperature. In the range of temperature from around zero on the Fahrenheit scale to about one-half the absolute melting temperature, the effects of temperature are slight in most cases. At higher temperatures the fatigue strength diminishes significantly. Further, alloys that exhibit a fatigue limit at room temperature tend to lose this characteristic at elevated temperatures, making infinite-life design at elevated temperatures impossible.

Grain size and *grain direction* may play a significant role in fatigue strength. Fine-grained materials tend to exhibit fatigue properties that are superior to coarse-grained materials of the same composition. This superiority becomes less significant at elevated temperatures when the characteristic room temperature transgranular cracking gives way to intergranular cracking paths. When the cyclic loading direction is across the grain (transverse direction) of an anisotropic specimen or machine part, fatigue strength properties are inferior to fatigue strength when the loading direction is along the grain (longitudinal direction).

Welding produces a metallurgically nonhomogeneous region ranging from unheated parent metal through the heat-affected zone (HAZ), to the weld metal zone. In some cases the entire welded joint may be post-heat-treated, in which case the structure of weld metal, HAZ, and parent metal may become nearly identical; in some critical cases postweld machining operations may be used to restore geometrical uniformity. Even with such care (and expense), welded joints (as well as bolted, riveted, or bonded joints) tend to have a fatigue strength inferior to that of a monolithic part of the same material. Factors contributing to fatigue strength reduction in welded joints, in addition to the gradient in homogeneity across the weld zone, include cracking in weld metal or base metal due to postcooling shrinkage stresses, incomplete penetration, lack of fusion between weld metal and parent metal from prior welding passes, undercut at the edge of weld metal deposit, overlap of weld metal flowing beyond the fusion zone, slag inclusions, porosity, misshapen welds, or welds with surface defects. Some of the effects of welding on fatigue strength properties are illustrated in Figure 5.32.

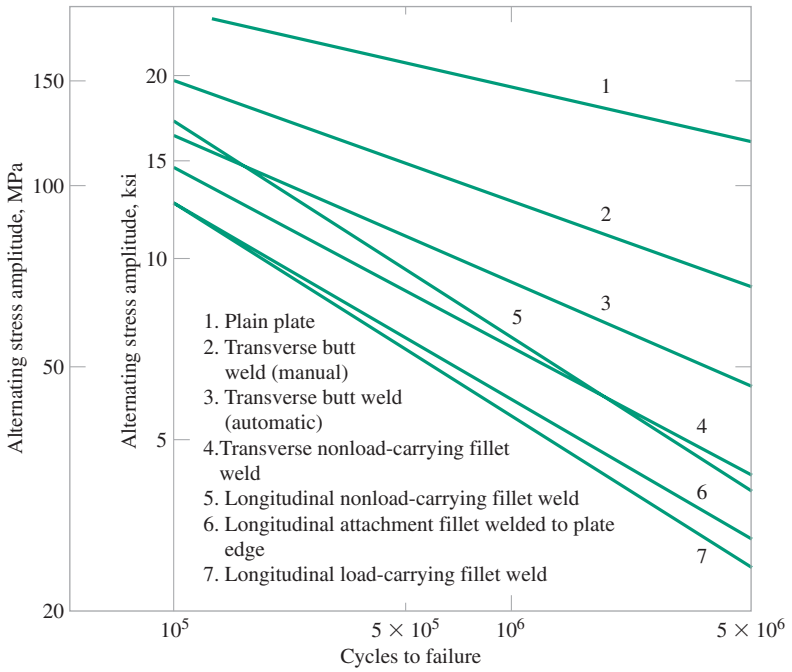

Figure 5.32
Effects of welding detail on the *S-N* curve of structural steels, with yield strengths in the range 30,000–52,000 psi. Tests were released tension ($\sigma_{min} = 0$) (Data from ref. 23.)

Stress concentration effects due to *geometrical discontinuities*, such as changes in shape or joint connections, may seriously diminish the fatigue strength of a machine part, even if the part is made of a ductile material. The severity of notches, holes, fillets, joints, and other stress raisers depends upon the relative dimensions, type of loading, and notch sensitivity of the material. A detailed discussion of stress concentration is presented in 5.3.

Surface condition is a very important factor in fatigue strength of a machine part since a very high proportion of all fatigue failures nucleate at the surface. Irregular surfaces and rough surfaces generally exhibit inferior fatigue properties as compared to smooth or polished surfaces, as illustrated in Figure 5.33. Cladding, plating, or coating may reduce the fatigue strength of the plated member because fatigue nuclei initiated in the plating continue to propagate into the base metal. This may cause a reduction in fatigue strength, as illustrated in Figure 5.34. Usually, however, the corrosion protection afforded by the plating more than offsets the strength loss due to plating.

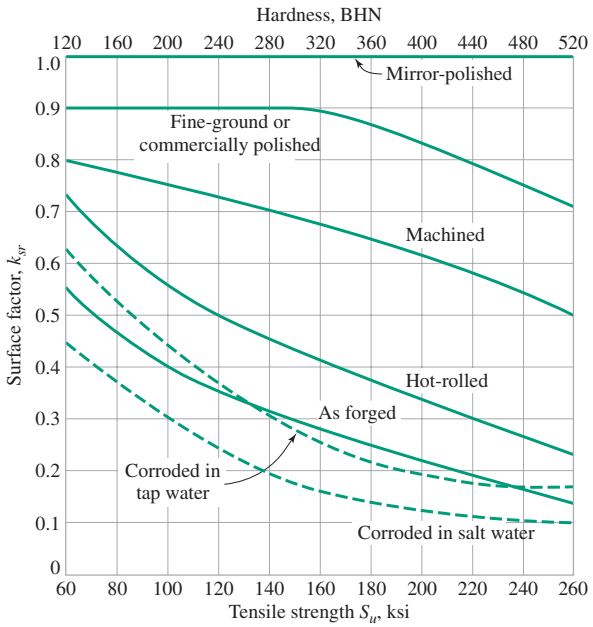

Figure 5.33
Reduction of fatigue strength due to surface finish (steel parts). (From ref. 6, reproduced with permission of The McGraw-Hill Companies.)

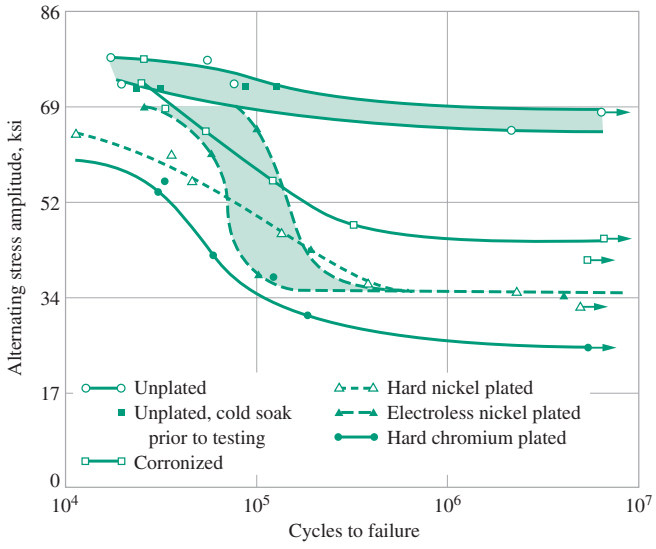

Figure 5.34
Effects of several electrodeposited coatings on the *S-N* curve of low-alloy steel at room temperature under axial tension-tension loading with $R = 0.02$. *Static ultimate strengths:* unplated, 172,300 psi; corronized, 177,700 psi; hard nickel plated, 176,100 psi; electroless nickel plated, 182,100 psi; hard aluminum plated, 162,400 psi. (Data from ref. 16, Copyright © 1969, adapted by permission from John Wiley & Sons, Inc.)

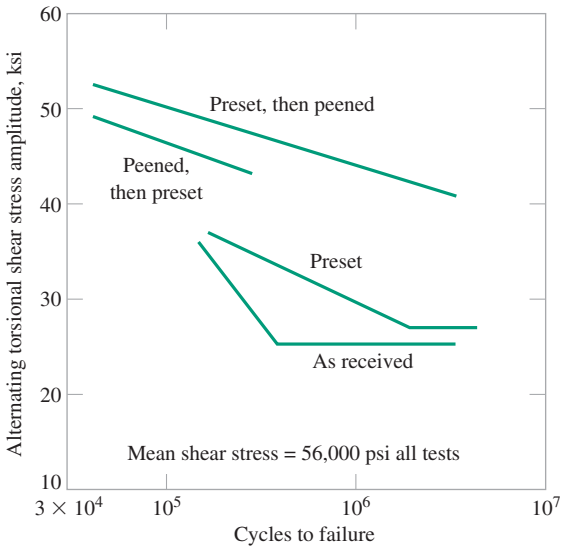

Figure 5.35
Effects of shot-peening and/or presetting on the *S-N* curve of hot wound helical coil springs made of 0.9 percent carbon steel. Spring details: hardness = Vickers DPH 550; wire diameter = $^1/_2$ inch; mean coil diameter = $2^5/_8$ inches; number of turns = 6; free length = $5^1/_{16}$ or 6 inches. (Data from ref. 24.)

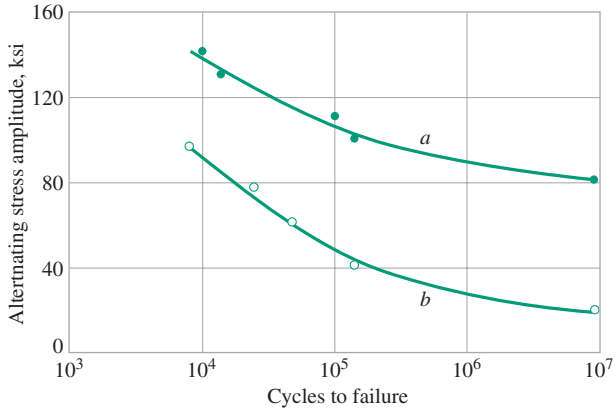

Figure 5.36
Effects of cold-rolling threads before and after heat treatment on the *S-N* curve for 220,000 psi ultimate strength bolts. (a) Rolled after heat treatment. (b) Rolled before heat treatment. (Data from ref. 16, Copyright © 1969, by permission from John Wiley & Sons, Inc.)

Larger specimens and machine parts exhibit a *size effect*, having lower fatigue strengths than smaller specimens of the same material. For example, the fatigue strength of a 6-inch-diameter machine part might be as much 15 or 20 percent lower than a one-half-inch-diameter specimen of the same material.

Residual stresses in the surface layer, whether induced intentionally or accidentally, may play an extremely important role in the overall fatigue response of a specimen or machine part. If the induced residual surface stresses are tensile, the fatigue strength is diminished. If the residual surface stresses are compressive, the fatigue strength is improved. Three common methods of inducing compressive residual surface stresses are shot-peening, cold-rolling, and presetting.[27] Figures 5.35 and 5.36 illustrate these effects. It is also notable that surface treatments such as shot-peening and cold-rolling not only improve the mean fatigue strength, but reduce the scatter (standard deviation) as well.

Fretting at the contacting surfaces of joints or connections may lead to a very significant reduction in fatigue strength of a machine part. As discussed in 2.9, the prediction of the fretting effect is difficult because many factors are involved. Experimental testing of the assembly under actual service conditions and loading should be undertaken for critical parts.

Corrosion tends to lower the fatigue strength, often by a large amount. Corrosive effects are specific to the combination of material composition and operating environment. Experimental testing of the machine part under service environment and loading should be employed for critical parts.

[27]Shot-peening involves uniform bombardment of the surface with a high-velocity stream of small steel spheres. Cold-rolling is accomplished by pressing a hard contoured-roller against the surface to be treated and uniformly rolling and translating the roller to cover the area to be cold worked. Presetting involves the application of a static overload on the part, in the direction of operational loads, to induce local yielding at stress concentrations and subsequent compressive residual stresses at these sites upon release of the static overload. Also, see 4.9.

Operating speeds in the range from about 200 cycles per minute (cpm) to about 7,000 cpm appear to have little effect on fatigue strength. Below 200 cpm there is often a small decrease in fatigue strength, and in the range 7,000 cpm to around 60,000 cpm many materials exhibit a significant increase in fatigue strength. Rest periods have no effect on fatigue strength.

Strength reliability, or reliability of fatigue strength, is usually based on the stresswise distribution of *S-N-P* data for small polished specimens of a particular material. Assuming the stresswise distribution of fatigue strengths to be *normal* is a reasonable and convenient procedure for estimating the strength reliability factor.[28] From any table for the cumulative distribution function[29] for the standard normal variable X, where

$$X = \left| \frac{S'_f(R) - S'_f}{\hat{\sigma}} \right| \tag{5-59}$$

and using the empirical estimate[30] for standard deviation of fatigue strength to be $\hat{\sigma} = 0.08S'_f$, the strength reliability factor may be expressed as

$$k_r = 1 - 0.08X \tag{5-60}$$

Based on this relationship, values for k_r are shown in Table 5.4 for a range of strength reliability values, R. If statistical data were available for the distributions of other factors listed in Table 5.3, a similar reliability approach could be taken for these influencing factors, but such data are not generally available.

In practice, the *configuration of the stress-time pattern* may take many forms, including sinusoidal, reversed ramp, superposed ripples, or distorted peaks as shown in Figure 5.37. Generally, the fatigue failure response seems to be relatively insensitive to changes

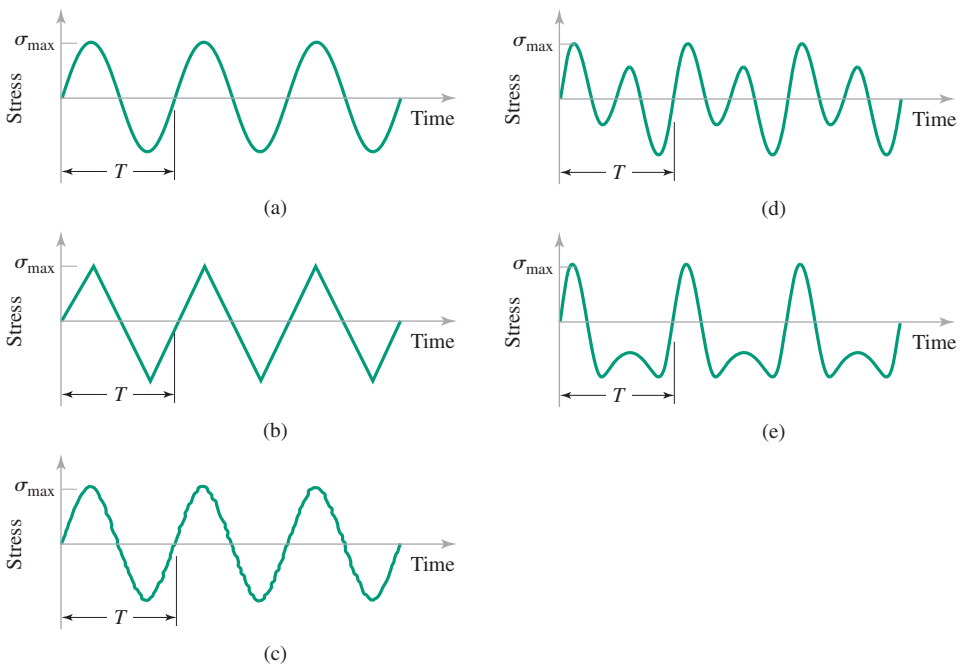

Figure 5.37
A variety of stress-time patterns used in evaluating fatigue behavior. (a) Completely reversed sinusoid. (b) Completely reversed ramp. (c) Superposed ripples. (d) Secondary peaks. (e) Distorted peaks.

[28]Although the Weibull distribution is widely agreed to be more accurate, its use is more cumbersome. See ref. 1, Ch. 9, for example.

[29]See, for example, Chapter 2, Table 2.9. [30]See ref. 24.

in wave shape as long as peak value and period are the same. When practical, however, it is better to account for each and every stress reversal by using a good *cycle counting method* such as the rain flow method discussed in the section "Cumulative Damage Concepts and Cycle Counting" below.

The magnitude of any *nonzero-mean stress* has an important influence on fatigue response and is discussed in detail in the next section. Likewise, the accumulation of fatigue damage caused by cyclic loading, or *cumulative damage*, is fully discussed in a later section.

Example 5.10 Estimating Fatigue Properties

A wrought carbon-steel alloy is known to have the static properties $S_u = 76{,}000$ psi, $S_{yp} = 42{,}000$ psi, and e (2 inches) $= 18$ percent, but fatigue properties cannot be located for the material. It is necessary to quickly estimate the fatigue properties for the preliminary design of a machine part for which the fluctuating loads will induce a stress spectrum with cyclic amplitudes in both the finite-life range and the infinite-life range.

a. How could the basic small-polished-specimen "*mean S-N* curve" be estimated for this material?

b. How could the $R = 99.9$ percent reliability *S-N* curve be estimated for the material?

Solution

a. Using the estimation guidelines for wrought-ferrous alloys with $S_{ut} < 200$ ksi (since $S_{ut} = S_u = 76{,}000$ psi),

$$S'_f = 0.5(S_u) = 0.5(76{,}000) = 38{,}000 \text{ psi}$$

$$S'_{N=1} = S_u = 76{,}000 \text{ psi}$$

Plotting these values on semilog coordinates and connecting them in accordance with the guideline procedures gives the mean ($R = 50$ percent) *S-N* curve shown in Figure E5.10.

b. To obtain an estimate of the $R = 99.9$ percent reliability *S-N* curve, the expression for standard normal variable X given in (5-59) may be utilized. Since the $R = 99.9$ percent

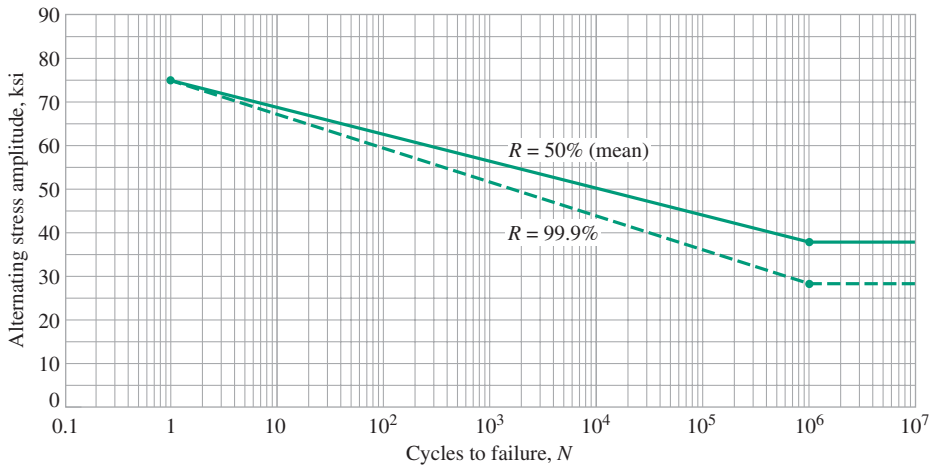

Figure E5.10
Estimated *S-N* curves for fatigue strength reliability levels of 50 percent (mean) and 99.9 percent.

curve must lie below the mean curve, $S'_f\,(R = 99.9)$ is less than the mean value S'_f. Hence, for this case, from (5-59)

$$X = \frac{S'_f - S'_f(R = 99.9)}{\hat{\sigma}} \tag{1}$$

Therefore

$$S'_f = 38{,}000 \text{ psi}$$

and using the estimated standard deviation $\hat{\sigma}$ discussed just after (5-59),

$$\hat{\sigma} = 0.08S'_f = 0.08(38{,}000) = 3040 \text{ psi}$$

with the Table 5.4 value for X corresponding to $R = 99.9$ percent reliability

$$X(R = 99.9) = 3.09$$

equation (1) may be solved for $S'_f\,(R = 99.9)$ to give

$$S'_f(R = 99.9) = S'_f - X\hat{\sigma}$$

or

$$S'_f(R = 99.9) = 38{,}000 - 3.09(3040) = 28{,}600 \text{ psi}$$

Plotting $S'_f(R = 99.9) = 25{,}600$ psi on the *S-N* coordinates of Figure E5.10 at 10^6 cycles, and connecting to the point S_{ut} at $N = 1$ cycle, results in the estimated 99.9 percent reliability *S-N* curve, as shown.

Example 5.11 Failure Mode Assessment

An axially loaded straight cylindrical bar of diameter $d = 12.5$ mm is to be made of 2024-T4 aluminum with ultimate strength of $S_u = 469$ MPa, yield strength $S_{yp} = 331$ MPa, and fatigue properties shown in Figure 5.31. The bar is to be subjected to a completely reversed axial force of 27 kN, and must last for at least 10^7 cycles.

a. What is the governing failure mode?

b. Is failure predicted to occur?

Solution

a. The two most probable candidates for governing failure mode are yielding and fatigue. Both should be calculated to determine which one governs.

b. For yielding, from (2-17) FIPTOI

$$\sigma \geq S_{yp}$$

Now

$$\sigma = \frac{F}{A_o} = \frac{4F}{\pi d^2} = \frac{4(27000)}{\pi(0.0125)^2} = 220 \text{ MPa}$$

Example 5.11 Continues

Hence, for yielding, FIPTOI

$$220 \geq 331$$

Therefore, failure by yielding is *not* predicted to occur.
For fatigue, at a design life requirement of $N_d = 10^7$ cycles, FIPTOI

$$\sigma_{max} \geq S_{N=10^7}$$

From Figure 5.31, using the curve for 2024-T4 aluminum for 10^7 cycles, the fatigue strength at $N = 10^7$ cycles may be read as

$$S_{N=10^7} = 23 \text{ ksi} \approx 159 \text{ MPa}$$

Hence, for fatigue at a design life requirement of $N_d = 10^7$ cycles, FIPTOI

$$220 \geq 159$$

Therefore, failure by fatigue is predicted. That is, fatigue failure would be expected before the design life of 10^7 cycles is achieved.

Example 5.12 Design for Infinite Fatigue Life

An axially loaded straight cylindrical bar is to be made of 1020 steel, with fatigue properties as shown in Figure 5.31. The bar is to be subjected to a completely reversed axial force of 7000 lb maximum. Fatigue is the governing failure mode.

If infinite life is desired for this part, what is the minimum diameter that the bar should be made?

Solution

Since fatigue is the governing failure mode and infinite life is desired, the stress in the bar must be just below the fatigue limit, read from Figure 5.31 for 1020 steel as

$$S_f' = 33{,}000 \text{ psi}$$

The maximum stress in the bar is

$$\sigma_{max} = \frac{F_{max}}{A_o} = \frac{F_{max}}{\left(\frac{\pi d^2}{4}\right)}$$

or

$$d = \sqrt{\frac{4F_{max}}{\pi \sigma_{max}}}$$

Setting $\sigma_{max} = S_f' = 33{,}000$ psi (incipient failure),

$$d = \sqrt{\frac{4(7000)}{\pi(33{,}000)}} = 0.52 \text{ inch}$$

Thus the minimum diameter for infinite life would be 0.52 inch. Again, it must be cautioned that this assumes that the *S-N* curve of Figure 5.31 properly reflects the conditions of the axially loaded bar in terms of size, surface finish, geometry, environment, and other influence factors. Further, statistical scatter or reliability level should also be

considered in establishing the bar diameter, using techniques such as the ones described in Example 5.9(b). As a practical matter, the small-polished-specimen *S-N* curve in Figure 5.31 would typically be modified by using appropriate factors from Table 5.3 to reflect the operating conditions, and a safety factor would be used to protect against remaining uncertainties.[31]

Example 5.13 Estimating Fatigue Properties of a Part

A wrought-carbon steel alloy with $S_u = 524$ MPa, $S_{yp} = 290$ MPa, and $e(50\text{ mm}) = 18\%$, is to be considered a candidate material for a proposed machine part to be used under the following conditions:

a. The part is to be lathe-turned from a bar of the wrought-steel alloy.

b. The part is uniform in shape at the critical point.

c. Operating speed is 3600 rpm.

d. A very long life is desired.

e. A strength reliability factor of 99.9% is desired.

It is desired to make a preliminary design estimate of the pertinent fatigue properties of the candidate material so that approximate size of the part can be estimated.

Solution

Since a very long life is desired, the fatigue property of primary interest is the fatigue limit of the part, S_f.

From (5-52) and (5-54),

$$S_f = k_\infty S_f' \quad \text{and} \quad k_\infty = (k_{gr}k_{we}k_f k_{sr}k_{sz}k_{rs}k_{fr}k_{cr}k_{sp}k_r)$$

Using estimation guidelines for wrought-ferrous alloys with $S_u < 200$ ksi(1379 MPa)

$$S_f' = 0.5(S_u) = 0.5(524) = 262 \text{ MPa}$$

To evaluate k_∞, each of the influence factors must be evaluated. Referring to Table 5.3 and the discussion following the table:

$k_{gr} = 1.0$ (from Table 5.3)
$k_{we} = 1.0$ (no welding anticipated)
$k_f = 1.0$ (uniform shape specified)
$k_{sr} = 0.65$ (see Figure 5.33)
$k_{sz} = 0.9$ (size unknown; use Table 5.3)
$k_{rs} = 1.0$ (no information available; later review essential)
$k_{fr} = 1.0$ (no fretting anticipated)
$k_{cr} = 1.0$ (no information available; later review essential)
$k_{sp} = 1.0$ (moderate; use Table 5.3)
$k_r = 0.75$(from Table 5.4 for $R = 99.9$)

Now we evaluate k_∞ as

$$k_\infty = (1.0)(1.0)(1.0)(0.65)(0.9)(1.0)(1.0)(1.0)(1.0)(0.75) = 0.43875 = 0.44$$

[31]See Chapter 2.

Example 5.13 Continues

The fatigue limit is therefore

$$S_f = 0.44(262) = 115.3 \text{ MPa}$$

Thus, the estimated fatigue limit for the part is 115.3 MPa. Using an appropriate safety factor with S_f would allow calculation of the approximate size of the part to produce infinite life.

Nonzero-Mean Stress

Fatigue failure data collected in the laboratory for small polished specimens are most often obtained for completely reversed, or *zero-mean* alternating stresses. Many, if not most, service applications involve *nonzero-mean* cyclic stresses. It is very important, therefore, to be able to predict the influence of mean stress on fatigue behavior so that completely reversed small-polished-specimen *S-N* data may be utilized to design machine parts subjected to nonzero-mean cyclic stresses.

High-cycle fatigue data collected from a series of experiments devised to investigate combinations of alternating stress amplitude σ_a and mean stress σ_m may be characterized by a plot of σ_a versus σ_m for any specified failure life of N cycles, such as Figure 5.38. As shown, the failure data points typically tend to cluster about a curve that passes through the point $\sigma_a = S_N$ at $\sigma_m = 0$ and the point $\sigma_m = S_u$ at $\sigma_a = 0$. As shown, failure is very sensitive to the magnitude of mean stress in the tensile mean-stress region but rather insensitive to the magnitude of mean stress in the compressive mean-stress region. Nonzero-mean failure data are available in the literature for some materials, usually presented as *constant lifetime diagrams*, or *master diagrams*, such as those shown in Figure 5.39. If a designer is fortunate enough to find such data for a proposed material that match the operating conditions for the application of interest, of course these data should be used. If pertinent data are not available, an estimate of the influence of nonzero-mean stress may be made by utilizing a mathematical model that approximates data of the type shown in Figure 5.38. Numerous successful models have been developed for this purpose.[32] Well known amongst these models and accepted as representing the experimental data are those due to Goodman (now called the *modified Goodman relationship*) and Gerber. The modified Goodman relationship provides a simple linear estimate, whereas Gerber provides a parabolic estimate. Modified Goodman lines used to approximate the data are constructed on a plot of σ_a

Figure 5.38
Simulated high-cycle fatigue failure data showing the influence of mean stress.

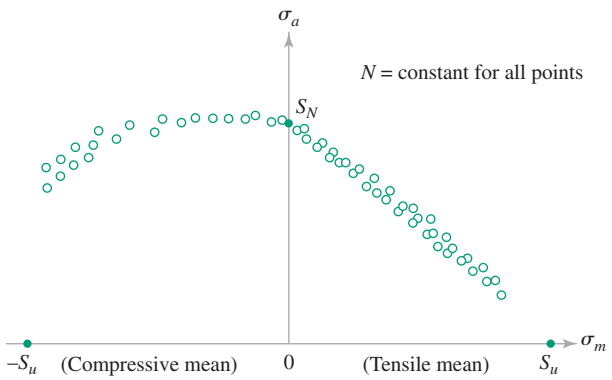

[32]See, for example, ref. 25, 26.

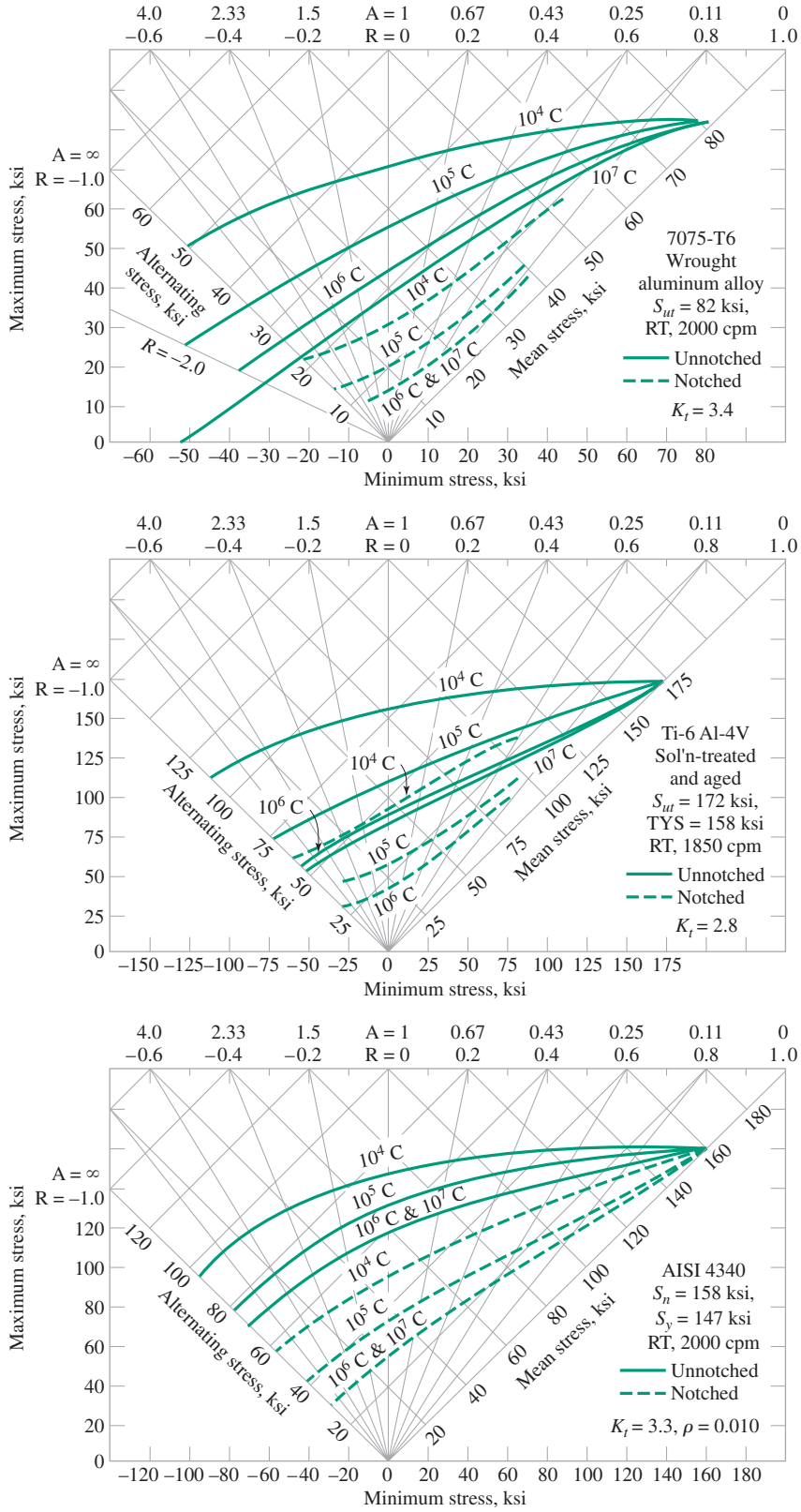

Figure 5.39
Master diagrams for alloys of steel, aluminum, and titanium. (From ref. 27, pp. 317, 322).

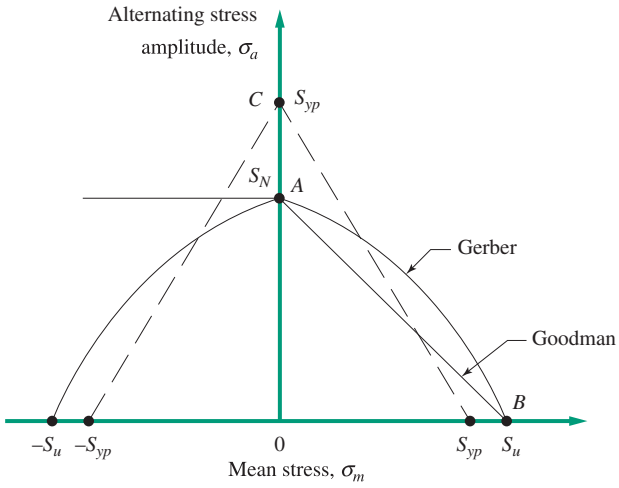

Figure 5.40
Modified Goodman and Gerber diagram representing fatigue failure at a life of N cycles.

versus σ_m by connecting the points S_N on the σ_a axis to S_u on the σ_m axis in the tensile mean-stress region and passing a second line horizontally through S_N in the compression mean-stress region. The Gerber parabola is constructed on a plot of σ_a versus σ_m by connecting the points S_N on the σ_a axis to S_u, and $-S_u$ on the σ_m axis in the tension-compression mean-stress region. These lines, shown in Figure 5.40, approximate the data illustrated in Figure 5.38 for a specified constant failure lifetime, N. Other failure lines would give similar curves but would change since the magnitude of S_N depends on failure life. Also it must be recognized that if $|\sigma_{max}|$ or $|\sigma_{min}|$ exceed yield strength values of the material, failure by yielding will occur. Thus yielding failure lines may be plotted from $\sigma_a = S_{yp}$ on the σ_a axis to $\sigma_m = \pm S_{yp}$ on the σ_m axis, as shown in Figure 5.40 by dashed lines.

Any combination of σ_a and σ_m that plots above either the solid or dashed lines in Figure 5.40 represents failure in a life shorter than N cycles, either by fatigue or by yielding. Writing an equation for line $S_N - S_u$ in the point-intercept form for the tensile mean-stress region,

$$y = mx + b \tag{5-61}$$

which becomes

$$\sigma_a = -\frac{S_N}{S_u}\sigma_m + S_N \tag{5-62}$$

Recalling that

$$\sigma_a = \sigma_{max} - \sigma_m \tag{5-63}$$

and substituting into (5-62),

$$\sigma_{max} - \sigma_m + \frac{S_N}{S_u}\sigma_m = S_N \tag{5-64}$$

or

$$\sigma_{max} - \sigma_m \left[\frac{S_u - S_N}{S_u}\right] = S_N \tag{5-65}$$

Defining the terms

$$m_t \equiv \frac{S_u - S_N}{S_u} \tag{5-66}$$

and

$$R_t \equiv \frac{\sigma_m}{\sigma_{max}} \tag{5-67}$$

equation (5-65) may be rewritten as

$$\sigma_{max} = \frac{S_N}{1 - m_t R_t} \tag{5-68}$$

To clarify, σ_{max} in this equation represents the cyclic maximum stress that, with the presence of mean stress σ_m, will cause failure in the same number of cycles as S_N at zero-mean stress. To recognize that this is therefore a "strength parameter," we set

$$\sigma_{max} \equiv S_{max-N} \tag{5-69}$$

Further, σ_{max} may not exceed S_{yp} either, or yielding will occur. Summarizing then, for the tensile mean-stress region,

$$S_{max-N} = \frac{S_N}{1 - m_t R_t} \qquad \text{for} \quad \sigma_m \geq 0 \quad \text{and} \quad S_{max-N} \leq S_{yp}$$

or

$$S_{max-N} = S_{yp} \qquad \text{for} \quad \sigma_m \geq 0 \quad \text{and} \quad S_{max-N} \geq S_{yp} \tag{5-70}$$

where

$$m_t = \frac{S_u - S_N}{S_u}$$

and

$$R_t = \frac{\sigma_m}{\sigma_{max}}$$

By a similar reasoning process for the compressive mean-stress region, σ_{min} represents the cyclic minimum stress that, with the presence of mean stress σ_m, will cause failure in the same number of cycles as S_N at zero-mean stress. Again, $|\sigma_{min}|$ may not exceed $|S_{yp}|$ or yielding will occur. Thus for the compressive mean-stress region

$$S_{min-N} = \frac{-S_N}{1 - m_c R_c} \qquad \text{for} \quad \sigma_m \leq 0 \quad \text{and} \quad S_{min-N} \geq -S_{yp}$$

or

$$S_{min-N} = -S_{yp} \qquad \text{for} \quad \sigma_m \leq 0 \quad \text{and} \quad S_{min-N} \leq -S_{yp} \tag{5-71}$$

where

$$m_c = 1$$

and

$$R_c = \frac{\sigma_m}{\sigma_{min}}$$

Referring to Note 1 of Figure 5-40, and solving (5-62) from a different perspective, modified Goodman expressions may be developed for an *equivalent completely reversed cyclic stress*, σ_{eq-CR}. This stress σ_{eq-CR} is a *calculated* completely reversed cyclic stress that would produce failure in exactly the same number of cycles N as would the actual

nonzero-mean cyclic stress that has amplitude σ_a and mean σ_m. Thus any nonzero-mean cyclic stress may be transformed into an *equivalent* completely reversed cyclic stress of amplitude σ_{eq-CR} that induces fatigue damage at the same rate cycle-by-cycle. Using this approach for the tensile mean-stress region

$$\sigma_{eq-CR} = \frac{\sigma_a}{1 - \dfrac{\sigma_m}{S_u}} \qquad \text{for} \quad \sigma_m \geq 0 \qquad \text{and} \quad \sigma_{max} \leq S_{yp}$$

or

$$\sigma_{eq-CR} = S_{yp} \qquad \text{for} \quad \sigma_m \geq 0 \qquad \text{and} \quad \sigma_{max} \geq S_{yp} \tag{5-72}$$

and for the compressive mean-stress region

$$\sigma_{eq-CR} = \sigma_a \qquad \text{for} \quad \sigma_m \leq 0 \qquad \text{and} \quad |\sigma_{min}| \leq |-S_{yp}|$$

or

$$\sigma_{eq-CR} = |-S_{yp}| \qquad \text{for} \quad \sigma_m \leq 0 \qquad \text{and} \quad |\sigma_{min}| \geq |-S_{yp}| \tag{5-73}$$

For the Gerber parabola, any combination of σ_a and σ_b that plots above either the dashed line or the solid curved line in Figure 5.40 again represents failure at a shorter life than N cycles, either by fatigue or yielding. Writing an equation for the Gerber parabola yields the form

$$y = -ax^2 + b$$

which becomes

$$\sigma_a = -\frac{S_N}{S_u^2}\sigma_m^2 + S_N \tag{5-74}$$

Again, referring to Note 1 of Figure 5.40 and solving (5-74) for an equivalent completely reversed cyclic stress, σ_{eq-CR}, we have only at the tensile mean-stress region

$$\sigma_{eq-CR} = \frac{\sigma_a}{\left[1 - \left(\dfrac{\sigma_m}{S_u}\right)^2\right]} \qquad \text{for } \sigma_m \geq 0 \text{ and } \sigma_{\max} \leq S_{yp}$$

or

$$\sigma_{eq-CR} = S_{yp} \qquad \text{for} \quad \sigma_m \geq 0 \quad \text{and} \quad \sigma_{\max} \geq S_{yp} \tag{5-75}$$

The Gerber parabola is limited to tensile mean stresses because it incorrectly predicts a harmful effect for compressive mean stresses.[33] For compressive mean stresses ($\sigma_m \leq 0$), equations (5-73) should be used.

In all equations from (5-70) through (5-75), it should be noted that if the design objective is infinite life, S_f should be substituted for S_N everywhere.

Example 5.14 Design to Account for Nonzero Mean Stress

A low-alloy steel link is to be made from a solid cylindrical bar subjected to an axial cyclic force that ranges from a maximum of 270 kN tension to a minimum of 180 kN compression. The static material properties are $S_u = 690$ MPa, $S_{yp} = 524$ MPa, and elongation in 50 mm of 25%. Calculate the diameter the link should be to provide infinite life.

[33] See ref. 28, page 430.

Solution

Since the link is cyclically loaded and infinite life is desired, the fatigue limit S_f is the material property of primary interest; yielding should also be checked. Using the estimation guidelines, since $S_u < 200$ ksi(1379 MPa),

$$S_f' = 0.5(S_u) = 0.5(690) = 345 \text{ MPa}$$

Following the procedures of Example 5.12, and utilizing Table 5.3, the fatigue limit for the part may be estimated as

$$S_f = k_\infty S_f' = k_\infty(345)$$

Since little information is given, the influencing factors of Table 5.3 may be estimated as:

$k_{gr} = 1.0$ (from Table 5.3)
$k_{we} = 1.0$ (no welding anticipated)
$k_f = 1.0$ (uniform shape specified)
$k_{sr} = 0.65$ (lathe-turned)
$k_{sz} = 0.9$ (from Table 5.3)
$k_{rs} = 1.0$ (no information available; later review essential)
$k_{fr} = 1.0$ (no fretting anticipated)
$k_{cr} = 1.0$ (no information available; later review essential)
$k_{sp} = 1.0$ (from Table 5.3)
$k_r = 0.9$ (from Table 5.4 For $R = 90$)

$k_\infty = (1.0)(1.0)(1.0)(0.65)(0.9)(1.0)(1.0)(1.0)(1.0)(0.9) = 0.5265 = 0.53$
$S_f = 0.53(345) = 182.9$ MPa

From the loading specification it may be noted that we have a case of nonzero-mean cyclic loading. Since stress is proportional to loading,

$$\sigma_m = \frac{P_m}{A} = \frac{\frac{1}{2}\left(P_{max} + P_{\min}\right)}{A} = \frac{\frac{1}{2}\left((270) + (-180)\right)}{A} = \frac{45}{A}$$

where A is the unknown cross-sectional area of the link.

Since the mean stress is tensile, (5-67) may be used with

$$S_{N=\infty} = S_f = 182.9 \text{ MPa}$$

$$m_t = \frac{690 - 182.9}{690} = 0.735$$

$$R_t = \frac{\sigma_m}{\sigma_{max}} = \frac{P_m/A}{P_{max}/A} = \frac{P_m}{P_{max}} = \frac{45}{270} = 0.167$$

so that (5-67) gives

$$S_{max-\infty} = \frac{S_N}{1 - m_t R_t} = \frac{182.9}{1 - (0.735)(0.167)} = 208.5 \text{ MPa} \qquad (1)$$

Since

$$S_{max-\infty} = 208.5 < S_{yp} = 524$$

Yielding does not occur and (1) is valid.

To obtain the required diameter, we set the maximum applied stress σ_{max} equal to the infinite-life strength for the specified nonzero-mean loading, giving

$$\sigma_{max} = S_{max-\infty}$$

Example 5.14 Continues

or

$$\frac{P_{max}}{A} = \frac{4P_{max}}{\pi d^2} = 208.5$$

Solving for the diameter

$$d = \sqrt{\frac{4P_{max}}{\pi(208.5)}} = \sqrt{\frac{4(270 \times 10^3)}{\pi(208.5 \times 10^6)}} = 0.0406 \text{ m} = 0.041 \text{ mm}$$

Thus the required link diameter is 41 mm to provide infinite life. It should be noted, however, that in practice a safety factor would also be imposed, and the required "safe" diameter would be somewhat larger than the 41 mm just calculated.

Example 5.15 Design for Selected Reliability

A one-inch-square bar is to be subjected to an axial cyclic force that ranges from a maximum of 36,000 lb (tension) to a minimum of −22,000 lb (compression). The material is the wrought-steel alloy of Example 5.10 and the operating conditions are the same as those specified in Example 5.10. A fatigue strength reliability level of 99.9 percent is desired. How many cycles of operation would be expected before failure occurs?

Solution

Since the material and the operating conditions are exactly the same as for Example 5.10, and a fatigue strength reliability level of 99.9 percent is specified, the R = 99.9 percent curve of Figure E5.10 in Example 5.10 represents the appropriate estimate of the S-N curve for the one-inch-square bar.

From the known loading and geometry,

$$\sigma_{max} = \frac{P_{max}}{A} = \frac{36{,}000}{(1)^2} = 36{,}000 \text{ psi}$$

$$\sigma_{min} = \frac{P_{min}}{A} = \frac{-22{,}000}{(1)^2} = -22{,}000 \text{ psi}$$

$$\sigma_m = \frac{\sigma_{max} + \sigma_{min}}{2} = \frac{36{,}000 + (-22{,}000)}{2} = 7000 \text{ psi}$$

$$\sigma_a = \frac{\sigma_{max} - \sigma_{min}}{2} = \frac{36{,}000 - (-22{,}000)}{2} = 29{,}000 \text{ psi}$$

Since the mean stress is tensile, from (5-72)

$$\sigma_{eq-CR} = \frac{\sigma_a}{1 - \dfrac{\sigma_m}{S_u}} = \frac{29{,}000}{1 - \left(\dfrac{7000}{76{,}000}\right)} = 31{,}940 \text{ psi}$$

Also,

$$\sigma_{max} = 36{,}000 < S_{yp} = 42{,}000$$

so yielding *does not* occur and σ_{eq-CR} is valid.

Since the mean stress is positive and yielding does not occur, Gerber's equation could also be applied. Hence, using (5-75)

$$\sigma_{eq-CR} = \frac{\sigma_a}{1 - \left(\dfrac{\sigma_m}{S_u}\right)^2} = \frac{29{,}000}{1 - \left(\dfrac{7{,}000}{76{,}000}\right)^2} = 29{,}248 \text{ psi}$$

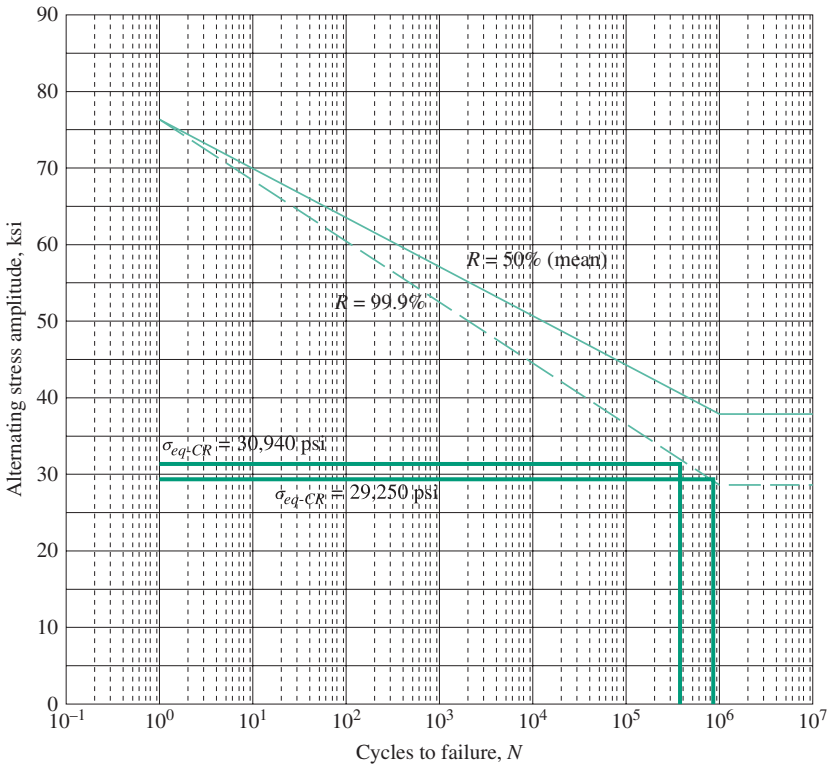

Figure E5.15
Estimated *S-N* curve for fatigue strength reliability levels of 50 percent (mean) and 99.9 percent.

Referring to the *S-N* curve of Figure E5.15 for $R = 99.9$ percent, repeated below as Figure E5.15, and reading from the curve on the stress axis at

$$S = \sigma_{eq-CR} = 31{,}940 \text{ psi}$$

and

$$S = \sigma_{eq-CR} = 29{,}248 \text{ psi}$$

Then across to intersect the *S-N* curve, the intersections occur at $N = 378{,}000$ cycles, using Goodman and $N = 827{,}000$ cycles using the Gerber approach.

The number of cycles to failure could also be obtained from the following equation since the *S-N* curve is taken as a straight line

$$S = c + b\log(N)$$

Applying the conditions that at $N = 1$, $S = S_u$ and at $N = 10^6$, $S'_f = 0.5S_u$, gives

$$c = S_u, \quad b = \frac{S'_f - S_u}{log(N)}$$

and

$$N = 10^{(S-c)/b}$$

From above, for $R = 99.9$ percent, $S'_f = 28{,}600$ psi (see example 5.10) and, therefore,

$$c = 76{,}000 \qquad b = \frac{28{,}600 - 76{,}000}{\log(10^6)} = -7900$$

Example 5.15 Continues

For $S = 31{,}940$ psi,

$$N = 10^{(31940-76000)/(-7900)} = 378{,}000 \text{ cycles}$$

and for $S = 29{,}250$ psi

$$N = 10^{(29250-76000)/(-7900)} = 827{,}000 \text{ cycles}$$

The appropriate fatigue failure curve to be used depends on how well the material property is known.

Cumulative Damage Concepts and Cycle Counting

Nearly all machines operate over a *spectrum* of speeds or loads, giving rise to a *spectrum* of alternating stress amplitudes and mean stresses, as illustrated for example in Figures 5.25 and 5.26. Such variations in stress amplitudes and mean stresses make the direct use of standard *S-N* curves inapplicable because these curves are developed and presented for *constant* stress amplitude operation (and usually for zero-mean stress). Therefore it becomes important to a designer to have available a theory or hypothesis, verified by experimental observations, that will permit good design estimates to be made for operation under conditions of spectrum loading using standard constant-amplitude *S-N* curves.

The basic postulate adopted by all fatigue investigators is that operation at any given cyclic stress amplitude will produce *fatigue damage*, the seriousness of which will be related to the number of cycles of operation at that stress amplitude and also related to the total number of cycles that would be required to produce failure of an undamaged specimen or part at that stress amplitude. It is further postulated that the damage incurred is permanent, and operation at several different stress amplitudes in sequence will result in an accumulation of total damage equal to the sum of damage increments accrued at all the different stress levels. When the total accumulated damage reaches a critical value, fatigue failure occurs.

Of the many damage theories proposed,[34] the most widely used is a linear theory first proposed by Palmgren in 1924 and later developed by Miner in 1945. This linear theory is referred to as the *Palmgren–Miner hypothesis* or the *linear damage rule*. The theory, based on the postulate that there is a linear relationship between fatigue damage and *cycle ratio n/N*, may be described using the *S-N* plot shown in Figure 5.41.

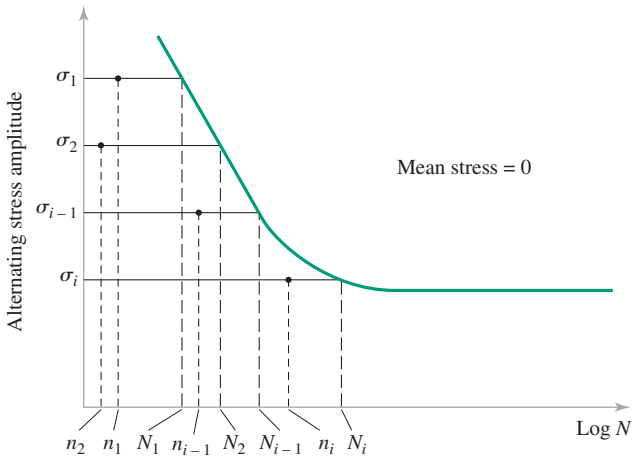

Figure 5.41
Illustration of spectrum loading where n_i cycles of operation are accrued at each of the different corresponding stress levels σ_i, and the N_i are cycles to failure at each σ_i.

[34]See, for example, ref. 1, Ch. 8.

By definition of the *S-N* curve, operation at a constant stress amplitude σ_1 will produce complete damage, or failure, in N_1 cycles. Operation at stress amplitude σ_1 for a number of cycles n_1, smaller than N_1, will produce a smaller fraction of damage, say D_1. D_1 is usually termed the *damage fraction*. Operation over a spectrum of i different stress levels results in a damage fraction D_i for each of the different stress levels σ_i in the spectrum. When these damage fractions sum to unity, failure is predicted; that is, failure is predicted to occur if (FIPTOI)

$$D_1 + D_2 + \cdots + D_i \geq 1 \tag{5-76}$$

The Palmgren–Miner hypothesis asserts that the damage fraction D_i at any stress level σ_i is linearly proportional to the ratio of number of cycles of operation n_i to the total number of cycles N_i that would produce failure at that stress level; that is,

$$D_i = \frac{n_i}{N_i} \tag{5-77}$$

By the Palmgren–Miner hypothesis then, (5-76) becomes FIPTOI

$$\frac{n_1}{N_1} + \frac{n_2}{N_2} + \cdots + \frac{n_i}{N_i} \geq 1 \tag{5-78}$$

or FIPTOI

$$\sum_{j=1}^{n} \frac{n_j}{N_j} \geq 1 \tag{5-79}$$

This is a complete statement of the Palmgren–Miner hypothesis, or the linear damage rule. It has one sterling virtue, namely, *simplicity;* and for this reason it is widely used. Further, other much more complicated cumulative damage theories typically do not yield a significant improvement in failure prediction reliability. Perhaps the most significant shortcomings of the linear damage rule are that no influence of the *order* of application of various stress levels is recognized, and damage is assumed to accumulate at the same rate at a given stress level *without regard to past history*. Nevertheless, the Palmgren–Miner hypothesis may be used with good success most of the time.

Example 5.16 Zero-Mean Spectrum Loading

An alloy steel strut for an experimental aircraft application is fabricated from a supply of material that has an ultimate strength of 135,000 psi, yield strength of 120,000 psi, elongation of 20 percent in 2 inches, and fatigue properties under test conditions that match the actual operating conditions, as shown in the table of experimental results in Table E5.16.

The cross-sectional area of the strut is 0.10 in^2 and buckling has been found not to be a problem due to the selected cross-sectional shape. In service, the strut is to be subjected to the following spectrum of completely reversed axial loads during each duty cycle:

$$P_a = 11{,}000 \text{ lb for } 1000 \text{ cycles}$$
$$P_b = 8300 \text{ lb for } 4000 \text{ cycles}$$
$$P_c = 6500 \text{ lb for } 500{,}000 \text{ cycles}$$

This duty cycle is to be repeated three times during the life of the strut.

Assuming fatigue to be the governing failure mode, would this strut be expected to survive all three duty cycles, or would it fail prematurely?

Example 5.16 Continues

TABLE E5.16 Fatigue Test Data for Strut Material

Stress Amplitude (psi)	Cycles to Failure, N
110,000	6,600
105,000	9,500
100,000	13,500
95,000	19,200
90,000	27,500
85,000	39,000
80,000	55,000
75,000	87,000
73,000	116,000
71,000	170,000
70,000	220,000
69,000	315,000
68,500	400,000
68,000	∞

Solution

Based on the data from Table E5.16, an *S-N* curve may be plotted as shown in Figure E5.16.

Since the completely reversed axial loads are given, and the cross-sectional area of the strut is given as 0.10 in^2, the completely reversed stress spectrum for each duty cycle may be calculated as

$$\sigma_a = \frac{P_a}{A} = \frac{11{,}000}{0.10} = 110{,}000 \text{ psi}; \qquad n_a = 1000 \text{ cycles}$$

$$\sigma_b = \frac{P_b}{A} = \frac{8300}{0.10} = 83{,}000 \text{ psi}; \qquad n_b = 4000 \text{ cycles}$$

$$\sigma_c = \frac{P_c}{A} = \frac{6500}{0.10} = 65{,}000 \text{ psi}; \qquad n_c = 500{,}000 \text{ cycles}$$

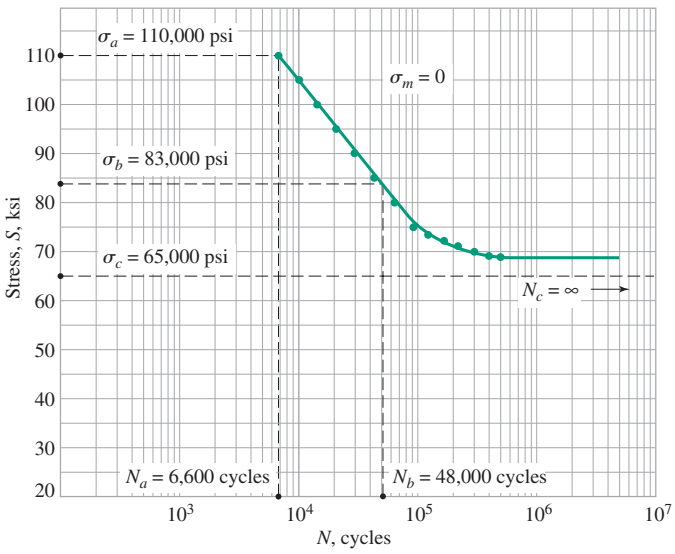

Figure E5.16
***S-N* curve for alloy steel data from Table E5.16.**

Reading from the *S-N* curve of Figure E5.16 for completely reversed stresses σ_a, σ_b, and σ_c, respectively,

$$N_a = 6600 \text{ cycles to failure}$$
$$N_b = 48{,}000 \text{ cycles to failure}$$
$$N_c = \infty \quad (\text{since } \sigma_c < S_f = 68{,}000)$$

Furthermore, three such duty cycles must be sustained without failure.

To determine whether failure would be predicted, the Palmgren–Miner linear damage rule formulated in (5-79) may be used. Hence FIPTOI

$$\sum_{j=1}^{n} \frac{n_j}{N_j} \geq 1$$

or, FIPTOI

$$3\left[\frac{n_a}{N_a} + \frac{n_b}{N_b} + \frac{n_c}{N_c}\right] \geq 1$$

Using the results above, FIPTOI

$$3\left[\frac{1000}{6600} + \frac{4000}{48{,}000} + \frac{500{,}000}{\infty}\right] \geq 1$$

or FIPTOI

$$3[0.152 + 0.083 + 0] = 0.706 \geq 1$$

Since this failure expression is not satisfied, the strut would be predicted to *survive* the three duty cycles.

For the simple case of a stress spectrum composed of a sequence of uniaxial completely reversed stresses of various amplitudes, the estimation of cumulative damage and prediction of failure are relatively straightforward, as illustrated by Example 5.16. If the stress spectrum is more complicated, as shown, for example, in Figures 5.25 or 5.26, the task of evaluating cumulative damage and even the task of *counting the cycles* in the spectrum become much more difficult. Although numerous cycle counting methods have been devised,[35] the *rain flow cycle counting method* is probably more widely used than any other method and will be the only method presented in this text.

To use the rain flow method, the stress-time history (stress-time spectrum) is plotted to scale on a stress-time coordinate system so that the time axis is vertically downward, and the lines connecting the stress peaks are imagined to be a series of sloping roofs, as shown, for example, in Figure 5.42. Several rules are imposed on "raindrops" flowing down these sloping roofs so that the rain flow may be used to define cycles and half-cycles of fluctuating stress in the spectrum.

Rain flow is initiated by placing raindrops successively at the inside of each peak (maximum) or valley (minimum).

The rules are as follows:

1. *The rain is allowed to flow on the roof and drip down to the next slope except that, if it initiates at a valley, it must be terminated when it comes opposite a valley more negative than the valley from which it initiated.* For example, in Figure 5.42 the flow begins at

[35]See, for example, ref. 1, p. 289.

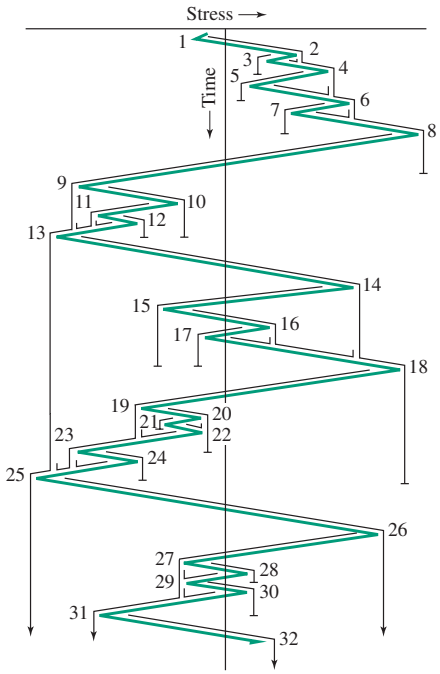

Figure 5.42
Example of rain flow cycle counting method. (After ref. 29.)

valley 1 and stops opposite valley 9, valley 9 being more negative than valley 1. A half-cycle is thus counted between valleys 1 and peak 8.

2. *Similarly, if the rain flow initiates at a peak, it must be terminated when it comes opposite a peak more positive than the peak from which it initiated.* For example, in Figure 5.42 the flow begins at peak 2 and stops opposite peak 4, thus counting a half-cycle between peak 2 and valley 3.

3. *A rain flow must also stop if it meets the rain from a roof above.* For example, in Figure 2.30, the flow beginning at valley 3 ends beneath peak 2. Using these rules, every part of the stress-time history is counted once and only once.

4. *If cycles are to be counted over the duration of a duty cycle or a "mission profile" block that is to be repeated block after block, the cycle counting should be started by initiating the first raindrop either at the most negative valley or the most positive peak, and continuing until all cycles in a complete block have been counted in sequence.* This procedure assures that a complete stress cycle will be counted between the most positive peak and most negative valley in the block.

The nonzero-mean stress cycles may be converted to equivalent completely reversed cycles by utilizing (5-72) or (5-73).

To determine the fatigue damage in each cycle associated with the equivalent completely reversed spectrum, an *S-N* curve for the material must be available or estimated using the techniques presented in Example 5.10 and the preceding discussion.

Finally, damage is summed by utilizing the Palmgren–Miner linear damage rule (5-79) as illustrated in Example 5.16.

It should be clear that for most real-life design cases the prediction techniques just described are practical only with the help of a digital computer program designed to carry forth the tedious cycle-by-cycle analyses involved. Many such programs are available.[36]

[36]See, for example, ref. 15, App. 5A.

Example 5.17 Cycle Counting, Nonzero-Mean Loading, and Fatigue Life

The stress-time pattern shown in Figure E5.17A is to be repeated in blocks. Using the rain flow cycle counting method and the *S-N* curve of Figure E5.17B, estimate the time in hours of testing required to produce failure.

Solution

The stress-time pattern of Figure E5.17A is first rotated so that the time axis is vertically downward, as shown in Figure E5.17C. Following the rules for rain flow cycle counting, the count is started at a minimum valley, as shown for raindrop (1) of the time-shifted block in Figure E5.17C.

Data for each raindrop, read from Figure E5.17C, are recorded in Table E5.17. Values for σ_{eq-CR} are calculated using (5-72) and (5-73). Values of N corresponding to each raindrop's σ_{eq-CR} value are read from the completely reversed *S-N* curve of Figure E5.17B.

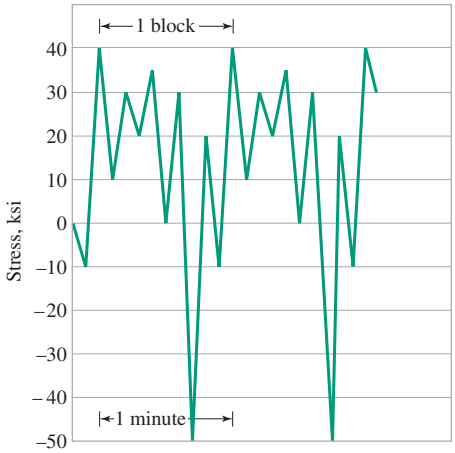

Figure E5.17A
Stress-time pattern applied.

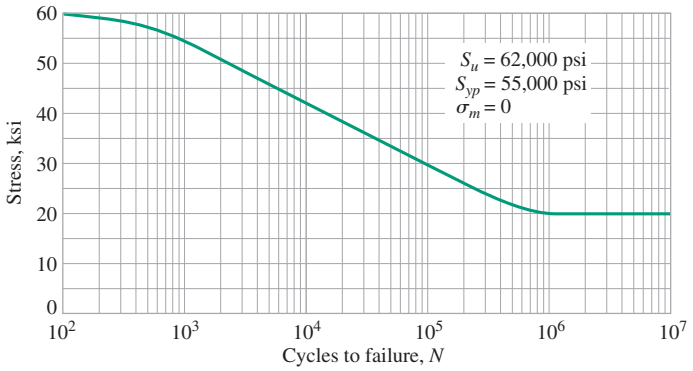

Figure E5.17B
***S-N* curve.**

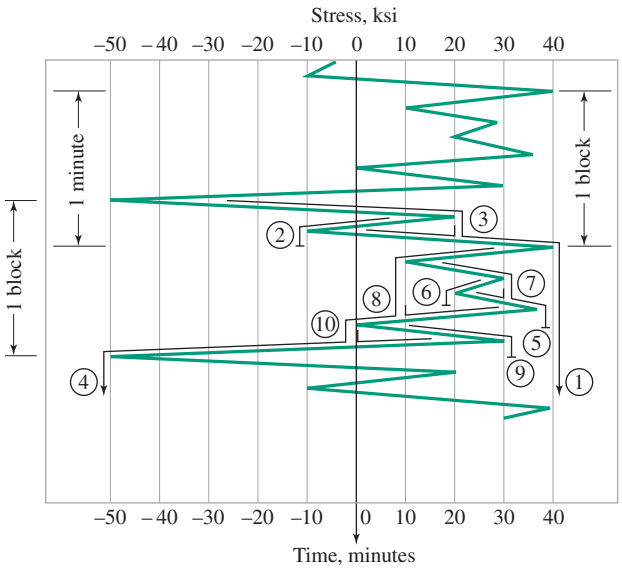

Figure E5.17C
Stress-time pattern oriented for rain flow cycle counting.

Example 5.17 Continues

TABLE E5.17 Rain Flow Data for One "Block" of the Stress-Time Pattern

Raindrop Number	n, cycles	σ_{max}, ksi	σ_{min}, ksi	σ_m, ksi	σ_a, ksi	σ_{eq-CR}, ksi	N, cycles
1,4 @ $\frac{1}{2}$ cycle each	1	40	–50	–5	45	45	6×10^3
2,3 @ $\frac{1}{2}$ cycle each	1	20	–10	5	15	16.3	∞
5,8 @ $\frac{1}{2}$ cycle each	1	35	10	22.5	12.5	19.6	∞
6,7 @ $\frac{1}{2}$ cycle each	1	30	20	25	5	8.4	∞
9,10 @ $\frac{1}{2}$ cycle each	1	30	0	15	15	19.8	∞

Based on the Palmgren–Miner linear damage rule of (5-79), FIPTOI

$$B_f \sum_{j=1}^{5} \frac{n_j}{N_j} \geq 1$$

using B_f to denote the number of block to failure.

From Table E5.17 it may be noted that only raindrops 1 and 4 will produce a nonzero cycle ratio.

Thus FIPTOI

$$B_f \left(\frac{n_{1,4}}{N_{1,4}} \right) \geq 1$$

Using the equal sign, which corresponds to incipient failure, and reading numerical values from Table E5.17,

$$B_f \left(\frac{1}{6 \times 10^3} \right) = 1$$

or

$$B_f = 6 \times 10^3 \text{ blocks to failure}$$

At 1 block/minute, as indicated in Figures E5.17A and E5.17C, the predicted time to failure in hours, H_f, would be

$$H_f = \left(\frac{6 \times 10^3 \text{ blocks}}{\text{min}} \right) \left(\frac{1 \text{ min}}{\text{block}} \right) \left(\frac{1 \text{ hr}}{60 \text{ min}} \right) = 100 \text{ hr to failure}$$

Multiaxial Cyclic Stresses

Uniaxial cyclic stressing has been implicit in all of the discussion thus far in 5.6. Most real design situations, including rotating shafts, pressure vessels, power screws, springs, gears, flywheels, and many other machine elements, may involve *multiaxial* states of cyclic stress. Because of the complexities and costs in producing multiaxial fatigue failure data, only a limited body of such data exists. Consequently, no consensus has yet been reached on the best approach to prediction of failure under multiaxial fatigue stresses; however, various proposals have been discussed in recent books on fatigue analysis.[37] The approach adopted in this text involves the concept of *equivalent stress* to define a uniaxial equivalent to the

[37]See, for example, refs. 1, 19, 21, and 25.

actual multiaxial state of cyclic stresses, including both the alternating stress amplitudes and mean stresses.

Fracture Mechanics (*F-M*) Approach to Fatigue

In the introductory paragraphs of section 5.6 it was noted that fatigue is a progressive failure process that involves three phases: the initiation of crack nuclei, propagation of cracks until one reaches an unstable size, and finally, a sudden catastrophic separation of the affected part into two or more pieces. In the discussion of the *S-N* approach to fatigue design and analysis just completed, the three phases are lumped together in an *S-N* curve that represents a final failure locus for a part or specimen subjected to known fluctuating loads. The transitions from initiation to propagation to final fracture cannot be identified from an *S-N* curve, and the *S-N* approach does not require such information. Physically, however, the three phases have been well documented and the separate modeling of each phase in sequence has been under intense development. The results of these efforts have led to an approach to fatigue called the *fracture mechanics (F-M)* approach. An extensive database has now been established to support the *F-M* method and it has in recent years been very successfully used in the analysis and design of machine parts subjected to cyclic loads. A brief discussion of the *F-M* approach is included here, but much more complete discussions may be found in the recent literature on fatigue.[38]

Crack Initiation Phase

The most widely accepted approach to the prediction of crack initiation life is the *local stress-strain* approach. While the details of the local stress-strain approach are complicated, the concepts are not. The basic premise is that the local fatigue response of the small critical zone of material at the crack initiation site, usually at the root of a geometrical discontinuity, is analogous to the fatigue response of a small smooth laboratory specimen subjected to the same cyclic strains and stresses as the critical zone. This concept is illustrated in Figure 5.43. The number of cycles required to *initiate a crack* in the critical zone, N_i, is postulated to be equal to the number of cycles to *produce failure* of the small smooth specimen in a laboratory test under the same cyclic strains and stresses. Digital computer simulation of the smooth specimen failure process then allows the prediction of N_i if appropriate cyclic material response data are available.

To proceed with the analysis, the prediction model must contain the ability to

1. Compute local stresses and strains, including means and ranges, from the applied loads and geometry of the structure or machine part.
2. Count cycles and associate mean and range values of stress and strain with each cycle.
3. Convert nonzero-mean cycles to equivalent completely reversed cycles.
4. Compute fatigue damage during each cycle from stress and/or strain amplitudes and cyclic materials properties.
5. Compute damage cycle-by-cycle and sum the damage to give the desired prediction of N_i.

Many of these steps may be accomplished using methods already developed earlier in 5.6. Rain flow cycle counting (Example 5.16) may be used for item (2), modified Goodman relationships (Example 5.15) for item (3), and Palmgren–Miner linear damage rule (Example 5.16) for item (5). Items (1) and (4) require further discussion.

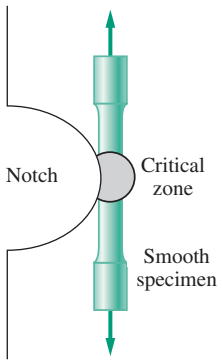

Figure 5.43
Smooth specimen analog of material at critical point in the structure. (See ref. 30.)

[38]See, for example, refs. 1, 19, 21, and 25.

To compute local stresses and strains from the external loading and geometry, a modified version of the Neuber Rule[39] for estimating theoretical stress concentration factors leads to the expression

$$\Delta\sigma\Delta\varepsilon = \frac{(K_f\ \Delta S)^2}{E} \tag{5-80}$$

where

$\Delta\sigma$ = local stress *range*
$\Delta\varepsilon$ = local strain *range*
ΔS = nominal[40] stress *range*
K_f = fatigue stress concentration factor[41]
E = Young's modulus of elasticity

From other work,[42] an empirical expression for the cyclic stress-strain curve[43] satisfactory for most engineering metals has been developed as

$$\frac{\Delta\varepsilon}{2} = \frac{\Delta\sigma}{2E} + \left[\frac{\Delta\sigma}{2k'}\right]^{1/n'} \tag{5-81}$$

where k' and n' are material constants, the *cyclic* strength coefficient and *cyclic* strain-hardening exponent, respectively. Values for k' and n' may be found from the intercept and slope of an experimentally determined log-log plot of cyclic stress amplitude $\Delta\sigma/2$ versus cyclic strain amplitude $\Delta\varepsilon/2$. Values for many materials may be found in the literature.[44] With known values of material properties E, k', and n', the fatigue stress concentration factor K_f, and readily calculable value of nominal stress range ΔS, equations (5-80) and (5-81) may be solved simultaneously to find values for local stress range $\Delta\sigma$ and local strain range $\Delta\varepsilon$.

To compute the local fatigue damage associated with equivalent completely reversed stress and strain ranges for each cycle, it is necessary to have experimental failure data for strain amplitude versus cycles to failure (crack initiation), N_i, often plotted as strain amplitude versus *reversals* to failure (crack initiation), $2N_i$, as illustrated in Figure 5.44.

Noting from Figure 5.44 that total strain amplitude may be expressed as the sum of elastic strain amplitude plus plastic strain amplitude, each linear with cycles or reversals to failure (crack initiation) on a log-log plot, an empirical expression for total strain amplitude versus cycles to crack initiation, N_i, has been developed as[45]

$$\frac{\Delta\varepsilon}{2} = \frac{\sigma'_f}{E}(2N_i)^b + \varepsilon'_f(2N_i)^c \tag{5-82}$$

The constants b and σ'_f/E are the slope and one-reversal intercept of the elastic line in Figure 5.44, and the constants c and ε'_f are the slope and one-reversal intercept of the plastic line in Figure 5.44. The values of the cyclic material properties σ'_f (cyclic true fracture strength) and ε'_f (cyclic true fracture ductility) must be experimentally determined. With

[39]See, for example, ref. 1, p. 283.

[40]Stress calculated assuming no stress concentration effect; note that the use here of S for *stress* deviates from the usual policy in this text of reserving S to denote strength.

[41]See 5.3.

[42]See ref. 30, p. 7.

[43]Usually significantly different from the static stress-strain curve. See, for example, ref. 1, pp. 284–285.

[44]See, for example, ref. 31.

[45]See ref. 29.

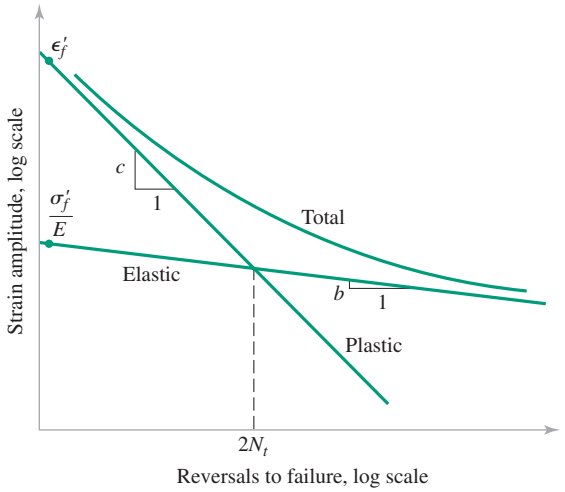

Figure 5.44
Schematic representation of elastic, plastic, and total strain amplitude versus fatigue life. (After ref. 29.)

known cyclic material properties equation (5-82) may be used to calculate the number of cycles to crack initiation, N_i, for any given total strain amplitude, $\Delta\varepsilon/2$.

All five steps of the local stress-strain approach may therefore be completed if the cyclic material properties data are available and the applied nominal stress spectrum is known.

Example 5.18 Fatigue Crack Initiation Life

Experimentally determined values for the properties of a martensitic steel have been found to be $S_u = 1482$ MPa, $S_{yp} = 1379$ MPa, $K_{Ic} = 81$ MPa$\sqrt{\text{m}}$, $e(50\text{ mm}) = 20\%$, $k' = 1069$ MPa, $n' = 0.15$, $\varepsilon'_f = 0.48$, $\sigma'_f = 2000$ MPa, $b = -0.091$, and $c = -0.60$. A direct tension member made of this alloy has a single semicircular edge notch that results in a fatigue stress concentration factor[46] of 1.6. The rectangular net section of the member at the root of the notch is 9 mm thick by 36 mm wide. A completely reversed axial force of 70 kN amplitude is applied to the tension member.

a. How many cycles would you estimate that it would take to initiate a fatigue crack at the notch root?

b. What length would you estimate this crack to be at the time it is initiated by the calculation of part (a)?

Solution

a. The nominal stress amplitude S_a may be calculated as

$$S_a = \frac{F_a}{A} = \frac{70\,000}{(0.009)(0.036)} = 216 \text{ MPa}$$

Hence the nominal stress range ΔS is given by

$$\Delta S = 2S_a = 2(216) = 432 \text{ MPa}$$

Using (5-75)

$$\Delta\sigma\Delta\varepsilon = \frac{[1.6(432 \times 10^6)]^2}{207 \times 10^9} = 2.31 \text{ MPa} \qquad (1)$$

[46]See 5.3.

Example 5.18 Continues

Next, from (5-76), using the results from (1)

$$\frac{\Delta\varepsilon}{2} = \frac{\Delta\sigma}{2(207 \times 10^9)}\left(\frac{\Delta\varepsilon}{\Delta\varepsilon}\right) + \left[\frac{\Delta\sigma}{2(1069 \times 10^6)}\left(\frac{\Delta\varepsilon}{\Delta\varepsilon}\right)\right]^{1/0.15}$$

$$\frac{\Delta\varepsilon}{2} = \frac{2.3 \times 10^6}{414 \times 10^9(\Delta\varepsilon)} + \left[\frac{2.3 \times 10^6}{2138 \times 10^6(\Delta\varepsilon)}\right]^{1/0.15}$$

$$\frac{(\Delta\varepsilon)^2}{2} = 5.56 \times 10^{-6} + 1.63 \times 10^{-20}(\Delta\varepsilon)^{(1-1/0.15)}$$

$$\Delta\varepsilon = \sqrt{1.11 \times 10^{-5} + 3.26 \times 10^{-20}(\Delta\varepsilon)^{-5.67}}$$

This can be iterated to the solution

$$\Delta\varepsilon = 3.64 \times 10^{-3} \text{ m/m}$$

Then, from (5-77)

$$\frac{3.64 \times 10^{-3}}{2} = \frac{2000 \times 10^6}{207 \times 10^9}(2N_i)^{-0.091} + 0.48(2N_i)^{-0.6}$$

$$1.82 \times 10^{-3} = 9.07 \times 10^{-3}(N_i)^{-0.091} + 0.317(N_i)^{-0.6}$$

This can be iterated to

$$N_i = 4.8 \times 10^7 \text{ cycles to initiation}$$

b. There is no known method for calculating the length of a newly initiated fatigue crack. The length must either be measured from an experimental test or estimated from experience. Often, if no other information is available, a newly initiated crack is assumed to be approximately $a_i = 1.3$ mm

Crack Propagation and Final Fracture Phases

As discussed in 5.5, the concepts of linear elastic fracture mechanics may be employed to predict the size of a crack in a given structure or machine part that will, under specified loadings, propagate spontaneously to final fracture. This *critical crack size*, a_{cr}, may be determined, for example, by solving (5-52) for crack size, which then (by definition) becomes a_{cr} when the applied stress σ is given its maximum value. Thus, from (5-52)

$$a_{cr} = \frac{1}{\pi}\left[\frac{K_c}{C\sigma_{max}}\right]^2 \tag{5-83}$$

Further, *if plane strain conditions are met*, as defined by (5-53), K_c becomes equal to the plane strain fracture toughness K_{Ic}, and (5-83) becomes

$$a_{cr} = \frac{1}{\pi}\left[\frac{K_{Ic}}{C\sigma_{max}}\right]^2 \tag{5-84}$$

A fatigue crack that has been initiated by cyclic loading, or any other preexisting flaw in the material, may be expected to grow under sustained cyclic loading until it reaches the critical size, a_{cr}, from which it will propagate spontaneously to catastrophic failure in accordance with the laws of fracture mechanics. Typically, the time for a fatigue-initiated crack to grow to critical size is a significant portion of the life of the machine part. Thus, not only is it necessary to understand the crack initiation phase and the definition of critical crack size but an understanding of the growth of a crack from initial size a_i to critical size a_{cr} is also essential.

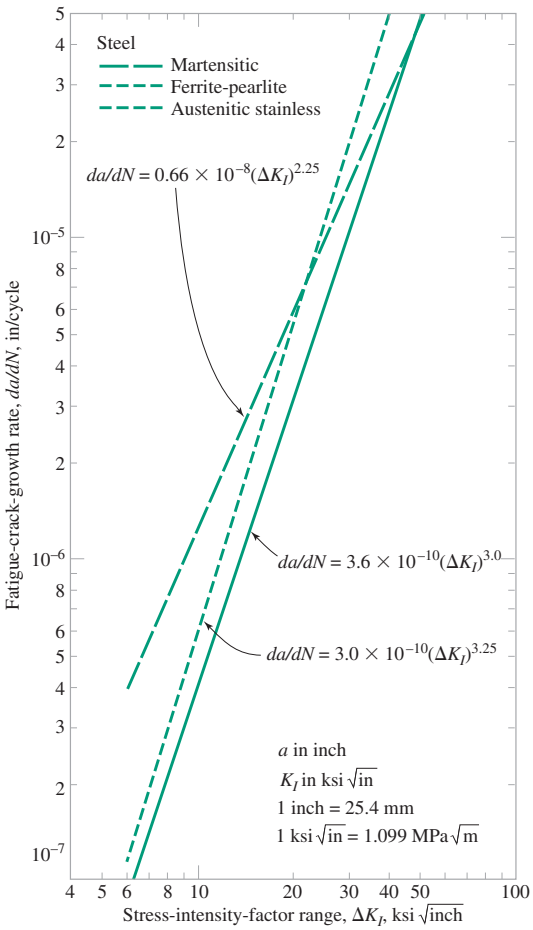

Figure 5.45
Fatigue crack propagation behavior of various steels. (Reprinted from ref. 34 by permission of Pearson Education, Inc., Upper Saddle River, N.J.)

The crack growth rate, da/dN, has been found to be related to the range of stress-intensity factor, ΔK, where

$$\Delta K = C\Delta\sigma\sqrt{\pi a} \tag{5-85}$$

and the range of stress is given by

$$\Delta\sigma = \sigma_{max} - \sigma_{min} \tag{5-86}$$

Most crack propagation data are presented as log-log plots of da/dN versus ΔK. Figure 5.45 shows such a plot for various types of steels. The study of such data has led to many different empirical models[47] for the prediction of crack growth rate da/dN as a function of ΔK. One such model, developed by Paris and Erdogan,[48] has become widely known as the *Paris Law*,

$$\frac{da}{dN} = C_{PE}(\Delta K)^n \tag{5-87}$$

where n is the slope of the log-log plot of da/dN versus ΔK, as shown in Figure 5.45, and C_{PE} is an empirical parameter that depends upon material properties, cyclic frequency, mean stress, and perhaps other secondary variables.

[47]See, for example, ref. 32. [48]See ref. 33.

If the parameters C_{PE} and n are known for a particular application, the crack length, a_N, resulting from the application of N cycles of loading after the crack is initiated, may be computed from the expression

$$a_N = a_i + \sum_{j=1}^{N_p} C_{PE}(\Delta K^n) \tag{5-88}$$

or

$$a_N = a_i + \int_1^{N_p} C_{PE}(\Delta K)^n \, dN \tag{5-89}$$

where a_i is the length of a newly initiated crack and N_p the number of loading cycles in the propagation phase following crack initiation. For complicated spectrum loading histories, these computations require block-by-block or cycle-by-cycle analyses, making the use of modern digital computer systems mandatory for the solution of most practical design problems. It should also be recognized that various other phenomena may take place in the zone of material around the tip of a growing crack to influence the crack growth prediction accuracy.[49] These may include crack growth retardation or acceleration due to plastic zones produced by preceding cyclic load histories, the influence of nonzero-mean stresses, and crack size effects. Typically, a designer would utilize (5-88) or (5-89) to obtain preliminary estimates of crack propagation life, but would enlist the help of a fracture mechanics specialist to improve prediction accuracy by including modifications to account for such factors as loading sequence, environment, frequency, multiaxial states of stress, and determination of applicable ΔK values in view of plasticity at the crack tip.

Example 5.19 Fatigue Crack Propagation Life

The martensitic alloy steel tension member of Example 5.17 is to be subjected to a continuation of completely reversed cyclic axial force of 70 kN amplitude, following the initiation of a fatigue crack. It may be assumed that the length of the newly initiated fatigue crack is 1.3 mm. Further, it may be assumed that the stress concentration effects are negligible for the propagating crack (because the initiated crack tip probably extends through most of the zone of stress concentration). How many cycles of continued loading would you estimate could be applied before catastrophic fracture would occur?

Solution

Since the applied axial force is completely reversed, the maximum and minimum normal stresses are

$$\sigma_{max,\,\min} = \pm\frac{F_a}{A} = \pm\frac{70\,000}{(0.009)(0.036)} = \pm 216 \text{ MPa}$$

Using (5-50) to check the plain strain conditions

$$B = 0.009 \geq 2.5\left(\frac{K_{Ic}}{S_{yp}}\right)^2 = 2.5\left(\frac{81}{1379}\right)^2 = 0.0086$$

Since this expression is satisfied, *plain strain conditions exist* and the critical crack size may be determined from (5-79). Thus,

$$a_{cr} = \frac{1}{\pi}\left[\frac{K_{Ic}}{C\sigma_{max}}\right]^2 = \frac{1}{\pi}\left[\frac{81}{216C}\right]^2 = \frac{0.0448}{C^2} \tag{1}$$

The parameter C may be evaluated from Figure 5.19 using the methods of Example 5.9, but must be iterated together with (1) above since the crack length a_{cr} must be known to

[49] See, for example, ref. 1, pp. 293–304.

find C, and C must be known to find a_{cr}. To illustrate the iteration, assume, for example, $a_{cr} = 15$ mm. Then from Figure 5.19,

$$a/b = 15/36 = 0.42$$

and

$$C(1 - 0.42)^{3/2} = 0.97 \quad \rightarrow \quad C = 2.2$$

From (1)

$$a_{cr} = \frac{0.0448}{(2.2)^2} = 0.0093 \text{ m} = 9.3 \text{ mm}$$

Iterating, try $a_{cr} = 12.5$ mm, giving $a/b = 12.5/36 = 0.35$ and $C = 0.98/(1 - 0.35)^{3/2} = 187$. This results in

$$a_{cr} = \frac{0.0448}{(1.87)^2} = 0.0128 \text{ m} = 12.8 \text{ mm}$$

This is considered close enough to the assumed value of $a_{cr} = 12.5$ mm. Corresponding to this critical crack length, we use $C_{cr} = 1.87$.

For the newly initiated crack of length $a_i = 1.3$ mm, the corresponding C_i may be found from Figure 5.19, with $a_i/b = 1.3/36 = 0.036$

$$C_i = 1.07/(1 - 0.036)^{3/2} = 1.13$$

Since this is a martensitic steel, from Figure 5.45 the applicable empirical crack growth model must be converted into SI and is

$$\frac{da}{dN} = 3.03 \times 10^{-10}(\Delta K)^{2.25} \tag{2}$$

where ΔK is in MPa$\sqrt{\text{m}}$ and da/dN is in meter per cycle.

Next we establish $\Delta\sigma$ using the maximum and minimum normal stresses

$$\Delta\sigma = 216 - (-216) = 432 \text{ MPa}$$

Substituting (5-80) into (2) above

$$\frac{da}{dN} = 3.03 \times 10^{-10}(C\Delta\sigma\sqrt{\pi a})^{2.25}$$

or

$$\frac{da}{a^{1.125}} = 3.03 \times 10^{-10}(C\Delta\sigma\sqrt{\pi})^{2.25}dN$$

Integrating both sides

$$\int_{a_i=0.0013}^{a_{cr}=0.0125} \frac{da}{a^{1.125}} = 3.03 \times 10^{-10}\left[\left(\frac{1.13 + 1.87}{2}\right)(432)\sqrt{\pi}\right]^{2.25}\int_0^{N_p} dN \tag{3}$$

Note that C is taken as the average of C_i and C_{cr}. A more accurate solution could be found by partitioning the crack growth into smaller increments and separately integrating each increment, summing the results to obtain N_p. Evaluating (3)

$$\frac{a^{-0.125}}{-0.125}\Bigg|_{0.0013}^{0.0125} = 0.00233N_p \quad \rightarrow \quad N_p = 1.94 \times 10^3$$

$N_p = 1.94 \times 10^3$ propagation cycles to final fracture

Design Issues in Fatigue Life Prediction

Using the *F-M* approach to estimate the total fatigue life of a proposed design configuration is simple in concept. The total fatigue life to failure N_f is the sum of the initiation life N_i plus the propagation life N_p. That is,

$$N_f = N_i + N_p \tag{5-90}$$

The initiation life may be calculated using the local stress-strain approach, as illustrated in Example 5.18. The propagation life may be calculated using an appropriate crack growth model together with LEFM estimates of critical crack size, as illustrated in Example 5.19. As a practical matter, however, several important additional issues must be addressed when attempting to use (5-90) as a design tool. These include the following: (1) determining or specifying the size of an initiated crack corresponding to N_i cycles; (2) accounting for geometric stress concentration effects and stress gradients; (3) accounting for strength gradients, especially as associated with metallurgical or mechanical surface treatments; (4) accounting for residual stress fields; (5) accounting for multiaxial states of stress, three-dimensional effects, and others. Most of these issues remain research topics, requiring designers to consult with fracture mechanics specialists and/or make appropriate simplifying assumptions when utilizing (5-90). In the final analysis, it is essential to conduct full-scale fatigue tests to provide acceptable reliability.

Example 5.20 Estimating Total Fatigue Life

Referring to the solutions of Examples 5.18 and 5.19, estimate the total fatigue life of the martenstic steel tensile member subjected to a completely reversed cyclic axial force of 70 kN amplitude.

Solution

The total fatigue life may be estimated using (5-90). With the results from Examples 5.18 and 5.19

$$N_f = N_i + N_p = 4.8 \times 10^7 + 1.94 \times 10^3 = 4.8 \times 10^7 \text{ cycles}$$

For this member, the fatigue life N_f is dominated by the crack initiation phase.

Fatigue Stress Concentration Factors and Notch Sensitivity Index

Unlike the theoretical stress concentration factor K_t, the fatigue stress concentration factor K_f is a *function of the material*, as well as geometry and type of loading. To account for the influence of material characteristics, a *notch sensitivity index q* has been defined to relate the actual effect of a notch on fatigue strength of a material to the effect that might be predicted solely on the basis of elastic theory. The definition of notch sensitivity index q is given by

$$q = \frac{K_f - 1}{K_t - 1} \tag{5-91}$$

where K_f = fatigue stress concentration factor
K_t = theoretical stress concentration factor
q = notch sensitivity index valid for high-cycle fatigue range

The magnitude of q ranges from *zero* for no notch effect to *unity* for full notch effect. The notch sensitivity index is a function of both material and notch radius, as illustrated in

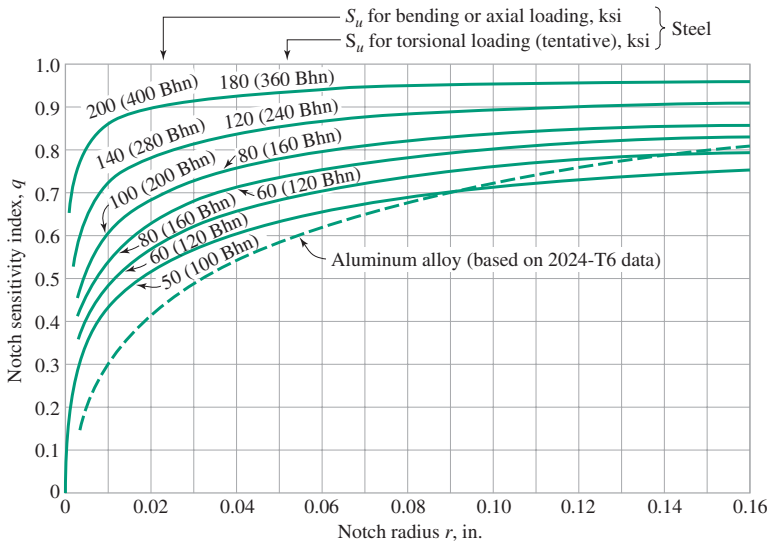

Figure 5.46
Curves of notch sensitivity index versus notch radius for a range of steels and an aluminum alloy subjected to axial, bending, and torsional loading. (After ref. 15; reprinted with permission of the McGraw-Hill Companies.)

Figure 5.46 for a range of steels and an aluminum aloy. For finer-grained materials, such as quenched and tempered steels, q is usually close to unity. For coarser-grained materials, such as annealed or normalized aluminum alloys, q approaches unity if the notch radius exceeds about one-quarter inch. In view of these facts it is tempting to recommend the use of $K_f = K_t$ as a simplifying assumption. Doing so, however, would ignore several important notch sensitivity effects, including:

1. Under fatigue loading, an alloy steel with superior *static* properties will often be found *not* to have superior *fatigue* properties when compared to a plain carbon steel, because of the difference in notch sensitivities.
2. There is a tendency to improperly assess the effects of tiny scratches and cavities unless notch sensitivity effects are recognized.
3. Serious errors in applying the results from models to large structures may be made if notch sensitivity effects are not recognized.
4. In critical design situations, inefficiencies may accrue if notch sensitivity effects are not considered.

Based on (5-91), an expression for fatigue stress concentration factor may be written as

$$K_f = q(K_t - 1) + 1 \tag{5-92}$$

The theoretical elastic stress concentration factor K_t may be determined, on the basis of geometry and loading, from handbook charts such as those depicted in Figures 5.4 through 5.12. The notch sensitivity index q may also be read from charts, such as the one shown in Figure 5.46.

For *uniaxial* states of cyclic stress it is sometimes convenient to use K_f as a "strength reduction factor" rather than as a "stress concentration factor." This may be done by *dividing* the fatigue limit *by* K_f rather than *multiplying* the applied nominal cyclic stress *times* K_f. Although conceptually it is more correct to think of K_f as a stress concentration factor, computationally it is often simpler to use K_f as a strength reduction factor when the cyclic stresses are uniaxial. For multiaxial states of stress, however, K_f *must* be used as a stress concentration factor.

The fatigue stress concentation factor (or strength reduction factor) determined from (5-92) is strictly applicable only in the high-cycle fatigue range (lives of 10^5–10^6 cycles

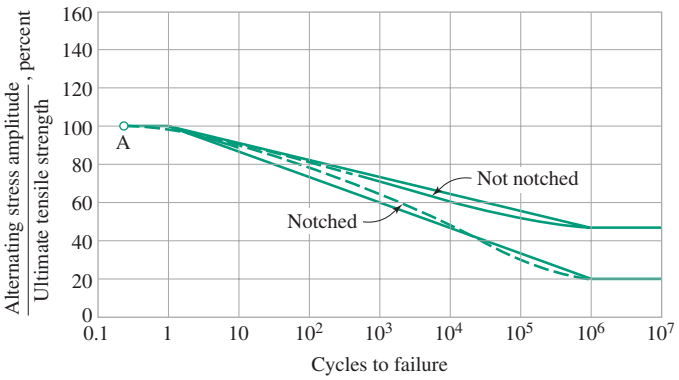

Figure 5.47
S-N curves for notched and unnotched specimens subjected to completely reversed axial loading. (After ref. 16.)

and greater). It has earlier been noted that for ductile materials and static loads, effects of stress concentration may usually be neglected. In the intermediate and low-cycle life range (from a quarter-cycle up to about 10^5–10^6 cycles), the stress concentration factor increases from unity to K_f, so the notched and unnotched *S-N* curves tend to converge toward the quarter-cycle point *A*, as shown in Figure 5.47.

Estimates for fatigue stress concentration factor can be made by constructing a straight line from the ultimate strength plotted at a life of 1 cycle to the unnotched fatigue strength divided by K_f plotted at a life of 10^6 cycles, on a semilogarithmic *S-N* plot.[50] The ratio of unnotched to notched fatigue strength at any selected intermediate life may be used as an estimate of fatigue stress concentration factor for that life.

Finally, experimental investigations have indicated that for evaluating fatigue of *ductile materials*, the fatigue stress concentration factor for any *nonzero mean* cyclic state of stress should be applied *only* to the *alternating* component of stress (and *not* to the *steady* component). In evaluating the fatigue loading of *brittle* materials, the stress concentration factor should be applied to *both* the alternating and the steady component.

Example 5.21 Fatigue Life Prediction Under Uniaxial Stress, Including Stress Concentration

A 60-mm-wide by 2.5-mm-thick rectangular plate of annealed 1040 steel has a 6-mm-diameter hole drilled through, as shown in Figure E5.21. The properties of the 1040 steel are $S_u = 372$ MPa, $S_{yp} = 330$ MPa, $e(50\text{ mm}) = 50\%$, and $S_f = 186$ MPa. The plate is to be subjected to a completely reversed alternating direct force of 8 kN. Buckling is not a problem. What life cycle would you predict for the bar if the not notched *S-N* curve of Figure 5.47 is valid?

Solution

The *actual* stress amplitude at the critical point adjacent to the hole is

$$(\sigma_a)_{act} = K_f(\sigma_a)_{nom} = K_f\left(\frac{P_a}{A_{net}}\right) = K_f\left(\frac{8000}{0.06(0.0025)}\right) = 53.3K_f\text{ MPa}$$

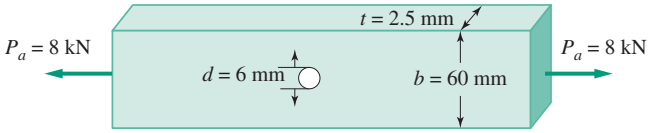

Figure E5.21
Steel bar with stress concentration subjected to cyclic loading.

[50]See Figure 5.47.

From (5-92)

$$K_f = q(K_t - 1) + 1$$

Using Figure 5.46 with $S_u = 372$ MPa $= 54$ ksi and $r = 3$ mm ≈ 0.125 in,

$$q = 0.76$$

From Figure 4.9 (b), with $b/d = 6/60 = 0.10$,

$$K_t = 2.7$$

Therefore,

$$K_f = 0.76(2.7 - 1) + 1 = 2.29$$

The actual stress is, therefore,

$$(\sigma_a)_{act} = 53.3K_f = 53.3(2.29) = 122 \text{ MPa}$$

Calculating the ordinate ratio

$$\frac{(\sigma_a)_{act}}{S_u} = \frac{122}{372} = 0.378 = 37.87\%$$

And using it to read into the "not notched" *S-N* curve of Figure 5.47, the predicted cyclic life of the plate is infinite.[51] It should be recognized, however, that there is virtually no margin of safety. It would be prudent, therefore, to impose an appropriate safety factor or reliability assessment before going further.

5.7 Multiaxial States of Cyclic Stress and Multiaxial Fatigue Failure Theories

An extensive discussion of the prediction and prevention of fatigue failure and fatigue life under *uniaxial* states of cyclic stress was presented in 5.6. As mentioned in that discussion, most real design situations involve fluctuating loads that produce *multiaxial* states of cyclic stress. *A consensus has not yet been reached on the best approach to prediction of failure under multiaxial states of cyclic stress*. However, one technique used for ductile materials subjected to fluctuating multiaxial stresses is to utilize a cyclic adaptation of the *equivalent stress* expression of (5-45). For brittle materials subjected to fluctuating multiaxial stresses, the principal normal stress expressions are utilized.

An *equivalent uniaxial alternating stress* expression σ_{eq-a} for ductile materials, based on the equivalent stress equation of (5-47), becomes

$$\sigma_{eq-a} = \sqrt{\frac{1}{2}[(\sigma_{x-a} - \sigma_{y-a})^2 + (\sigma_{y-a} - \sigma_{z-a})^2 + (\sigma_{z-a} - \sigma_{x-a})^2] + 3(\tau_{xy-a}^2 + \tau_{yz-a}^2 + \tau_{xz-a}^2)} \tag{5-93}$$

An *equivalent uniaxial mean stress* expression σ_{eq-m} for ductile materials, based on the equivalent stress equation of (5-47), is

$$\sigma_{eq-m} = \sqrt{\frac{1}{2}[(\sigma_{x-m} - \sigma_{y-m})^2 + (\sigma_{y-m} - \sigma_{z-m})^2 + (\sigma_{z-m} - \sigma_{x-m})^2] + 3(\tau_{xy-m}^2 + \tau_{yz-m}^2 + \tau_{xz-m}^2)} \tag{5-94}$$

[51] Because the ordinate ratio 0.42 lies below the *S-N* curve.

or, for plane stress,

$$\sigma_{eq-a} = \sqrt{\sigma_{x-a}^2 + \sigma_{y-a}^2 - \sigma_{x-a}\sigma_{y-a} + 3\tau_{xy-a}^2} \tag{5-95}$$

$$\sigma_{eq-m} = \sqrt{\sigma_{x-m}^2 + \sigma_{y-m}^2 - \sigma_{x-m}\sigma_{y-m} + 3\tau_{xy-m}^2} \tag{5-96}$$

The equations (5-93) through (5-96) may be substituted into any of the expressions discussed in 5.6 as equivalents for their uniaxial counterparts, σ_a and σ_m . For example, in using (5-72), if the loading conditions produce a *multiaxial* state of cyclic stress the equations become

$$\sigma_{eq\text{-}CR} = \frac{\sigma_{eq\text{-}a}}{1 - (\sigma_{eq\text{-}m}/S_u)} \qquad \text{for } \sigma_{eq\text{-}m} \geq 0 \qquad \text{and} \qquad \sigma_{max} \leq S_{yp} \tag{5-97}$$

or

$$\sigma_{eq\text{-}CR} = S_{yp} \qquad \text{for } \sigma_{eq\text{-}m} \geq 0 \qquad \text{and} \qquad \sigma_{max} \geq S_{yp} \tag{5-98}$$

where

$$\sigma_{max} = \sigma_{eq\text{-}a} + \sigma_{eq\text{-}m} \tag{5-99}$$

For brittle materials subjected to multiaxial states of cyclic stress, if the convention $\sigma_1 \geq \sigma_2 \geq \sigma_3$ is adopted, the expressions σ_{1a} and σ_{1m} may be substituted into any of the uniaxial procedures discussed in 5.6. With brittle materials, for example, equations (5-73) would become, under multiaxial states of cyclic stress,

$$\sigma_{eq\text{-}CR} = \frac{\sigma_{1a}}{1 - (\sigma_{1m}/S_u)} \qquad \text{for } \sigma_{1m} \geq 0 \qquad \text{and} \qquad \sigma_{max} \leq S_u \tag{5-100}$$

Example 5.22 Fatigue Failure Prediction Under Fluctuating Multiaxial Stresses

A power transmission shaft of solid cylindrical shape is to be made of 1020 hot-rolled steel with $S_u = 65{,}000$ psi, $S_{yp} = 43{,}000$ psi, $e = 36$ percent elongation in 2 in, and fatigue properties as shown for 1020 steel in Figure 5.31. The shaft is to transmit 85 horsepower at a rotational speed of $n = 1800$ rpm, with no fluctuations in torque or speed. At the critical location, midspan between bearings, the rotation shaft is also subjected to a pure bending moment of 1500 in-lb, fixed in a vertical plane by virtue of a system of symmetrical external forces on the shaft. If the shaft diameter is 1.0 in, what operating life would be predicted before fatigue failure occurs?

Solution

From the horsepower equation (4-39), the steady shaft torque is

$$T = \frac{63{,}025(hp)}{n} = \frac{63{,}025(85)}{1800} = 2976 \text{ in-lb (steady)}$$

And from the problem statement, the bending moment is completely reversed (due to shaft rotation), giving

$$M = 1500 \text{ in-lb (completely reversed)}$$

Since the maximum shearing stress due to torque T occurs at the surface, and cyclic bending stresses range from maximum to minimum and back to maximum at the surface with each rotation, all midspan surface points are equally critical.

A typical volume element at a midspan critical point is shown in Figure E5.22. The steady torsional shearing stress may be calculated from (4-37) as

$$\tau_{xy} = \frac{Ta}{J} = \frac{16T}{\pi d^3}$$

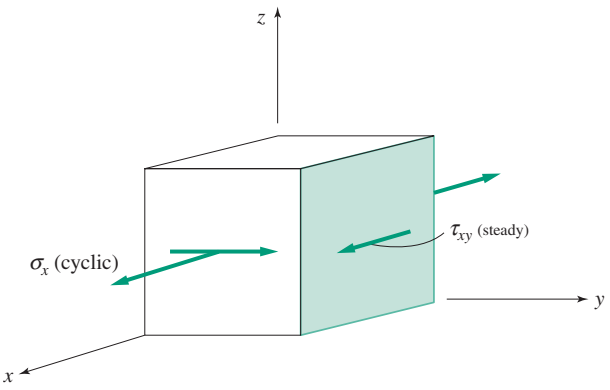

Figure E5.22
State of stress at a typical midspan critical point.

and cyclic bending stress from (4-5) as

$$\sigma_x = \frac{Mc}{I} = \frac{32M}{\pi d^3}$$

Noting that $T_{max} = T_{min} = T_m = T = 2976$ in-lb, $M_{max} = +1500$ in-lb, $M_{min} = -1500$ in-lb, and $M_m = 0$, the alternating and mean components stresses are

$$\tau_{xy-m} = \frac{16(2976)}{\pi(1)^3} = 15{,}157 \text{ psi}, \tau_{xy-a} = 0 \text{ psi}$$

$$\sigma_{x-m} = 0 \text{ psi}, \qquad \sigma_{x-a} = \frac{32(1500)}{\pi(1)^3} = 15{,}279 \text{ psi}$$

Since $e = 36$ percent, the material is ductile and the equivalent stress concepts of (5-95) and (5-96) may be used to write

$$\sigma_{eq-a} = \sqrt{(15{,}279)^2 + 0^2} = 15{,}279 \text{ psi}$$
$$\sigma_{eq-m} = \sqrt{0^2 + 3(15{,}157)^2} = 26{,}253 \text{ psi}$$

Using the expressions in (5-99), the condition of σ_{max} may be checked by calculating

$$\sigma_{max} = 15{,}279 + 26{,}253 = 41{,}532 < 43{,}000 \text{ psi}$$

Thus, (5-97) is valid, and gives

$$\sigma_{eq-CR} = \frac{15{,}279}{1 - \dfrac{26{,}253}{65{,}000}} = 25{,}631 \text{ psi}$$

Checking Figure 5.31, this value, $\sigma_{eq\text{-}CR} = 25{,}631$ psi, corresponds to infinite life for 1020 steel. No strength-influencing factors such as surface finish, corrosion, and so forth, have been considered. A more accurate prediction could be made by considering such factors, as was done in Example 5.13.

Example 5.23 Fatigue Life Predication Under Multiaxial Stresses, Including Stress Concentration Effects

Refer to Figure E5.23A, in which a torsionally oscillating shaft of 1.25-in diameter has a 0.25-inch diametral hole all the way through it. By the way the shaft is loaded, it is subjected to a *released* torsional moment of 8300 in-lb, and an in-phase released cyclic

Example 5.23 Continues

bending moment, in the plane of the through-hole axis, of 3700 in-lb. If the shaft is made of 4340 steel with S_u = 150,000 psi, S_{yp} = 120,000 psi, e = 15 percent in 2 in, and the fatigue properties shown in Figure E5.23B, how many torsional oscillations would you expect could be completed before fatigue failure of the shaft takes place? (Assume that the critical point for bending and torsion coincide.)

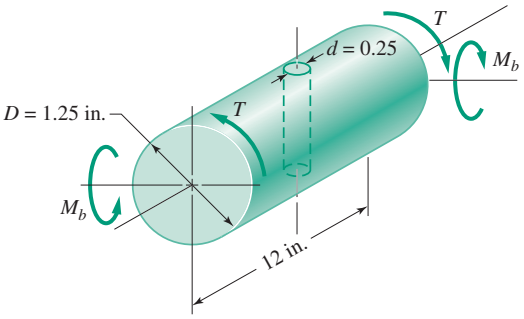

Figure E5.23A
Oscillating shaft with through hole.

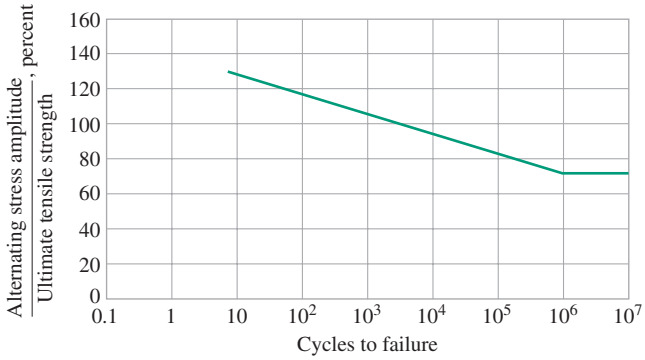

Figure E5.23B
Uniaxial fatigue properties of 4340 steel used in the torsionally oscillating shaft.

Figure E5.23C
State of stress at the critical point.

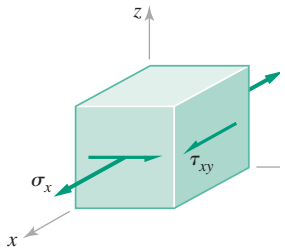

Solution

The critical points for bending and torsion are assumed to be at the same location, adjacent to the edge of the hole at top and bottom surface elements. The state of stress at the critical point is shown in Figure E5.23C.

From Figure 5.6, the nominal bending and torsional stresses as well as bending and torsional stress concentration factors may be found. The nominal bending stress is

$$\sigma_{nom} = \frac{M}{\frac{\pi D^3}{32} - \frac{dD^2}{6}} = \frac{M}{\frac{\pi(1.25)^3}{32} - \frac{0.25(1.25)^2}{6}} = 7.9M$$

and the nominal torsional stress is

$$\tau_{nom} = \frac{T}{\frac{\pi D^3}{16} - \frac{dD^2}{6}} = \frac{T}{\frac{\pi(1.25)^3}{16} - \frac{0.25(1.25)^2}{6}} = 3.14T$$

Referring again to Figure 5.6, for

$$\frac{d}{D} = \frac{0.25}{1.25} = 0.2$$

It may be found that

$$(K_t)_{tor} = 1.50$$

and

$$(K_t)_{bend} = 2.03$$

Also, from Figure 5.46

$$q_{tor} = 0.94$$

and

$$q_{bend} = 0.92$$

Then from (5-92)

$$K_{f-tor} = 0.94(1.50 - 1) + 1 = 1.47$$

and

$$K_{f-bend} = 0.92(2.03 - 1) + 1 = 1.95$$

Then

$$\tau_{xy} = 1.47(3.14T) = 4.62T$$

and

$$\sigma_x = 1.95(7.90M) = 15.41M$$

Since the shaft is subjected to a released torsional moment of 8300 in-lb and a released cyclic bending moment of 3700 in-lb, the maximum and minimum values are

$$M_{\max} = 3700 \text{ in-lb}, \; M_{\min} = 0$$
$$T_{\max} = 8300 \text{ in-lb}, \; T_{\min} = 0$$

The alternating and mean values are

$$M_a = M_m = \frac{3700}{2} = 1850 \text{ in-lb}$$
$$T_a = T_m = \frac{8300}{2} = 4150 \text{ in-lb}$$

Based on the above equations, the alternating and mean component stresses are

$$\sigma_{x-a} = \sigma_{x-m} = 15.41(1850) = 28{,}509 \text{ psi}$$
$$\tau_{xy-a} = \tau_{xy-m} = 4.62(4150) = 19{,}173 \text{ psi}$$

Since $e = 15$ percent, the material is ductile, and the equivalent stress concepts of (5-95) and (5-96) may be used to give

$$\sigma_{eq-a} = \sqrt{(28{,}509)^2 + 3(19{,}173)^2} = 43{,}767 \text{ psi}$$

And

$$\sigma_{eq-m} = \sqrt{(28{,}509)^2 + 3(19{,}173)^2} = 43{,}767 \text{ psi}$$

Example 5.23 Continues

Using these expressions in (5-99), the condition on σ_{max} may be checked by calculating

$$\sigma_{max} = 43{,}767 + 43{,}767 = 87{,}534 \text{ psi}$$

Based on the validity criteria

$$\sigma_{eq-m} \geq 0$$

And

$$\sigma_{max} = 87{,}534 < S_{yp} = 120{,}000 \text{ psi}$$

If (5-72) is chosen, the result is

$$\sigma_{eq-CR} = \frac{43{,}767}{1 - (43{,}767/150{,}000)} = 61{,}800 \text{ psi}$$

If (5-75) is chosen, the result would be

$$\sigma_{eq-CR} = \frac{43{,}767}{1 - (43{,}767/150{,}000)^2} = 47{,}840 \text{ psi}$$

Since the fatigue limit in Figure E5.23B is shown as $S_f = 75{,}000$ psi, both values calculated for σ_{eq-CR} would be predicted to give infinite life (an infinite number of torsional oscillations) for this part. Strength-influencing factors such as surface finish, corrosion, and so on, should be reviewed, however, to improve the life assessment. (See Example 5.13.)

Example 5.24 Fatigue Life Improvement Resulting from Shot-Peening (Favorable Residual Stresses)

A cylindrical support bar is to be subjected to a *released* cyclic tensile load of $P_{max} = 23{,}000$ lb. The critical section in the bar is at the root of a circumferential groove of semicircular profile, having the dimensions shown in Figure E5.24A. The material is to be a wrought carbon steel alloy with $S_u = 76{,}000$ psi, $S_{yp} = 42{,}000$ psi, and e (2 inches) = 18 percent when in hot rolled condition, and $S_u = 70{,}000$ psi, $S_{yp} = 54{,}000$ psi, and e (2 inches) = 15 percent when in cold drawn condition. Fatigue properties are defined by the *S-N* curve from Example 5.10, and repeated here as Figure E5.24B.

a. Using a fatigue strength reliability level of 99.9 percent, estimate the life of the bar under the conditions given, if the material is in hot-rolled condition.

b. Estimate the improvement in life (if any) that might be expected from the hot-rolled bar if the groove is properly shot-peened, assuming that the shot-peening process results in a compressive residual surface stress of about 50 percent of the strain-hardened yield strength.

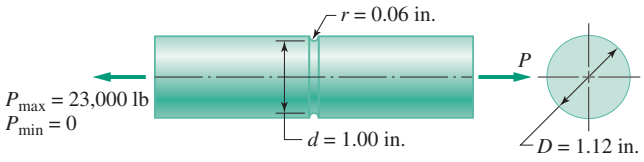

Figure E5.24A
Cyclically loaded cylindrical steel support bar with circumferential groove of semicircular profile.

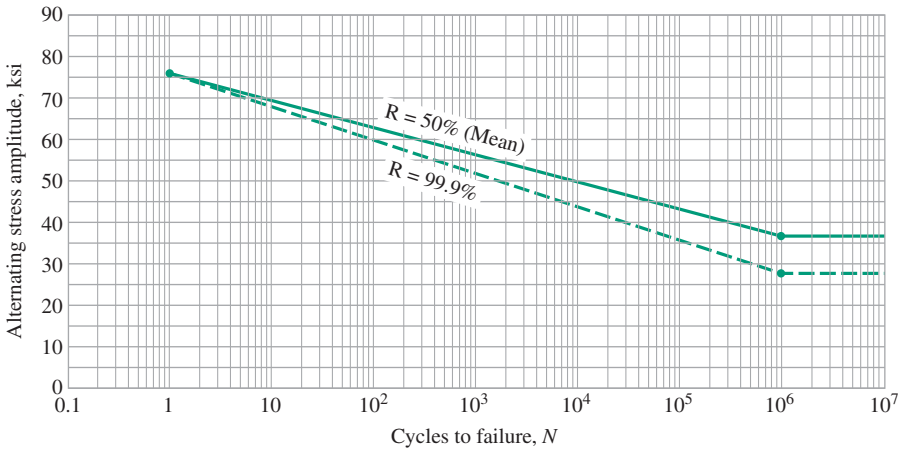

Figure E5.24B
Estimated *S-N* curves for fatigue strength reliability levels of 50% and 99.9% (repeat of Figure E5.10A). Note that S_f for $R = 50\%$ is 38,000 psi and S_f for $R = 99.9\%$ is 28,600 psi.

Solution

a. For the *released* loading applied, with $P_{max} = 23{,}000$ lb, the nominal cyclic stress ranges from

$$(\sigma_{min})_{nom} = 0$$

to

$$(\sigma_{max})_{nom} = \frac{P_{max}}{A_{net}} = \frac{23{,}000}{\frac{\pi(1.00)^2}{4}} = 29{,}285 \text{ psi}$$

giving nominal values of stress amplitude and tensile mean stress of

$$(\sigma_a)_{nom} = \frac{29{,}285 - 0}{2} = 14{,}642 \text{ psi}$$

and

$$(\sigma_m)_{nom} = \frac{29{,}285 + 0}{2} = 14{,}642 \text{ psi}$$

Using methods developed in 5.3, since the material is ductile,

$$(\sigma_a)_{act} = K_f (\sigma_a)_{nom}$$

and

$$(\sigma_m)_{act} = (\sigma_m)_{nom}$$

Then from (5-91)

$$K_f = q(K_t - 1) + 1$$

where q may be read from Figure 5.11 with $r = 0.06$ and $S_u = 76{,}000$ psi, as

$$q = 0.74$$

From Figure 5.5(b), with $r/d = 0.06$ and $D/d = 1.12$, K_t may be read as

$$K_t = 2.18$$

Example 5.24 Continues

giving

$$K_f = 0.74(2.18 - 1) + 1 = 1.87$$

From this,

$$(\sigma_a)_{act} = 1.87(14{,}642) = 27{,}381 \text{ psi}$$

and

$$(\sigma_m)_{act} = 14{,}642 \text{ psi}$$

Therefore, *effective* values for σ_{max} and σ_{min} are

$$(\sigma_{max})_{eff} = 27{,}381 + 14{,}642 = 42{,}023 \text{ psi}$$

and

$$(\sigma_{min})_{eff} = 14{,}642 - 27{,}381 = -12{,}739 \text{ psi}$$

Now, using (5-72),

$$\sigma_{eq\text{-}CR} = \frac{(\sigma_a)_{act}}{1 - \dfrac{\sigma_m}{S_u}} = \frac{27{,}381}{1 - \dfrac{14{,}642}{76{,}000}} = 33{,}915 \text{ psi}$$

Taking this equivalent completely reversed stress amplitude to the 99.9 percent reliability *S-N* curve of Figure E4.20B, the estimated life is read as

$$N = 2 \times 10^5 \text{ cycles}$$

b. If the groove were shot-peened to give a residual compressive stress of 50 percent of the strain-hardened yield strength, the compressive residual stress at the surface would be

$$\sigma_{res} = -0.5(54{,}000) = -27{,}000 \text{ psi}$$

Superposing the residual stress on the effective operational stresses at the notch root, we get

$$(\sigma_{max})_{sp\text{-}eff} = 42{,}023 + (-27{,}000) = 15{,}023 \text{ psi}$$

and

$$(\sigma_{min})_{sp\text{-}eff} = -12{,}739 + (-27{,}000) = -39{,}739 \text{ psi}$$

so

$$(\sigma_a)_{sp\text{-}eff} = \frac{15{,}023 - (-39{,}739)}{2} = 27{,}381 \text{ psi}$$

and

$$(\sigma_m)_{sp\text{-}eff} = \frac{15{,}023 + (-39{,}739)}{2} = -12{,}358 \text{ psi}$$

For the shot-peened groove, then, since mean stress is compressive, using (5-73),

$$\sigma_{eq\text{-}CR} = (\sigma_a)_{sp\text{-}eff} = 27{,}381 \text{ psi}$$

Taking the equivalent completely reversed stress amplitude to the 99.9 percent reliability *S-N* curve of Figure E5.24B, the estimated life is read as

$$N_{sp} = \infty \text{ cycles}$$

because

$$\sigma_{eq\text{-}CR} = 27{,}381 < S_f\,(R = 99.9\%) = 28{,}600 \text{ psi}$$

Shot-peening the groove in this case is estimated to increase fatigue life of the part from about 200,000 cycles to infinite life. Shot-peening is widely used to improve fatigue failure resistance.